DISCLAIMER

This book was prepared as an account of work sponsored by an agency of the United States Government. Neither the United States Government nor any agency thereof, nor any of their employees, makes any warranty, express or implied, or assumes any legal liability or responsibility for the accuracy, completeness, or usefulness of any information, apparatus, product, or process disclosed, or represents that its use would not infringe privately owned rights. Reference herein to any specific commercial product, process, or service by trade name, trademark, manufacturer, or otherwise, does not necessarily constitute or imply its endorsement, recommendation, or favoring by the United States Government or any agency thereof. The views and opinions of authors expressed herein do not necessarily state or reflect those of the United States Government or any agency thereof.

Preparation and Spectroscopic Properties of Three New Actinide (IV) Borohydrides

Rodney Howard Banks *

Abstract

New tetrakis-borohydrides of Pa, Np, and Pu have been synthesized by similar reactions as those used in the preparation of thorium and uranium borohydrides,

$$AnF_4 + 2Al(BH_4)_3 \rightarrow An(BH_4)_4 + 2AlF_2BH_4;\ An = Th - Pu.$$

The crystal structure of $Pa(BH_4)_4$ is isostructural to those of $Th(BH_4)_4$ and $U(BH_4)_4$ and is of the tetragonal space group $P4_32_12$, where a = 7.53 (3) Å, c = 13.22 (5) Å, and Z = 4. Its calculated density is 2.57 $gm\text{-}cm^{-3}$. $Pa(BH_4)_4$ is an orange, air-sensitive compound which is soluble in THF and sublimes at 55° in vacuum.

Due to the thermal instabilities of $Np(BH_4)_4$ and $Pu(BH_4)_4$, their reaction temperatures are maintained at 0° and the compounds must be stored at low temperature. Neptunium and plutonium borohydrides are pyrophoric liquids and are very soluble in organic solvents. The vapor pressure of $Np(BH_4)_4$, 10 mmHg/25°, was measured as a function of temperature in the range of -5 to 25° and is described by the equations, $\log p(mmHg) = -3168/T + 11.80$ (solid) and $\log p = -1858/T + 7.24$ (liquid), where T is in degrees K.

* Lawrence Berkeley Laboratory, University of California, Berkeley, California 94720

DISTRIBUTION OF THIS DOCUMENT IS UNLIMITED

Low temperature Xray diffraction studies have shown that $Np(BH_4)_4$ and $Pu(BH_4)_4$ are isomorphous and exhibit a unique crystal structure which is very similar to that of $Zr(BH_4)_4$. The details of this new structure were determined by single crystal Xray diffraction methods at 130K for $Np(BH_4)_4$. Neptunium borohydride is monomeric and crystallizes into the tetragonal space group $P4_2/nmc$, where a = 8.559 (9) Å, c = 6.017 (9) Å, and Z = 2. The 12 coordinate Np atom is triply hydrogen-bridged bonded to four terminal BH_4^- groups disposed tetrahedrally around it giving Np-B distances of 2.46 (3) Å.

Solid-state, low temperature infrared (25-7400 cm^{-1}) and Raman (100-2600 cm^{-1}) spectra were taken for $Np(BH_4)_4$ and $Np(BD_4)_4$. A normal coordinate analysis was carried out using the assigned fundamental frequencies obtained from the spectra and determined a reasonable set of force constants and calculated values for the frequencies of the unobserved T_1 modes. Based on results of the analysis, isotopic impurity, overtone, and combination bands were identified in the infrared spectra.

Electron paramagnetic resonance spectra of $Np(BH_4)_4/Zr(BH_4)_4$ and $Np(BD_4)_4/Zr(BD_4)_4$ at X, K, and Q bands have established the ground electronic states as $\Gamma_6(^4I_{9/2})$ having g values of 1.894 (1) and 1.892 (1), respectively. The hyperfine coupling constant was found to be large, $|A| = .1140 \pm .001$ cm^{-1} for both isotopes.

Optical absorption spectra of pure $Np(BH_4)_4$, $Np(BD_4)_4$, and these compounds diluted in $Zr(BH_4)_4$ and $Zr(BD_4)_4$ single crystals were obtained at 2, 77, and 300K in the region 300-2500 nm. Although the other pure

electronic transitions were not assigned, the transition Γ_6 ($^4I_{9/2}$) → $\Gamma_8^{(1)}$ ($^4I_{11/2}$) and its accompanying vibronic bands have been assigned, based on the results of the normal coordinate analysis and crystal field energy level calculations. Similar spectra of $Pa(BH_4)_4$ and $Pa(BD_4)_4$ in an organic glass have been taken and a preliminary analysis of the spectra is given.

ACKNOWLEDGMENT

I would like to thank the many people who have made my graduate years in Berkeley a memorable experience and without whose help this thesis could not have been written.

My research directors--Dr. Glenn Seaborg, whose inspiration and guidance is greatly appreciated; and Dr. Norman Edelstein, who contributed enormously to all phases of this project--deserve special gratitude.

Deep appreciation goes to Dr. William Gwinn for his patience and numerous rewarding discussions.

The excellent assistance from the glass and machine shops and the Xray crystallography group is gratefully acknowledged.

I am indebted to Gerda Bolz, E. Calhoon, and Bob McCracken of the Environmental Health and Safety Department whose expert help and advice insured the safety and completion of this work.

Sincere thanks also go to my family for their unfailing support and encouragement during these years.

This work was supproted by the U. S. Department of Energy under Contract number W-7405-ENG-48.

TABLE OF CONTENTS

	Page
LIST OF FIGURES	iv
LIST OF TABLES	vi
CHAPTER 1. SYNTHESIS AND CHEMISTRY OF $Pa(BH_4)_4$, $Np(BH_4)_4$, AND $Pu(BH_4)_4$	1
Introduction	1
Preparation of Anhydrous Actinide Tetrafluorides	5
Protactinium Tetrafluoride	5
Neptunium Tetrafluoride	9
Plutonium Tetrafluoride	10
Preparation of Actinide Tetrakis-Borohydrides	10
Protactinium Borohydride	12
Neptunium and Plutonium Borohydrides	12
Preparation of Actinide Borodeuterides	13
Thermal Stability of Np, Pu Borohydrides	17
Preparation of Actinide (IV) TMCOT Complexes from $An(BH_4)_4$	19
Attempted Synthesis of $Ce(BH_4)_4$	20
References and Notes	23
CHAPTER 2. PHYSICAL PROPERTIES AND MOLECULAR STRUCTURES OF THE ACTINIDE BOROHYDRIDES	27
Introduction	27
Experimental	28
Infrared Spectra	28
Xray Powder Diffraction	28
Single Crystal Xray Diffraction	29
Vapor Pressure Measurement	32
Results and Discussion	33
Polymeric Actinide Borohydrides	33
Monomeric Actinide Borohydrides	34
Volatilities of the Metal Tetrakis-Borohydrides	49
References	54
CHAPTER 3. VIBRATIONAL ANALYSIS OF NEPTUNIUM BOROHYDRIDE	56
Introduction	56
Experimental	61
Infrared Spectroscopy	61
Raman Spectroscopy	62

TABLE OF CONTENTS (continued)

Page

Assignment of Fundamentals..... 67
2600-2500 cm^{-1} (2000-1900 cm^{-1}) Region..... 68
2200-2000 cm^{-1} (1600-1500 cm^{-1}) Region..... 78
1300-1050 cm^{-1} (950- 800 cm^{-1}) Region..... 80
600- 450 cm^{-1} (450- 400 cm^{-1}) Region..... 83
200- 25 cm^{-1} Region..... 86
Teller-Redlich Isotopic Product Rules..... 87
Normal Coordinate Analysis..... 90
The Program NORCRD..... 90
The Least Squares Fit..... 93
Assignment of Nonfundamental Bands..... 103
4000- 200 cm^{-1} Region..... 103
7400-4000 cm^{-1} Region..... 120
Other Calculations..... 131
Pictures of A_1 Normal Modes..... 131
Partition Functions and Thermodynamic Quantities..... 131
Conclusion..... 139
References and Notes..... 142
Appendix A..... 147
Appendix B..... 152

CHAPTER 4. ELECTRON PARAMAGNETIC RESONANCE OF NEPTUNIUM BOROHYDRIDE..... 153
Introduction..... 153
Experimental..... 153
Theory and Results..... 155
Calculation of Hamiltonian Parameters..... 157
References..... 168

CHAPTER 5. OPTICAL SPECTRA OF NEPTUNIUM BOROHYDRIDE AND PROTACTINIUM BOROHYDRIDE..... 169
Introduction..... 169
Experimental..... 170
Pure Compound Spectra..... 170
Diluted Compound Spectra..... 170
Theory..... 171
Results and Discussion..... 175
Neptunium Borohydride..... 175
Protactinium Borohydride..... 191
References..... 194

CONCLUSIONS AND FUTURE WORK..... 196

LIST OF FIGURES

Page

CHAPTER 1.
1. Pa-231 Purification Process..... 7
2. Actinide Borohydride Reaction Vessels..... 11

CHAPTER 2.
1. Solid-State Molecular Structure of $U(BH_4)_4$..... 39
2. ORTEP Stereo View of $Np(BH_4)_4$..... 42
3. Schematic Diagram of Packing in $Np(BH_4)_4$..... 47
4. Vapor Pressure vs. $10^3/T$ for U, Np, Hf, and Zr Borohydrides..... 50

CHAPTER 3.
1. Schematic of $M(BH_4)_4$ Infrared Spectra..... 60
2. Raman Spectrum of $Np(BH_4)_4$..... 64
3. Raman Spectrum of $Np(BD_4)_4$..... 65
4. Raman Liquid Nitrogen Cryostat..... 66
5. Gas Phase Infrared Spectra of $Np(BH_4)_4$ and $Np(BD_4)_4$..... 69
6. Solid State Infrared Spectra of $Np(BH_4)_4$ and $Np(BD_4)_4$ at 77K..... 70
7. Far Infrared Spectrum of $Np(BH_4)_4$ at 77K..... 71
8. Near Infrared Spectra of $Zr(BH_4)_4$ and $Np(BH_4)_4$..... 121
9. Near Infrared Spectrum of $Zr(BD_4)_4$..... 129
A1. $\nu_1^{A_1}$ Normal Mode of $Np(BD_4)_4$..... 148
A2. $\nu_2^{A_1}$ Normal Mode of $Np(BD_4)_4$..... 149
A3. $\nu_3^{A_1}$ Normal Mode of $Np(BD_4)_4$..... 150
A4. $\nu_4^{A_1}$ Normal Mode of $Np(BD_4)_4$..... 151

CHAPTER 4.
1. Energy Level Diagram for the Γ_6, $\Gamma_8^{(1)}$, and $\Gamma_8^{(2)}$ States for the J = 9/2 Manifold..... 156
2. EPR Spectrum of $Np(BD_4)_4/Zr(BD_4)_4$ at K Band..... 158
3. EPR Spectra of $Np(BH_4)_4/Zr(BH_4)_4$ at X and Q Bands..... 159
4. Zeeman Energy Levels for $Np(BH_4)_4$..... 164

CHAPTER 5.
1. Crystal Field States of $Np(BH_4)_4$ as a Function of B_0^4 When $B_0^4/B_0^6 = 1.31$..... 176
2. Crystal Field States of $Np(BH_4)_4$ as a Function of B_0^4 When $B_0^4/B_0^6 = .85$..... 177
3. Crystal Field States of $Np(BH_4)_4$ as a Function of B_0^4 When $B_0^4/B_0^6 = .33$..... 178

LIST OF FIGURES (continued)

Page

4. Optical Absorption Spectra of $Np(BH_4)_4$ and $Np(BD_4)_4$ in the Region 2000-2500 nm..... 180
5. Optical Absorption Spectra of $Np(BH_4)_4$ and $Np(BD_4)_4$ in the Region 2000-1500 nm..... 181
6. Optical Absorption Spectra of $Np(BH_4)_4$ and $Np(BD_4)_4$ in the Region 1400-1000 nm..... 182
7. Optical Absorption Spectra of $Np(BH_4)_4$ and $Np(BD_4)_4$ in the Region 900-350 nm..... 183
8. Plot of the g Value for the Γ_6 Ground State of $Np(BH_4)_4$ as a Function of B_0^4 for Various Values of B_0^4/B_0^6..... 189
9. Lines of Constant g Value for the Γ_6 Ground State of $Np(BH_4)_4$ as a Function of B_0^4 vs. B_0^6 for Various Values of ζ_{5f}..... 190
10. Optical Absorption Spectra of $Pa(BH_4)_4$/MCH-d_{14} and $Pa(BD_4)_4$/MCH-d_{14} in the Region 2000-1400 nm..... 193

LIST OF TABLES

Page

CHAPTER 2.

1. Xray Powder Diffraction Data for $Th(BH_4)_4$ 35
2. Xray Powder Diffraction Data for $Pa(BH_4)_4$ 36
3. Xray Powder Diffraction Data for $U(BH_4)_4$ 37
4. Lattice Constants and Calculated Densities for Th, Pa, and U Borohydrides 38
5. Positional and Thermal Parameters for $Np(BH_4)_4$ 43
6. Molecular Structure Parameters for $Np(BH_4)_4$ 44
7. Physical Properties of Metal Tetrakis-Borohydrides 52

CHAPTER 3.

1. Observed Bands in Gas Phase IR Spectra of $Np(BH_4)_4$ and $Np(BD_4)_4$ 72
2. Observed Bands in 77K IR (4000-25 cm^{-1}) and Raman (2600-100 cm^{-1}) Spectra of $Np(BH_4)_4$ 74
3. Observed Bands in 77K IR (4000-25 cm^{-1}) and Raman (2300-100 cm^{-1}) Spectra of $Np(BD_4)_4$ 76
4. Teller-Redlich Isotopic Product Rules 88
5. Molecular Structure Parameters for $Np(BH_4)_4$ 92
6. Best-Fit Force Constants for $Np(BH_4)_4$ 99
7. Fundamental Vibrations (cm^{-1}) of $Np(BH_4)_4$ and $Np(BD_4)_4$ 101
8. Calculated Frequencies for the Eclipsed ($\omega = 0°$) Structure 102
9. Calculated Frequencies for $Np(^{10,11}B^{1,2}H_4)_4$ 107
10. Calculated Frequencies for $Np(^{11}BH_4)_3{}^{10}BH_4$ 108
11. Calculated Frequencies for $Np(^{11}BD_4)_3{}^{10}BD_4$ 110
12. Calculated Frequencies for $Np(^{11}BH_4)_2(^{10}BH_4)_2$ 111
13. Calculated Frequencies for $Np(^{11}BD_4)_2(^{10}BD_4)_2$ 113
14. Calculated Frequencies for $Np(^{11}BD_4)_3{}^{11}BD_3H_t$ 115
15. Calculated Frequencies for $Np(^{11}BH_4)_3{}^{11}BH_3D_t$ 116
16. Calculated Frequencies for $Np(^{11}BH_4)_3{}^{11}BH_3D_b$ and $Np(^{11}BD_4)_3{}^{11}BD_3H_b$ 117
17. Observed IR Bands (7400-4000 cm^{-1}) of $Np(BH_4)_4$ at 2K 122
18. Observed IR Bands (7500-4000 cm^{-1}) of $Zr(BH_4)_4$ at 2K 123
19. Observed IR Bands (4800-4000 cm^{-1}) of $Zr(BD_4)_4$ at 2K 130
20. Entropies and Heat Capacities of $Hf(BH_4)_4$, $Np(BH_4)_4$, and $M(CH_3)_4$ 141

LIST OF TABLES (continued)

Page

CHAPTER 4.
1. Observed X and Q Band Resonances of $Np(BH_4)_4$ 160
2. Observed and Calculated Field Values (gauss) at K Band for $Np(BH_4)_4$ and $Np(BD_4)_4$ 160
3. Spin Hamiltonian Parameters 162

CHAPTER 5.
1. Vibronic Bands of the $\Gamma_6(^4I_{9/2}) \rightarrow \Gamma_8^{(1)}(^4I_{11/2})$ 0-0 Stark Transition 186

Chapter 1

SYNTHESIS AND CHEMISTRY OF $Pa(BH_4)_4$, $Np(BH_4)_4$, AND $Pu(BH_4)_4$

Introduction

The first volatile metal borohydrides, $Be(BH_4)_2$[1] and $Al(BH_4)_3$,[2] were prepared around 1940 by the reaction of $Be(CH_3)_2$ or $Al(CH_3)_3$ with B_2H_6. This procedure proved to be very tedious however, and in 1953 Schlesinger et al.[3] reported a more facile method using the metal halide and an alkali metal borohydride. The most popular method is the reaction of the metal chloride with lithium borohydride,

$$MCl_x + xLiBH_4 \rightarrow M(BH_4)_x\uparrow + xLiCl;\ x = 2,3,4 \qquad (1)$$

Since that time many other metal borohydrides were synthesized by Eq. (1) including the very volatile Ti,[4] Zr,[5] and Hf[6] borohydrides, and some of the d-block metal compounds.[7,8] Tetrahydrofuran adducts of the lanthanide tris-borohydrides were made by Zange[9] who reacted the anhydrous lanthanum trichlorides with a solution of diborane and THF. The only synthesis of an actinide borohydride by Eq. (1) is $Th(BH_4)_4 \cdot 2THF$, which upon heating in a vacuum gives the free tetrakis-borohydride.[10]

During the time of the Manhattan Project, thorium[4] and uranium[11] tetrakis-borohydrides were prepared by a different reaction which involves

the actinide tetrafluoride and $Al(BH_4)_3$:

$$AnF_4 + 2Al(BH_4)_3 \rightarrow An(BH_4)_4 \uparrow + 2AlF_2BH_4 \qquad (2)$$

Many other procedures were found unsatisfactory[12(a)] but $U(BH_4)_4$ was reported to be synthesized by Eq. (1) in a vacuum ball mill.[12(b)]

These actinide borohydrides are among the most volatile compounds of uranium and thorium. They form numerous coordination[10,13] and organo-actinide borohydride complexes[14] which recently have been the subject of many structural[13,15,16] and spectroscopic studies.[14(a),17]

The new actinide (IV) borohydrides, $Pa(BH_4)_4$, $Np(BH_4)_4$, and $Pu(BH_4)_4$ have been synthesized and details of the experimental procedures and some of their physical properties are given in this chapter. A few miscellaneous reactions involving these compounds are also discussed. Before the syntheses are described, a summary of some of the properties of actinide borohydrides is given.

There are two structural types of actinide borohydrides, polymeric and monomeric, which require different handling methods since their physical and chemical properties are very dissimilar and are treated separately. Specific experimental techniques and apparatus, however, are described later in the appropriate chapters.

The first three actinides Th, Pa, and U form polymeric tetrakis-borohydrides. The most obvious characteristic distinguishing them from the monomeric compounds is their relatively low volatility. Vapor pressures of the solids increase smoothly from $Th(BH_4)_4$ to $U(BH_4)_4$;[18]

$Th(BH_4)_4$ requires heating to 120°C to sublime,[4] while $U(BH_4)_4$ sublimes slowly at room temperature. Sublimation is nearly quantitative and is recommended immediately before use to insure high purity. Thorium and uranium borohydrides can be handled and stored in ordinary inert-atmosphere dryboxes but the high radioactivity of Pa-231 requires the use of special dryboxes designed for active materials.

Since all actinide borohydrides are extremely reactive, especially towards oxidation, only the most nonacidic organic solvents can be used. Due to the polymeric structures, Th and Pa borohydrides are virtually insoluble in nonpolar, aliphatic hydrocarbons ($U(BH_4)_4$ is slightly soluble) but are quite soluble in coordinating ethers. The solvents must be thoroughly dried, usually by refluxing with Na/benzophenone and then degassed. When making solutions of low concentration, such as that for spectroscopy, much more care is necessary in insuring that the solvents are completely dry.

Thorium borohydride can be separated from the coordinated ethers by heating and pumping.[10] However, uranium borohydride decomposes under these conditions and the ethers cannot be removed.[13] Unsaturated and other hydrocarbons containing atoms besides ethereal oxygen give decomposition within a week or two. It is never wise to store any metal borohydride in any solvent for long periods as decomposition will inevitably occur.

Thermal stability is another important difference between the two types of actinide borohydrides. Unlike the monomeric compounds, the polymeric ones are thermally stable at room temperature. Uranium boro-

hydride has been observed to show signs of degradation after long periods in the form of surface discoloration,[11] but this is probably due to traces of O_2 or H_2O. $Pa(BH_4)_4$ turns black after a month, which is most likely caused by radiation damage. Above the sublimation temperature, thermal decomposition is very noticeable and H_2 and B_2H_6 are evolved. At temperatures greater than 200° - 300° total decomposition takes place rapidly.[4,11]

Disposing of unwanted material is accomplished by carefully condensing methanol onto the borohydride before admitting air and then finally washing with water and dilute HCl.

The two monomeric actinide compounds, $Np(BH_4)_4$ and $Pu(BH_4)_4$, are pyrophoric and much more volatile than the polymeric borohydrides. Therefore, they must be confined to a high-vacuum line employing grease-free stopcocks and Viton or Teflon O-ring connections. The borohydrides easily sublime at 0° and quantitative amounts of material are transferred using known vapor pressures.

The absence of polymeric chains holding molecules together makes $Np(BH_4)_4$ and $Pu(BH_4)_4$ very soluble in paraffinic hydrocarbons such as pentane and also in coordinating ethers. Standard solvent-drying methods seem to be inadequate unless undue care is taken and very concentrated solutions are prepared. Thorough drying is successfully achieved by mixing the predried solvent with the same or other borohydride (e.g. $Zr(BH_4)_4$, but not B_2H_6), degassing, and then vacuum transferring the solvent at low temperature into the apparatus. Glassware (optical cells,

esp.) which come into direct contact with the liquid or solid borohydride should be baked out under vacuum to remove surface water.

The above discussion also applies to the monomeric Zr, Hf, and Al borohydrides which are important optical matrix materials (Zr, Hf) and reagent for synthesis (Al).

Neptunium and plutonium borohydrides are unstable at room temperature and must be kept at dry-ice or liquid-nitrogen temperatures in grease-free storage tubes. Decomposition is particularly rapid in the liquid phase with half-lives of roughly a day or less. In the gaseous state or when incorporated in $Zr(BH_4)_4$ crystals, the compounds have much longer half-lives, on the order of a few weeks at room temperature.

Reactions with air, water, alcohols, etc. are violent and care should be taken when handling large amounts and when disposing of waste material. Ethanol or isopropanol are good for the initial clean-up, then methanol, water, and dilute HCl are used in the final stages.

All actinide tetrakis-borohydrides are synthesized by Eq. (2) with variations (depending on An) being necessary in the purification steps.[18]

The preparation of very dry tetrafluorides is essential and is discussed in the next section.

Preparation of Anhydrous Actinide Tetrafluorides[19,20]

Protactinium Tetrafluoride

Purification of Pa(V) oxides. The protactinium-231 was present in a 15M HF stock solution composed of old discarded waste material from

which the Pa had to be recovered. Early purification techniques for Pa involved tedious fractional crystallization[21,22] or anion exchange column separations.[23-26] At about the time when this work was beginning, Brown and Whittaker[27] reported a new, simple procedure for separating Pa-231 from a wide variety of elements including its radioactive daughters.

Their method is based on the insolubility of Pa (V) hydrous oxide in various aqueous acidic and basic media (except when F^- is present) in which the impurities are soluble and easily separated from the Pa oxide precipitate. A slightly modified version of the process is given as a flow diagram in Fig. 1.

Since aqueous HF plays an important role in the beginning of the purification procedure, Nalgene centrifuge cones, presoaked in conc. HCl and washed with distilled water, were used throughout. Reagent grade NH_4OH, NaOH, HNO_3, and H_2O_2 from Mallinckrodt, Inc. were used without further purification.

Protactinium hydrous oxides were precipitated from the HF solution by careful addition of excess NH_4OH. The resulting precipitate was washed with 5M NaOH and water to effect decontamination from some impurities and to completely remove fluoride before the later acid washes. It is important that the precipitate age overnight during these steps in order to minimize dissolution of the oxide in the acid washes which follow.

The .5M HNO_3 - 3% H_2O_2 solution, made by substituting 3% H_2O_2 for distilled water in the dilution of conc. HNO_3, greatly improves the decontamination from Fe, Cr, Mn, Mo, Ti, V, Pt, and Zn.[27] Removal of Sb is accomplished by adding 12M HCl and evaporating the solution to dryness,

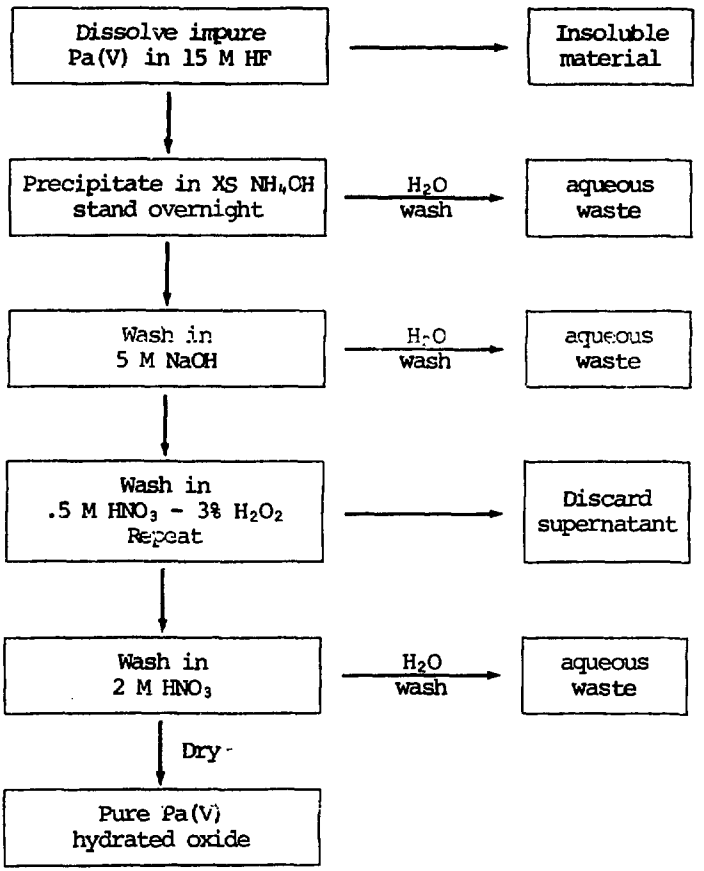

Figure 1.

Pa-231 Purification Process

driving off the volatile $SbCl_3$. Although some Si is removed in the NaOH washings, the remainder is effectively eliminated from the product by dissolving the dried Pa oxide in 20M HF and evaporating. This step is not necessary in this case since later it is driven off as SiF_4 during hydrofluorination.

After washing the solid oxide with water, it was dried in the Nalgene cone by placing it in a beaker of water on a hot plate. Tapping the inverted cone causes the entire lump to fall out with very little loss of material.

A small amount of the Pa oxide was dissolved in 20M HF and a known quantity (~ 25 λ) was transferred to a Pt counting planchet and flamed dry in an induction heater. Results from an α pulse-height analysis showed that 98% of the α activity was due to Pa-231, 1.25% to Th-227 (the short-lived α-decay daughter), and .7% due to other isotopes (e.g. Ra-223).

From the calculated concentration of Pa in the above 20M HF solution, an amount containing 50 μg of Pa was evaporated on a Cu electrode for spectrochemical analysis. The only significant impurities found within the detection limits[28] were Mg and Ca (~ .02 wt. % ea.).

Preparation of PaF_4. PaF_4 was prepared according to Stein[29] by treating the pentoxide with anhydrous HF and excess H_2 at 500°:

$$Pa_2O_5 + 8\ HF \xrightarrow[500^\circ]{H_2} 2PaF_4 + 5H_2O \qquad (3)$$

The dried Pa_2O_5 was placed into a Pt boat and inserted into a nickel

furnace. The hydrogen gas served both as a reductant and as a carrier gas by which the pre-purified HF was circulated through the furnace and finally into an Al_2O_3 absorption tower. The flow rate of HF from its transparent Kel-F container was monitored visually while the flow of H_2 was observed with an oil bubbler.

After a 3-hour reaction time, the furnace and the flow of HF were turned off but the H_2 flow continued overnight to flush out all traces of H_2O and HF. The brown solid was identified to be PaF_4 by its Xray powder pattern. Approximately 110 mg of the anhydrous tetrafluoride was obtained.

Neptunium Tetrafluoride

The dioxide, $^{237}NpO_2$, was available in gram quantities and was of high purity. The tetrafluoride was initially prepared by a hydrofluorination reaction[19,20,30] similar to Eq. (3):

$$NpO_2 + 4\ HF \xrightarrow[500^\circ]{Ar\ or\ O_2} NpF_4 + 2H_2O \qquad (4)$$

This gives NpF_4 suitable for the borohydride synthesis but later it was discovered that its preparation from aqueous solution was much easier and gave very reactive NpF_4. The ultimate success of this method is due to the rather unique property of NpF_4 as compared with the other actinide compounds in that it can be made anhydrous by simply heating the solid under vacuum. The tetrafluorides of Th,[20] Pa,[24] and Pu[31] decompose and must be dried under the conditions of Eq. (3) or (4).

Approximately 400 mg NpO_2 was put in 30 ml of hot 10M HNO_3 to which 3 drops of 5M HF had been added to aid dissolution of the oxide. When the solution appeared saturated, the liquid was decanted into a 50 ml Nalgene centrifuge cone. Five ml of 48% aqueous HF was added and NpF_4 immediately precipitated. After centrifugation, the liquid was discarded and the process was repeated until all NpO_2 was converted into NpF_4. Initial drying was done similarly to that for Pa_2O_5 discussed in the previous section. Although the NpF_4 was amorphous, it was identified by its characteristic green color.

Plutonium Tetrafluoride

The long-lived isotope of plutonium, Pu-242, was obtained as the dioxide. PuF_4 prepared from aqueous solution is a hydrate of the formula $2PuF_4 \cdot 5H_2O$ which when dehydrated at 300° under vacuum gives PuF_3 and PuO_2.[31] Therefore the anhydrous tetrafluoride must be prepared by reaction (5) where O_2 is necessary to prevent the formation of PuF_3.

$$PuO_2 + 4\ HF \xrightarrow[400\ -\ 500^\circ]{O_2} PuF_4 + 2H_2O \qquad (5)$$

Approximately 300 mg of PuF_4 was obtained using the same apparatus that was used in making PaF_4.

Preparation of the Actinide Tetrakis-borohydrides[18]

Two basic designs shown in Fig. 2 were employed in the construction of reaction vessels—one for Th and Pa borohydrides (A) and the other for U, Np, and Pu borohydrides (B). Each type comes apart at the 15 mm

Actinide Borohydride Reaction Vessels

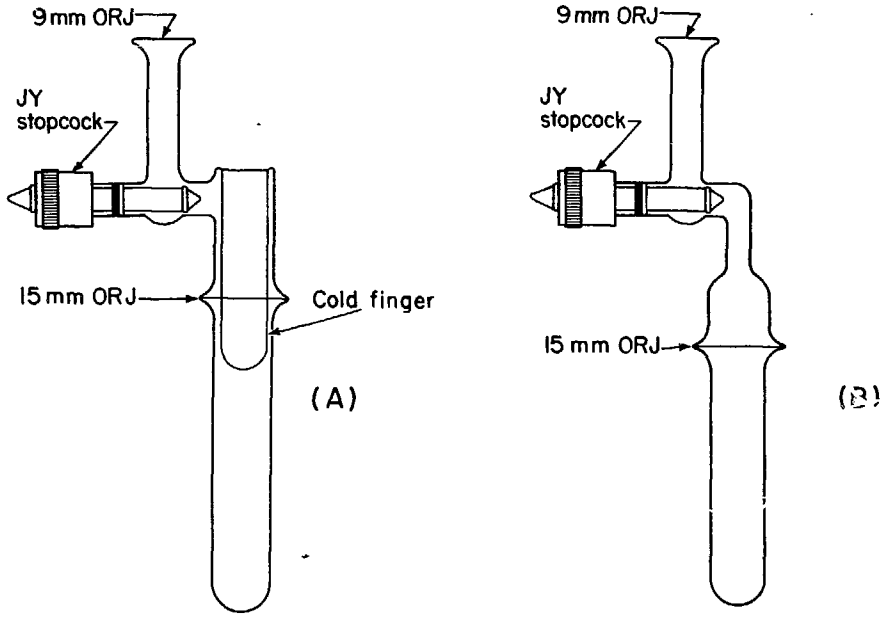

Figure 2.

XBL7911-13256

O-ring joint (ORJ) for the addition of a stir bar and the tetrafluoride, removal of the borohydride product (A), and for cleaning. The $Al(BH_4)_3$ comes in contact only with glass, Teflon, and Viton.

Protactinium Borohydride

The tetrafluoride and a small Teflon stir bar were added to the lower section of vessel (A). It was evacuated and a stoichiometric amount of $Al(BH_4)_3$ was condensed in and the stopcock closed. After warming to room temperature, some bubbling occurred which later subsided. Periodically the solid-liquid mixture was stirred.

In a few days, the initially clear liquid $Al(BH_4)_3$ turned light yellow in color as the concentration of dissolved $Pa(BH_4)_4$ increased. After about 5 days the unreacted $Al(BH_4)_3$ was collected in a liquid nitrogen trap and the orange $Pa(BH_4)_4$ was sublimed at 55° onto the -78° cold finger. Yields were very low, less than 10%. Identification of the orange product was made by its infrared spectrum and its Xray powder pattern (see chapter 2).

Neptunium and Plutonium Borohydrides

The two actinide borohydrides exhibit nearly identical physical properties, as do the analogous Zr and Hf compounds and the syntheses of $Np(BH_4)_4$ and $Pu(BH_4)_4$ are also very similar. Since neither compound is thermally stable at room temperature, the reactions were carried out below 25°. The desired tetrafluoride and a Teflon stir bar were put into the bottom of reaction vessel (B) which was then assembled and evacuated. PuF_4 was made sufficiently anhydrous during its formation but

NpF_4 needed further dehydration by heating the reaction vessel containing it to 80° while evacuating for several hours. Then the stoichiometric or a small excess of $Al(BH_4)_3$ was condensed in.

After a 4-hour reaction period at 0°, the $An(BH_4)_4$ was collected in a dry-ice trap while the unreacted $Al(BH_4)_3$ passed through and into a liquid-nitrogen trap. Returning the $Al(BH_4)_3$ to the tetrafluoride again produced more $An(BH_4)_4$ but not nearly as much as was obtained in the first period. In the case of Pu, this usually does not work since large amounts of trivalent Pu have already formed after four hours and it is best to start over with fresh PuF_4.

The unreacted $Al(BH_4)_3$ recovered from these syntheses is easily separated from the accompanying B_2H_6 by passing the mixture vapors through a trap immersed in an n-pentane slush (- 130°). The unreacted actinide fluoride mixture remaining in the reaction vessel is revitalized by *carefully* neutralizing it with methanol. After exposing it to the air, the vessel is dismantled. Final washing with water and dilute HCl and drying prepares the fluoride residue for the usual hydrofluorination reaction appropriate to the particular actinide.

Preparation of Actinide Borodeuterides

All glassware which comes in contact with the borodeuterides should be passivated with B_2D_6 or $Al(BD_4)_3$ or treated with D_2O and then baked out thoroughly under vacuum. This step is especially important for optical cells. Those cells which use alkali halide windows should only be treated with B_2D_6.

The borodeuterides of Th, Pa, and U are prepared in the same manner as the borohydrides except that $Al(BD_4)_3$ is used. The resulting isotopic impurity is approximately 2% if the $Al(BD_4)_3$ is made from commercial grade $LiBD_4$. Higher purity products can be obtained by further deuterium enrichment of the $Al(BD_4)_3$ as explained below in the syntheses of Np and Pu borodeuterides.

$Np(BD_4)_4$ and $Pu(BD_4)_4$ can also be prepared using $Al(BD_4)_3$ but an easier and more effective method was employed which takes advantage of the high volatilities of the covalent borohydrides. Intermolecular exchange reactions have been observed between the volatile metal borohydrides and B_2D_6[33-35] and D_2,[34] in which a hydrogen-deuterium interchange occurs. If the B_2D_6 or D_2 is maintained in large excess over the metal borohydride, all hydrogen is eventually replaced by deuterium. D_2 was used in this work as it was readily obtainable and easily handled in a vacuum line.

Sufficient $Np(BH_4)_4$ was condensed into a 500 ml glass bulb such that all of it would be in the gas phase at room temperature (~ .25 mmol). Approximately 1 atm of dry, O_2-free D_2 was admitted into the bulb which was then closed off from the rest of the vacuum line. After letting the two gases stand at room temperature for 2 days, the bulb was cooled to -78°[36] and the volatile compounds were pumped out. Another volume of D_2 was added and the exchange reaction continued for another 2-day period. Three such cycles[37] were found sufficient for complete conversion to $Np(BD_4)_4$ with an isotopic purity as high as the deuterium used (99.7%).

An attempt was made to prepare $Np(BT_4)_4$ by the above method. Five mg of $Np(BH_4)_4$ and 600 mm Hg T_2 were added to a 35 ml passivated glass vessel. After 2 days, all the $Np(BH_4)_4$ was decomposed to the usual yellow solid by the intense β^- emission (56 Ci) of the tritium gas and no volatile Np compound was recovered.

This method is generally applicable to all volatile metal borohydrides including $Be(BH_4)_2$, $Al(BH_4)_3$, $Zr(BH_4)_4$, and $Hf(BH_4)_4$ where the number and durations of cycles depend on the particular borohydride. Exchange rates and decomposition rates are higher for the more unstable molecules and procedures must be modified accordingly.[38] The unstable $Pu(BH_4)_4$, for example, requires less time than the more stable $Zr(BH_4)_4$.

The reason for the variance in H $\leftrightarrow$ D exchange rates can be explained by a mechanism shown below,[33,34] where the metal borohydride-dependent, rate-determining step is that in which a $BH_3\cdot$ fragment breaks away from the metal borohydride molecule in Eq. (6).

$$M(BH_4)_x \underset{k_2}{\overset{k_1}{\rightleftharpoons}} MH(BH_4)_{x-1} + BH_3\cdot \tag{6}$$

$$BH_3\cdot + D_2 \xrightarrow[k_4]{k_3} BH_2D\cdot + HD \text{ etc.} \tag{7}$$

$$BH_yD_{3-y} + MH(BH_4)_{x-1} \xrightarrow{k_5} M(BH_4)_{x-1}(BH_{y+1}D_{3-y}) \tag{8}$$

The ratio k_1/k_2 would depend on the stability of the borohydride; for $Zr(BH_4)_4$, $k_1/k_2 \ll 1$, while for $Pu(BH_4)_4$ the ratio would be closer

to unity. In Eq. (7) $k_3 = k_4$ and the exchange reaction takes place rapidly since the borane radical is very reactive. From symmetry considerations, $k_1 = xk_5$, where Eq. (8) is basically Eq. (6) in the k_2 direction. It can be seen that with enough D_2 in the system, $y = 0$ in Eq. (8) and the fluxional behavior of the H atoms[7,39] insures the eventual complete replacement of H by D.

Experimental evidence in support of Eq. (6) are the observations of $^{11}B \leftrightarrow {}^{10}B$ exchanges between $M(^{11}BH_4)_x$ and $^{10}B_2H_6$,[33,35,40] and the presence of B_2H_6 in partially decomposed samples of $M(BH_4)_x$ compounds.[11,18]

By perhaps a somewhat different mechanism, alkyl substitution reactions have been reported in which the terminal hydrogen atoms of the tridentate BH_4^- group was replaced by CH_3[12,41] and C_2H_5[14(d)] in $U(BH_4)_4$ and $ThCOT(BH_4)_2$ in THF, respectively. For $U(BH_4)_4$, Eq. (6) would remain as such ($x = 4$, $M = U$) but Eq. (7) would become

$$BH_3 + B(CH_3)_3 \underset{k_4'}{\overset{k_3'}{\rightleftharpoons}} BH_2CH_3 + BH(BH_3)_2 \qquad (9)$$

from which only BH_2CH_3 could react with the metal compound as in Eq. (10).

$$BH_2CH_3 + UH(BH_4)_3 \xrightarrow{k_5'} U(BH_4)_3(BH_3CH_3) \qquad (10)$$

With large excesses of $B(CH_3)_3$, the tetramethyl compound, $U(BH_3CH_3)_4$, is obtained and can be separated from the monomethyl derivative by fractional sublimation.[41]

Alkyl exchange reactions of the type given above, involving $Np(BH_4)_4$ and $B(CH_3)_3$ in the gas phase also showed that methyl groups replace terminal hydrogen atoms in $Np(BH_4)_4$. Several green compounds differing in volatility were isolated and the presence of CH_3 in them was confirmed by their infrared spectra. The compounds were not further characterized.

Thermal Stability of Np, Pu Borohydrides

All metal borohydrides evolve H_2 and B_2H_6 during thermal decomposition.[4,11,18] This can be seen in Eq. (6) which can be rewritten as

$$M(BH_4)_x \rightarrow MH(BH_4)_{x-1} + \tfrac{1}{2}B_2H_6 \qquad (11)$$

where two borane radicals have combined to give diborane. The additional presence of an equimolar amount of H_2 is explained if the metal ion is reduced, forming a lower borohydride, i.e.

$$M(BH_4)_x \rightarrow M(BH_4)_{x-1} + \tfrac{1}{2}H_2 + \tfrac{1}{2}B_2H_6 \qquad (12)$$

Schlesinger and Brown[11] characterized the reddish-brown $U(BH_4)_3$ obtained by heating $U(BH_4)_4$ to 100°. Based on the quantities of H_2 and B_2H_6 evolved, the color, and the fact that the solid generated 12 mols of H by hydrolysis per mol of $U(BH_4)_4$ decomposed in its formation, they suggested that Eq. (13) occurred.

$$U(BH_4)_4 \xrightarrow{100^\circ} U(BH_4)_3 + \tfrac{1}{2}H_2 + \tfrac{1}{2}B_2H_6 \qquad (13)$$

The gas and liquid phase decompositions of $Np(BH_4)_4$ at 25° were followed by IR spectroscopy and by visual means of the liquid in a glass capillary. It was found that its stability in the gas phase is roughly 50 times higher than in the liquid. This phenomenon indicates that an intermolecular process, in addition to the inherent thermodynamic instability of the compound, is important in determining the overall stability of $Np(BH_4)_4$. Similar effects were seen in $Pu(BH_4)_4$ but not in $Zr(BH_4)_4$ or $Hf(BH_4)_4$. The $H \leftrightarrow T$ exchange experiment and observations of $Pa(BH_4)_4$ suggest that radiation damage[42] is important in these borohydrides. This effect, which would cause greater decomposition rates in the condensed phases of Np and Pu borohydrides, would be nonexistent in the Zr and Hf compounds.

Since $Np(BH_4)_4$ and $Pu(BH_4)_4$ also liberate H_2 and B_2H_6 on decomposition and that Np^{3+} and Pu^{3+} are well-known,[19,20] the tris-borohydrides are assumed to be formed analogously to $U(BH_4)_4$. However, Xray powder diffraction photographs show that the solids of decomposition for U and Np borohydrides are not isomorphous.

The trend of thermal stabilities: $U(BH_4)_4 > Np(BH_4)_4 > Pu(BH_4)_4$ follows from the general stabilities of the tetravalent oxidation states: $U^{4+} > Np^{4+} > Pu^{4+}$.[20,32,43] Similar conclusions were drawn for Ti borohydride [4,8] whose +4 oxidation state is so unstable that all routes to Ti (IV) borohydride lead to $Ti(BH_4)_3$. The other members of Group IVB with stable +4 oxidation states, Zr, Hf, and Th, give very stable tetrakis-borohydrides.

At very high temperatures (> 300°), metallic, amorphous, mirrors are formed which may be Np, Pu, NpB_4, or PuB_4.[4,11]

Preparation of Actinide (IV) TMCOT Complexes from $An(BH_4)_4$[44]

The high solubility of the Np and Pu borohydrides in various types of organic solvents such as pentane, THF, and benzene make these actinide compounds useful in the preparation of organoactinide complexes. For the tetravalent actinides, usually the tetrachloride is used with THF as the solvent. Although the early actinide tetrachlorides are reasonably soluble in THF, $NpCl_4$ is not very soluble and that of Pu is unknown in the solid state so the slightly soluble $(NEt_4)_2PuCl_6$ is substituted.

The syntheses of some organoactinide compounds, the bis(η^8-tetramethylcyclooctatetraene) complexes, $Np(TMCOT)_2$ and $Pu(TMCOT)_2$, prepared by the reaction of the tetrakis-borohydrides and the TMCOT dianion in THF were investigated.[45,46] The reaction can be written as

$$An(BH_4)_4 + 2K_2TMCOT \xrightarrow{THF} An(TMCOT)_2 + 4KBH_4 \qquad (14)$$

The actinide TMCOT compounds were identified by their visible spectra[47(b)] and Xray powder patterns.[45] The formation of KBH_4 was confirmed by an Xray powder pattern of the insoluble reaction product. The above method was found particularly attractive for Pu since analogous reactions of K_2TMCOT with complex Pu (IV) halides were reported to give reduction to Pu (III).[47(a)]

Although the polymeric actinide borohydrides were not tried in this synthesis, it is presumed that they would also give the desired product since the borohydrides are very soluble in THF. Very low yields of

$Pa(TMCOT)_2$ were obtained from $PaCl_4$,[45] possibly due to the relative ease of oxidation of Pa (IV) to Pa (V). Perhaps the same kinds of effects which seem to inhibit the reduction of Pu (IV) in Eq. (14) will also stabilize the Pa^{4+} ion and give higher yields.

Attempted Synthesis of $Ce(BH_4)_4$

When the synthesis of the tetrakis-borohydrides of the Group IVB elements were reported for Zr, Hf, and Th and the tris-borohydride of Ti, no mention was made of the cerium compound.[4] Even if the tetravalent oxidation state of Ce were not sufficiently stable for it to form the tetrakis compound the tris-borohydride should have resulted as in the case of Ti. Although Ce^{4+} is significantly less stable to reduction than Pu^{4+},[32] stable organometallic borohydride derivatives of Ce (IV), $(C_5H_5)_3CeBH_4$ and $(C_9H_7)_2Ce(BH_4)_2$, have been prepared.[48]

Since a solid-state structure transformation takes place between Hf and Th borohydride (ionic radii[49] are Hf^{4+} = .83 Å, Th^{4+} = 1.06 Å), the molecular structure of $Ce(BH_4)_4$ (Ce^{4+} = .97 Å) would be interesting. If its solid-state structure were of high symmetry, it could be useful as a host matrix for optical studies of actinide borohydrides (see chapter 5). Therefore an attempt to prepare $Ce(BH_4)_4$ was made.

The nonexistence of $CeCl_4$ ruled out Eq. (1) as a route to $Ce(BH_4)_4$. Since Eq. (2) works well for the actinides and CeF_4 exists as a stable compound, this method was tried first. All commercially obtained CeF_4 was identified to be CeF_3 by Xray diffraction and so the tetrafluoride had to be made. The aqueous solution method of preparing CeF_4 gives a hydrate which decomposes upon dehydration[50] and is not satisfactory.

Two syntheses of CeF_4 were tried by the reactions given below.

$$CeCl_3 + 2F_2 \xrightarrow{25^\circ} CeF_4 + \tfrac{3}{2}Cl_2 \qquad (15)$$

$$CeF_3 + \tfrac{1}{2}F_2 \xrightarrow{250^\circ} CeF_4 \qquad (16)$$

Eq. (15)[51] proved to be a problem because the stated 25° reaction temperature is erroneous as $CeCl_3$ ignites in fluorine and severe boat contamination results. The charred mass also contained some CeF_3 as well. Eq. (16)[52,53] was then considered.

CeF_3 was prepared in aqueous solution by the method of Cunningham et al.[52] and was dried at 80° overnight. Reaction at 250° for 6 hours with 2 atm F_2 gave pure CeF_4.

The CeF_4 was added to reactor (B) (Fig. 2) in a drybox and $Al(BH_4)_3$ was condensed in after evacuation. After 4 days at 25°, the CeF_4 turned grey and no cerium borohydride was obtained even after attempted sublimation at 110°. An Xray powder pattern showed that the solid was still CeF_4. Similar negative results were observed for ZrF_4 and HfF_4[4] which did not react with $Al(BH_4)_3$ although their double salts, e.g. Na_2ZrF_6, did.

The double salt of Ce (IV), Na_2CeF_6, was prepared by the reaction between NaCl and CeO_2 in excess F_2 at 500°:[54]

$$2NaCl + CeO_2 \xrightarrow[500^\circ]{F_2} Na_2CeF_6 + \text{mixed O, Cl, F products} \qquad (17)$$

and being isostructural to β_2 - K_2UF_6,[54] was identified by its Xray powder pattern.

No reaction occurred between Na_2CeF_6 and $Al(BH_4)_3$ at 25° and the Na_2CeF_6 and nearly all $Al(BH_4)_3$ were recovered. Perhaps double salts of other alkali metals, M_xCeF_{4+x}, x = 1, 2, 3 may be reactive. Although many other reactions exist which could prove fruitful,[7,8] the synthesis of $Ce(BH_4)_4$ was not further investigated.

References and Notes

[1]Schlesinger, H. I.; Sanderson, R. T.; Burg, A. B. J. Am. Chem. Soc. 62 3421 (1940).

[2]Burg, A. B.; Schlesinger, H. I. J. Am. Chem. Soc. 62 3425 (1940).

[3]Schlesinger, H. I.; Brown, H. C.; Hyde, E. K. J. Am. Chem. Soc. 75 209 (1953).

[4]Hoekstra, H. R.; Katz, J. J. J. Am. Chem. Soc. 71 2488 (1949).

[5]Reid, Jr., W. E.; Bish, J. M.; Brenner, A. J. Electrochem. Soc. 104 21 (1957).

[6]James, B. D.; Nanda, R. K.; Wallbridge, M. G. H. J. Chem. Soc. (A) 182 (1966).

[7]James, B. D.; Wallbridge, M. G. H. Prog. Inorg. Chem. 11 99 (1970).

[8]Marks, T. J.; Kolb, J. R. Chem. Rev. 77 263 (1977).

[9]Zange, E. Chem. Ber. 93 652 (1960).

[10]Eheman, Von M.; Noth, H. Z. Anorg. Allg. Chem. 386 87 (1971).

[11]Schlesinger, H. I.; Brown, H. C. J. Am. Chem. Soc. 75 219 (1953).

[12(a)]Katz, J. J.; Rabinowitch, E. "The Chemistry of Uranium," McGraw-Hill Book Co., Inc. New York, N.Y. 1951. p. 550-557.

[(b)]Volkov, V.; Myakishev, K. G. (USSR) Radiokhimya 18 512 (1976).

[13(a)]Rietz, R. R.; Zalkin, A.; Templeton, D. H.; Edelstein, N. M.; Templeton, L. K. Inorg. Chem. 17 653 (1978).

[(b)]Rietz, R. R.; Edelstein, N. M.; Ruben, H. W.; Templeton, D. H.; Zalkin, A. Inorg. Chem. 17 658 (1978).

[(c)]Zalkin, A.; Rietz, R. R.; Templeton, D. H.; Edelstein, N. M. Inorg. Chem. 17 661 (1978).

[14(a)]Marks, T. J.; Kennelly, W. J.; Kolb, J. R.; Shimp, L. A. Inorg. Chem. 11 2540 (1972).

[(b)]Marks, T. J.; Seyam, A. M.; Wachter, W. A. Inorg. Syn. 16 147 (1976).

[14(c)] Levanda, C.; Solar, J. P.; Streitwieser, Jr., A. J. Am. Chem. Soc., submitted (1979).

[(d)] Solar, J. P.; Streitwieser, Jr., A.; Edelstein, N. M. In "Lanthanides and Actinides, ACS Symposium Series," Edelstein, N. M. Ed.; American Chemical Society: Washington, D.C. 1980; in press.

[15] Bernstein, E. R.; Hamilton, W. C.; Keiderling, T. A.; La Placa, S. J.; Lippard, S. J.; Mayerle, J. J. Inorg. Chem. 11 3009 (1972).

[16] Turner, H. S.; Andersen, R. A.; Zalkin, A.; Templeton, D. H. Inorg. Chem. 18 1221 (1979).

[17(a)] Bernstein, E. R.; Keiderling, T. A. J. Chem. Phys. 59 2105 (1973).

[(b)] Paine, R. T.; Light, R. W.; Nelson, M. Spectrochim. Acta 35A 213 (1979).

[(c)] Ghiassee, N.; Clay, P. G.; Walton, G. N. Inorg. Nucl. Chem. Lett. 14 117 (1978).

[(d)] Volkov, V. V.; Myakishev, K. G.; Grankina, Z. A. Russ. J. Inorg. Chem. 15 1490 (1970).

[18] Banks, R. H. Edelstein, N. M.; Rietz, R. R.; Templeton, D. H.; Zalkin, A. J. Am. Chem. Soc. 100 1958 (1978).

[19] Brown, D. "Halides of the Lanthanides and Actinides," John Wiley & Sons, Ltd. Great Britain, 1968.

[20] Seaborg, G. T.; Katz, J. J. "The Actinide Elements," McGraw-Hill Book Co., Inc. New York, N.Y., 1954.

[21] Brown, D.; Maddock, A. G. Quart. Rev. 17 289 (1963).

[22] Cunningham, B. B. "Physico-Chimie du Protactinium," Centre National de la Recherche Scientifique. Paris, 1966, p. 45.

[23] Chetham-Strode, A.; Keller, O. L. ibid., p. 189.

[24] Stein, L. ibid., p. 101.

[25] Jenkins, I. L.; Scargill, E.; Wein, A. G. J. Inorg. Nucl. Chem. 37 257 (1975).

[26] Dod, R. L. Ph.D. Thesis. University of California, 1972.

[27] Brown, D.; Whittaker, B. U.K.A.E.A. Harwell Rept. AERE-R 8315, 1976.

[28]For a table of detection limits for this analysis, see Ref. 26, Table 3, p. 9.

[29]Stein, L. Inorg. Chem. 3 995 (1964).

[30]Fried, S.; Davidson, N. J. Am. Chem. Soc. 70 3539 (1948).

[31]Dawson, J. K.; Elliott, R. M.; Hurst, R.; Truswell, A. E. J. Chem. Soc. 558 (1954).

[32]Nugent, L. J.; Baybarz, R. D.; Burnett, J. L.; Ryan, J. L. J. Phys. Chem. 77 1528 (1973).

[33]Maybury, P. C.; Larrabee, J. C. Inorg. Chem. 2 885 (1963).

[34]Maybury, P. C.; Larrabee, J. C. Abstracts of Papers. 135th National Meeting, American Chemical Society. 1959, p. 28M.

[35]Davies, N.; Saunders, D.; Wallbridge, M. G. H. J. Chem. Soc. (A) 2915 (1970).

[36]The reaction bulb must be evacuated at -78° and not at lower temperatures in order that ^1H impurities in the form of diboranes will be removed between cycles.

[37]Longer or more cycles do not, in fact, increase the deuterium content of the product but only lower the final yield.

[38]Unpublished results in our laboratory. 1978.

[39]Marks, T. J.; Shimp, L. A. J. Am. Chem. Soc. 94 1542 (1972).

[40]Marks, T. J.; Kolb, J. R. J. Am. Chem. Soc. 97 27 (1972).

[41]Schlesinger, H. I.; Brown, H. G.; Horvitz, L.; Bond, A. C.; Tuck, L. D.; Walker, A. C. J. Am. Chem. Soc. 75 222 (1953).

[42]For discussions on radiation damage in chemical compounds, see

(a)McDonald, R. E. Gov't. Rep. Announce. 74 210 (1974).

(b)Asmus, K. D. Adv. Study Inst. Ser., Ser. E 8 435 (1975).

[43]Seaborg, G. T. "Encyclopedia of Chemical Technology." Vol. 1, 3rd Ed. John Wiley. New York, N.Y., 1978.

[44]A collaborative effort of J. P. Solar, H. P. G. Burghard, R. H. Banks, A. Streitwieser, Jr., and D. Brown.

[45]Solar, J. P.; Burhard, H. P. G.; Banks, R. H.; Streitwieser, Jr., A.; Brown, D. Inorg. Chem., submitted, 1979.

[46]For a review of actinide COT compounds, see

(a)Baker, E. C.; Halstead, G. W.; Raymond, K. N. Structure and Bonding 25 23 (1976).

(b)Streitwieser, Jr., A. "Topics in Nonbenzenoid Aromatic Chemistry," Vol. 1, 221 (1973).

(c)Streitwieser, Jr., A. "Organometallic Compounds of the f-Elements," Marks, T. J.; Fisher, R. D. Eds., Reidel Publishing Co. Amsterdam, 1979.

[47](a)Streitwieser, Jr., A.; Dempf, D.; La Mar, G. N.; Karraker, D. G.; Edelstein, N. M. J. Am. Chem. Soc. 93 7343 (1971).

(b)Karraker, D. G. Inorg. Chem. 12 1105 (1973).

[48]Kapur, S.; Kalostra, B. L.; Multani, R. K.; Jain, B. D. J. Inorg. Nucl. Chem. 35 1689 (1973).

[49]Shannon, R. D.; Prewitt, C. T. Acta Cryst. B25 925 (1969).

[50]Asher, W. J.; Wylie, A. W. Aust. J. Chem. 18 959 (1965).

[51]Klemm, Von W.; Henkel, P. Z. Anorg. Chem. 220 180 (1934).

[52]Cunningham, B. B.; Feay, D. C.; Rollier, M. A. J. Am. Chem. Soc. 76 3361 (1954).

[53]Wartenberg, H. Z. Anorg. Chem. 244 339 (1940).

[54]Hoppe, R.; Rödder, K. M. Z. Anorg. Chem. 313 154 (1961).

Chapter 2

PHYSICAL PROPERTIES AND MOLECULAR STRUCTURES OF THE ACTINIDE BOROHYDRIDES

Introduction

All five actinide (IV) borohydrides have the same molecular geometry in the gas phase and are monomeric.[1-4] In the solid state however, they crystallize into two different structure types, polymeric and monomeric, each of which exhibits unique chemical and physical properties.[5] Some of these properties were discussed in chapter 1. Xray powder diffraction patterns have shown that Th, Pa, and U borohydrides are isostructural, a result also verified by their solid state infrared spectra. Lattice parameters, 2θ values, and densities for all these compounds were obtained from their powder patterns and are given in Tables 1-4. The molecular structures of the first three actinide borohydrides are polymeric and that of $U(BH_4)_4$, determined by single crystal Xray[6] and neutron[7] diffractions methods by Bernstein et al., is discussed later in this chapter.

Neptunium and plutonium borohydrides are monomeric and low-temperature Xray powder patterns have shown that they are isomorphous and are of a different structure type than that displayed by the three earlier actinide compounds. The structure of $Np(BH_4)_4$ was determined by single crystal Xray diffraction at 130K[5] and found to be very similar to that of the monomeric Zr and Hf borohydrides although the crystal structures

are slightly different. Both molecular structures are described in this chapter and are contrasted to that of the polymeric compounds.

The volatilities and some calculated thermodynamic quantities of the seven metal tetrakis-borohydrides are given and qualitatively compared on the basis of their solid state structures.

Experimental

Infrared Spectra

Solid-state infrared spectra of Th, Pa, and U borohydrides were taken from 4000-400 cm^{-1} on a Perkin-Elmer 283 infrared spectrophotometer at room temperature. The samples were prepared as a suspension of the powder in predried Nujol between two KBr disks. A gas phase spectrum of $U(BH_4)_4$ at 50° was recorded by heating the compound in a 10 cm KBr gas cell placed in the sample beam. Similar spectra of $Pa(BH_4)_4$ could not be obtained even while heating to 100° due to the low vapor pressure of the borohydride. Gas phase infrared spectra of $Np(BH_4)_4$ and $Pu(BH_4)_4$ were taken at 18°[1] and solid state infrared and Raman spectra were obtained for $Np(BH_4)_4$ at 77K (see chapter 3).

Xray Powder Diffraction

Xray powder samples of freshly sublimed Th, Pa, and U borohydrides were prepared in an argon atmosphere drybox by adding 1 cm of the powdered compound into a predried 0.3 mm diameter quartz capillary. The diffraction photographs were taken with a 114.6 mm Debye-Scherrer powder camera using Cu Kα radiation (λ = 1.5418 Å). The exposures were made on Ilford Industrial G Xray film from which the diffraction lines were measured

to an accuracy of ± .05 mm with a Phillips-Norelco film reader. The indexed lines were fitted by a least squares routine to calculated lines using unit cell parameters by the lattice constant refinement program, LCR-2, with the Nelson-Riley correction.[8]

The Xray samples of $Np(BH_4)_4$ and $Pu(BH_4)_4$ were prepared by condensing the compounds into quartz capillaries and sealing them off to a length of approximately 1½ cm. A 114.6 mm Debye-Scherrer camera was modified for low temperature use. A stryofoam block which had a hole drilled through its center to fit around the capillary, was inserted into the camera. Cold nitrogen gas entered the camera through a hole in the camera cover, flowed through the stryofoam block, bathed the sample, and exited via another hole in the cover, thereby traversing a U-shaped path. This method permitted the film to remain at room temperature during the exposure. Although the sample of $Pu(BH_4)_4$ was cooled to -20°, a faster cooling rate and lower temperature of -150° was used for $Np(BH_4)_4$ since it tended to freeze amorphously in these experiments.

Single Crystal Xray Diffraction

A sample of the dark green liquid $Np(BH_4)_4$ was sealed into a 0.3 mm ID quartz capillary and stored in liquid nitrogen prior to use. The capillary was mounted on a Picker FACS-I automated diffractometer equipped with a Syntex LT-1 temperature controller. Slow cooling through the melting point resulted in substantial supercooling followed by rapid freezing giving polycrystalline samples. Partial melting of the solid followed by slow refreezing provided a crystal suitable for structure determination.

During unit cell measurements and intensity data collection, the sample was maintained at 130 ± 5K, as determined from prior calibration with a thermocouple in place of the capillary.

Unit cell parameters were obtained from carefully centered settings on the $K\alpha_1$ peaks of the (14,0,0), (0,14,0), and (0,0,10) reflections using graphite-monochromated Mo radiation ($\lambda(K\alpha_1)$ = 0.70930 Å). Cell dimensions obtained before and after intensity data collection did not differ significantly and yielded the values a = 8.559(9) Å and c = 6.017(9) Å for the tetragonal unit cell. The full width at half height for ω-scans of low-angle reflections before and after intensity data collection was typically 0.15°.

Intensity data were collected using the θ-2θ scan technique to 68° in 2θ for positive h, k, and ℓ with scans from 0.9° below $K\alpha_1$ to 0.9° above $K\alpha_2$ and with background counts of four seconds at each end of the scan. Two standards, measured every 100 reflections, showed a decrease in intensity of 17% during the course of data collection and the measured intensities of the 1000 reflections were corrected accordingly. Crystal faces were not clearly visible through the capillary so an absorption correction was not attempted (μ is 40 cm^{-1} and r is approximately 1×10^{-2} cm). The intensities were corrected for Lorentz and polarization effects. When the double data set was merged, the estimated standard deviation of the intensity of a reflection based on counting statistics was replaced by the scatter in measured intensities for 137 reflections (out of a total of 511 unique reflections) for which the scatter exceed four times the estimated standard deviations. The diffraction

symmetry and systematically absent reflections were consistent with the space group $P4_2/nmc$.

With $Z = 2$, the Np atom must occupy a special position with $\bar{4}2$ m symmetry as noted from the earlier Xray powder data[1] which showed a body-centered pattern and intensities consistent with Np at the origin. The single crystal experiment detected the weak non-body-centered reflections. The boron atom was initially placed 2.5 Å from the neptunium in an eightfold position on a mirror plane by analogy with the tetrahedral $Hf(BH_4)_4$ structure.[9] After several cycles of least-squares refinement with anisotropic thermal parameters for Np and an isotropic thermal parameter for B, inspection of the agreement between observed and calculated structure factors for the strongest reflections suggested that an extinction correction was appropriate. An empirical correction was applied where $F_{corr} = F_{obs}(1 + 2.4 \times 10^{-7} I)$; F_{corr} and F_{obs} are the corrected and observed structure factors and I is the observed intensity. Several additional cycles of least-squares refinement with anisotropic thermal parameters for both Np and B then converged with $R = \Sigma||F_o| - |F_c||/\Sigma|F_o| = 0.115$ for nine parameters and 352 data with $F^2 > \sigma(F^2)$.

A difference-Fourier map was calculated to see whether the hydrogen atoms could be located. Peaks with an electron density of approximately one electron per A^3 were found in positions expected for three bridging hydrogens and one terminal hydrogen as in the structure of $Hf(BH_4)_4$. An initial attempt to refine the hydrogen atom positions would not converge and an attempt to refine a single isotropic thermal parameter converged to a negative value. Finally, with all hydrogens given the

same fixed isotropic thermal parameter and with positional parameters allowed to shift only half of the indicated full matrix value in each cycle, several additional cycles of least-squares refinement converged smoothly to the values given in Table 5. The full matrix least-squares program minimizes the function $\Sigma w|\Delta F|^2/\Sigma wF_0^2$ where the assigned weights $w = [\sigma(F)]^{-2}$ were derived from $\sigma(F^2) = [S^2 + (pF^2)^2]^{\frac{1}{2}}$ where S^2 is the variance due to counting statistics and $p = 0.10$. The final R-factor was 0.114 for 16 parameters and 352 data with $F^2 > \sigma(F^2)$ and 0.125 for all 511 data. The weighted $Rw = (\Sigma w(|F_o|-|F_c|)^2/\Sigma wF_o^2)^{\frac{1}{2}}$ was 0.140 and the estimated standard deviation for an observation of unit weight was 2.15. The scattering factors used were those of Doyle and Turner[10] for neural boron, those of Steward, Davidson, and Simpson[11] for hydrogen, and those from the International Tables[12] for Np^{4+} corrected for anomalous dispersion.

Vapor Pressure Measurement

The extreme chemical reactivity of $Np(BH_4)_4$ precluded the use of a mercury manometer and only an all-glass-and-Teflon Bourdon gauge was found satisfactory for these measurements. The exposed surfaces of the gauge were passivated with the Np borohydride vapor prior to use to minimize a decomposition reaction which evolves hydrogen and diborane. Excess $Np(BH_4)_4$ was condensed into the passivated gauge and the gauge was pumped out at -78°. At various temperatures, the compound was allowed to vaporize and deflect a pointer, whose initial position was precisely determined by a cathetometer. Shortly after equilibrium was established, the pointer was nulled to its original position by pressurizing the outer

chamber of the gauge with argon. The argon pressure, as measured by a standard pressure gauge, then equaled the vapor pressure of the $Np(BH_4)_4$. Care was taken to remove all traces of H_2 and B_2H_6 before and after each measurement. Vapor pressure readings were taken at room temperature and below until the vapor pressure of the compound approached the sensitivity of the Bourdon gauge.

Results and Discussion

Polymeric Actinide Borohydrides

The orange sublimate obtained from the $PaF_4/Al(BH_4)_3$ reaction gave a solid-state infrared spectrum almost identical to those of Th[13] and U[3,13] borohydrides and identified it to be $Pa(BH_4)_4$. It was further characterized by its Xray powder pattern which also showed that Th, Pa, and U borohydrides are isostructural.

From the single-crystal Xray study of $U(BH_4)_4$,[6] it was determined that $U(BH_4)_4$ crystallizes in the tetragonal space group $P4_32_12(P4_12_12)$ where a = 7.49(1) Å, c = 13.24(1) Å, and Z = 4. The calculated density is 2.66 gm/cm^3. These values agree (within experimental error) with those given in Table 4 obtained from our powder patterns. The Xray patterns of Th and Pa borohydrides were indexed on the basis of the $U(BH_4)_4$ structure and the diffraction data are listed in Table 1-4. The trend in lattice parameters reflect the effect of increasing ionic radii of the An^{4+} ions from U^{4+} to Th^{4+} with the concomitant decrease in density. Metal-boron distances, which are accurately known for $U(BH_4)_4$, are not truly functions of a and c only and so corresponding distances in the

Th and Pa compounds cannot be obtained from the powder diffraction data. Approximate values can be calculated by adding to the U-B distances the differences between the ionic radii of Th^{4+} and U^{4+} (.06 Å)[14] or Pa^{4+} and U^{4+} (.01 Å).[14] The c/a ratios are almost equivalent for all three compounds and therefore the intermolecular van der Waals forces are similar.

The structure of $U(BH_4)_4$, as determined by single-crystal neutron diffraction, is shown in Fig. 1. Like those in the well-known boron hydrides,[15] hydrogen bridge bonds are found in the actinide borohydrides. There are two types of borohydride groups in the molecule, bidentate and tridentate. Each of the four bidentate groups are bound to the uranium atom via two hydrogen bridge bonds and use their remaining two hydrogen atoms to link neighboring uranium atoms in a polymeric structure of C_2 symmetry at uranium. The two tridentate BH_4^- groups are in a cis configuration about the metal and are connected to it by three hydrogen bridge bonds. The terminal H atom is nearly colinear with the U-BT vector and is bonded only to the boron atom. While the bidentate borohydride groups exhibit a U-B distance of 2.87 Å, the terminal borohydrides are closer to the uranium atom with a U-B distance of 2.53 Å. The U atom in $U(BH_4)_4$ is 14 coordinate and the 14 bridging hydrogen atoms form a slightly distorted capped hexagonal antiprism with a mean U-H distance of 2.35 Å. The BH_4^- groups themselves are nearly tetrahedral with B-H distances in the range 1.2-1.3 Å.

Monomeric Actinide Borohydrides

Gas phase infrared spectra of Np and Pu borohydrides are almost identical to that of $U(BH_4)_4$ and therefore similar gas-phase structures

Table 1

Xray Powder Diffraction Data for $Th(BH_4)_4$

Intensity	hkl	2Θ(obs)	2Θ(calc)[a]
M	101	13.68	13.55
S	110	16.63	16.65
VS	111	17.83	17.95
M-	200	23.58	23.58
M	201	24.53	24.53
W	113	26.33	26.17
W	004	26.93	26.89
S	211	27.23	27.26
S	212	29.68	29.68
M	203	31.13	31.14
S	114	31.63	31.75
S	213	33.23	33.37
W	221	34.13	34.24
S	204	36.03	36.01
S	214	38.08	37.99
W	223	39.33	39.38
W	205	41.63	41.55
S	106	42.48	42.55
W	320	43.28	43.14

In Tables 1-3: S = strong, M = medium, W = weak, V = very.

Cu Kα radiation of wavelength 1.5418 Å was used.

[a]See Table 4 for lattice parameters.

Table 2

Xray Powder Diffraction Data for $Pa(BH_4)_4$

Intensity	hkl	2Θ(obs)	2Θ(calc) [a]
M	101	13.49	13.47
S-	110	16.62	16.59
VS	111	17.77	17.90
M-	200	23.54	23.57
M	201	24.59	24.53
W	113	26.27	26.20
M-	211	27.28	27.27
M	212	29.71	29.72
W	203	31.24	31.19
M	114	31.82	31.82
M	213	33.42	33.44
W	221	34.28	34.30
S-	222	36.28	36.32
M+	302	38.24	38.30
VW	223	39.54	39.49
W	312	40.24	40.20
W	303	41.35	41.34
VW	205	41.65	41.69
W	106	42.70	42.71
M-	320	43.20	43.27

[a]See Table 4 for lattice parameters.

Table 3

Xray Powder Diffraction Data for $U(BH_4)_4$

Intensity	hkl	2Θ(obs)	2Θ(calc) [a]
M	101	13.83	13.75
S	110	16.94	16.92
VS	111	18.04	18.22
W	103	23.61	23.59
W	200	23.91	23.97
M	201	25.01	24.92
W	113	26.56	26.49
M	004	27.06	27.13
M	211	27.72	27.70
S	212	30.12	30.13
W	203	31.68	31.56
S	114	32.13	32.11
S	213	33.83	33.83
W	221	34.78	34.81
M	204	36.39	36.47
M	222	36.79	36.82
W	214	38.49	38.49
M	302	38.84	38.82
W	223	39.95	39.97
W	312	40.70	40.74
M	303	42.00	41.85

[a]See Table 4 for lattice parameters.

Table 4

Lattice Constants and Calculated Densities

for Th, Pa, and U Borohydrides

	a [a]	c	c/a	ρ [b]
$Th(BH_4)_4$	7.58 ± .03	13.31 ± .05	1.76	2.53
$Pa(BH_4)_4$	7.53 ± .03	13.22 ± .05	1.76	2.57
$U(BH_4)_4$	7.46 ± .03	13.19 ± .05	1.77	2.69

[a] Values of a and c are in Å.

[b] Densities are in $gm\text{-}cm^{-3}$.

All compounds are of the tetragonal space group $P4_32_12$ ($P4_12_12$) with 4 molecules/unit cell.

The Nelson-Riley correction was used in the fitting procedures.

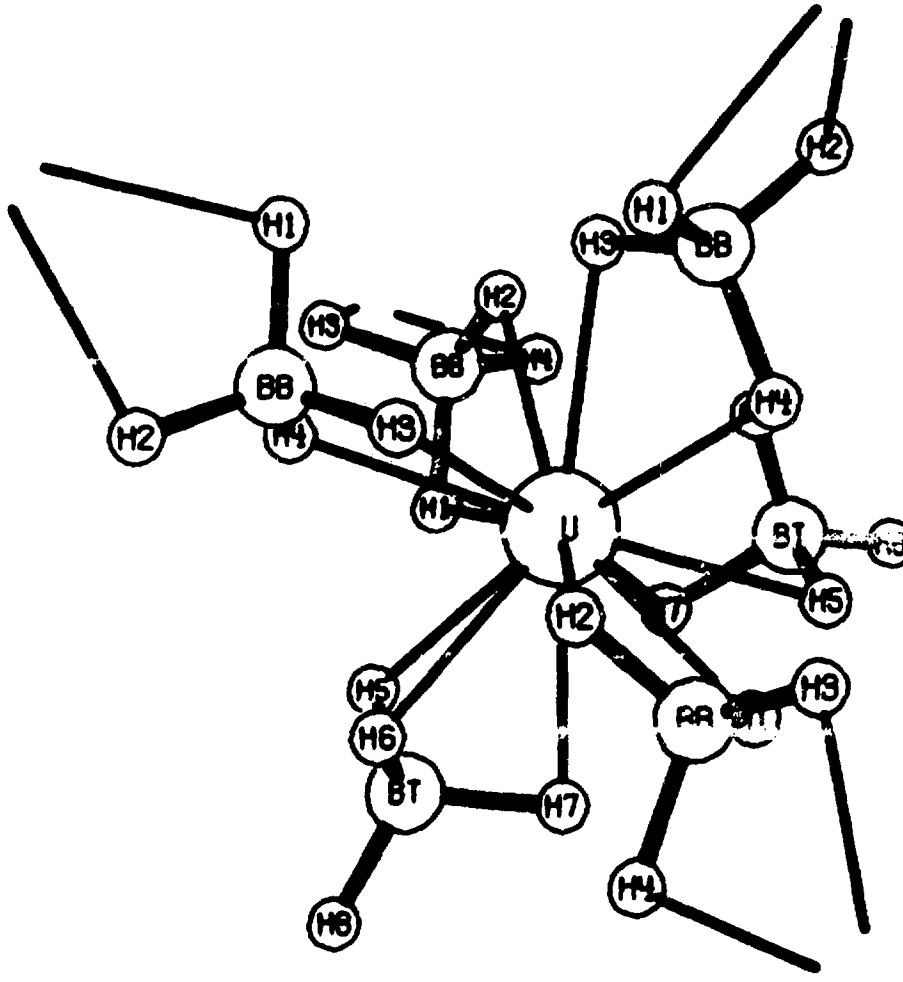

XBL 771-7338

Figure 1. Solid-State Molecular Structure of $U(BH_4)_4$.

are expected for them. In the solid state, $Np(BH_4)_4$ (and presumably $Pu(BH_4)_4$ also) gives basically the same spectrum as in the gaseous state, while $U(BH_4)_4$ produces much different spectra in the two phases. The polymeric structure of $U(BH_4)_4$ transforms into a different one upon vaporizing but $Np(BH_4)_4$ retains its solid-state structure in the gaseous state.

Low temperature powder diffraction photographs of $Np(BH_4)_4$ and $Pu(BH_4)_4$[1] showed that they are isostructural and crystallize into a tetragonal structure different than the tetragonal structure of the polymeric compounds. Dissimilar molecular structures were also predicted by the solid-state infrared spectra. Since the $Np(BH_4)_4$ and $Pu(BH_4)_4$ crystals were preferentially oriented, the powder patterns did not show any reflection with ℓ values greater than 2 and therefore the c dimensions were not accurately determined. The diffraction patterns suggested that the Np and Pu compounds are monomeric but did not define the boron and hydrogen atom positions. It was concluded both from the powder patterns and solid state vibrational spectra that the $Np(BH_4)_4$-type structure is very similar to that of $Zr(BH_4)_4$[16,17] and $Hf(BH_4)_4$[16,18] described below.

The molecular and crystal structures of $Zr(BH_4)_4$[19,20] and $Hf(BH_4)_4$[9] were determined by electron, Xray, and neutron diffraction methods. $Hf(BH_4)_4$ and $Zr(BH_4)_4$ are monomeric and crystallize into a simple cubic lattice of space group $P\bar{4}3$ m. The metal atom is bonded to four tetrahedrally arranged borohydride groups by triple hydrogen bridge bonds giving the molecule T_d symmetry. Corresponding Zr-B and Hf-B distances

are 2.34(3) Å[20] and 2.28(1)[9(a)] Å, respectively. The coordination sphere around the Zr or Hf atoms consists of only 12 H atoms in the form of a distorted cube octahedron.

A single crystal Xray crystallographic investigation of $Np(BH_4)_4$ was undertaken[5] to determine its detailed molecular structure and compare it to the structures of the other metal tetrakis-borohydrides.

The monomeric nature of solid $Np(BH_4)_4$ is established by the Xray diffraction results. The molecule is shown in the ORTEP diagram in Fig. 2 (see also Appendix A, chapter 3) and is also representative of the structure of $Zr(BH_4)_4$ and $Hf(BH_4)_4$. The molecular structure parameters are given in Table 6. The $Np(BH_4)_4$ crystals are tetragonal and of the space group $P4_2/nmc$; a = 8.559(9) Å, c = 6.017(9) Å, Z = 2.

The Np atom is coordinated to four borohydrides through three bridging hydrogen atoms each, with all B-Np-B angles being tetrahedral to within less than one estimated standard deviation, even though the crystallographic site symmetry for Np does not require regular tetrahedral geometry.

Bernstein et al.[7] observed that bridging borohydride groups give larger M-B distances than do the terminal ones in $U(BH_4)_4$. They suggested an "ionic radius" of a terminal BH_4^- group be approximately 1.3(1) Å and that of a bridging BH_4 group be about 1.6(1) Å. Using the value from Shannon and Prewitt[14] for the radius of Np^{4+} and the Np-B distance of 2.46 Å, it is found that the BH_4^- radius is 1.34 Å. This is in good agreement with the values calculated for other triply bridged borohydride groups: $U(BH_4)_4$ 1.38 Å,[7] 1.37 Å;[21] $Zr(BH_4)_4$ 1.36 Å,[20] 1.33 Å;[19(a)] $Hf(BH_4)_4$ 1.31 Å.[9(a)]

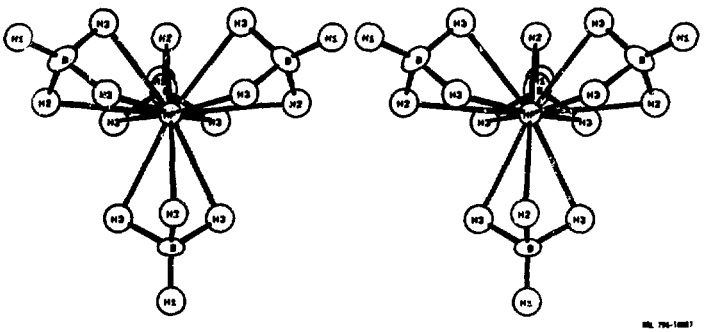

Figure 2. ORTEP Stereo View of $Np(BH_4)_4$.

Table 5

Positional and Thermal Parameters for $Np(BH_4)_4$ [a]

Atom	x	y	z	B_{11}	B_{22}	B_{33}	B_{23}
Np	0	0	0	1.94(5)	1.94(5)	2.07(6)	0
B	0	0.235(4)	0.233(5)	2.8(11)	3.0(12)	2.4(7)	-1.6(8)
H(1) [b]	0	0.33(3)	0.33(4)				
H(2) [b]	0	0.26(6)	0.05(4)				
H(3) [b]	0.10(3)	0.15(2)	0.24(6)				

[a]The anisotropic temperature factor has the form $\exp(-0.25(B_{11}h^2a^{*2} + 2B_{12}hka^*b^* + \ldots))$. Symmetry restraints of the thermal parameters of Np are: $B_{11} = B_{22}$ and $B_{12} = B_{13} = B_{23} = 0$; and for B they are $B_{12} = B_{13} = 0$.

[b]The isotropic thermal parameter of the hydrogen atoms was constrained to a value of 3.0 $Å^2$ and its isotropic temperature factor has the form $\exp(-B((\sin\theta)/\lambda^2))$.

Table 6

Molecular Structure Parameters for $Np(BH_4)_4$

Interatomic Distances (Å)

Np-4B	2.46(3)	H(1)-H(2)	1.8(5)
Np-H(2)	2.3(5)	H(1)-2H(3)	1.9(3)
Np-2H(3)	2.1(3)	H(2)-2H(3)	1.8(3)
B-H(1)	1.0(3)	H(3)-H(3)	1.8(4)
B-H(2)	1.1(2)	H(2)-2H(3)[a]	2.5(4)
B-2H(3)	1.2(2)	H(3)-H(3)[a]	2.5(4)

[a]Distance to H(3) on an adjacent BH_4^- group.

Angles (deg)

B-Np-B[a]	110.3(18)	Np-B-H(1)	179(16)
B-Np-B[b]	109.1(9)	Np-H(2)-B	85(26)
H(1)-B-H(2)	112(32)	Np-H(3)-B	93(16)
H(1)-B-H(3)	122(15)		
H(2)-B-H(3)	99(20)		
H(3)-B-H(3)	100(22)		

[a]Symmetry operation $0,\bar{x},z$.

[b]Symmetry operations $x,0,\bar{z}$ and $\bar{x},0,\bar{z}$.

The borohydride group in $Np(BH_4)_4$ is tetrahedral within the estimated standard deviation with an average B-H bond length of 1.1(2) Å. Neutron diffraction investigations on "covalent" $U(BH_4)_4$ and $Hf(BH_4)_4$ revealed departures from T_d symmetry of the tridentate BH_4^- groups manifesting themselves as wider H_t-B-H_b (113°) and smaller H_b-B-H_b (106°) angles with respect to the tetrahedral angle, and as a shorter B-H_t (1.15 Å) distance compared to the longer B-H_b (1.24 Å) distances. Unfortunately the present Xray diffraction results are not accurate enough to determine if these deviations from T_d symmetry are present in $Np(BH_4)_4$. A neutron structure determination of the "ionic" KBH_4 compound[22] indicated that the BH_4^- group was symmetrical with all B-H bond lengths being 1.260(2) Å and the H-B-H angle of 109.5°. Whether the distortion of the BH_4^- groups in these compounds can be used to test for covalency[23] must await further neutron diffraction results.

Although the hydrogen atom positions have large estimated standard deviations and the inclusion of the hydrogen atoms in the refinement lowered the R-factor a trivial amount, the hydrogen atoms refined to chemically reasonable positions. The terminal hydrogen atom is properly oriented away from the neptunium with a Np-B-H(1) angle of 179(16)°. The 12 bridging hydrogen atoms around the neptunium are all 2.5 Å away from it and form a coordination polyhedron in which each hydrogen atom is 1.8 Å from two other hydrogen atoms in the same borohydride group, and 2.5 Å from two hydrogen atoms in adjacent borohydride groups. This polynedron is similar to the cube-octahedron which describes the coordination in the cubic-closest-packing structure with six neighbors in a

plane, three above, and three below. The inequality of the H-H distances corresponds to a tetrahedral distortion of this figure which changes the square faces into rectangles and the triangular faces into four larger ones and four smaller ones.

James et al.[17,24] have suggested that $Zr(BH_4)_4$ may be of slightly lower T symmetry which is obtained by rotating all four BH_4^- groups from the staggered orientation by an angle of less than 60° about the Zr-B vector.[24] They based their argument on an uncertain interpretation of an electron diffraction study on *gaseous* $Zr(BH_4)_4$[19] and on weak infrared transitions[17] which they assigned as fundamental modes. However, the staggered arrangement of bridging hydrogen atoms offers the least amount of inter-hydrogen repulsion. Our work gives no evidence for symmetry lower than T_d for $Np(BH_4)_4$.

Despite the close similarity between the ionic radii of Np^{4+} and U^{4+} (difference is .02 Å)[14] as compared to those of Np^{4+} and Hf^{4+} (difference is .15 Å),[14] the solid-state structure and physical properties of $Np(BH_4)_4$ resemble those of $Hf(BH_4)_4$. If the metal ion size is the determining factor in the number of bridging hydrogen atoms that can be accommodated in the coordination sphere of the metal in these borohydrides, this work establishes the transition from 14 to 12 coordination between U^{4+} (r = 1.00 Å) and Np^{4+} (r = .98 Å).

The solid-state molecular structure of $Np(BH_4)_4$ has the same basic geometry as $Hf(BH_4)_4$ and $Zr(BH_4)_4$ yet the crystal structures are different. The tetragonal unit cell (Fig. 3) has one molecule at the origin and another (with inverted configuration) at the body center. If the

Figure 3. Schematic diagram of packing in $Np(BH_4)_4$. Solid line is the tetragonal $Np(BH_4)_4$ cell, the dotted line shows the cubic $Zr(BH_4)_4$ cell if the metal atoms were at $z = 0$. The H atoms are not shown.

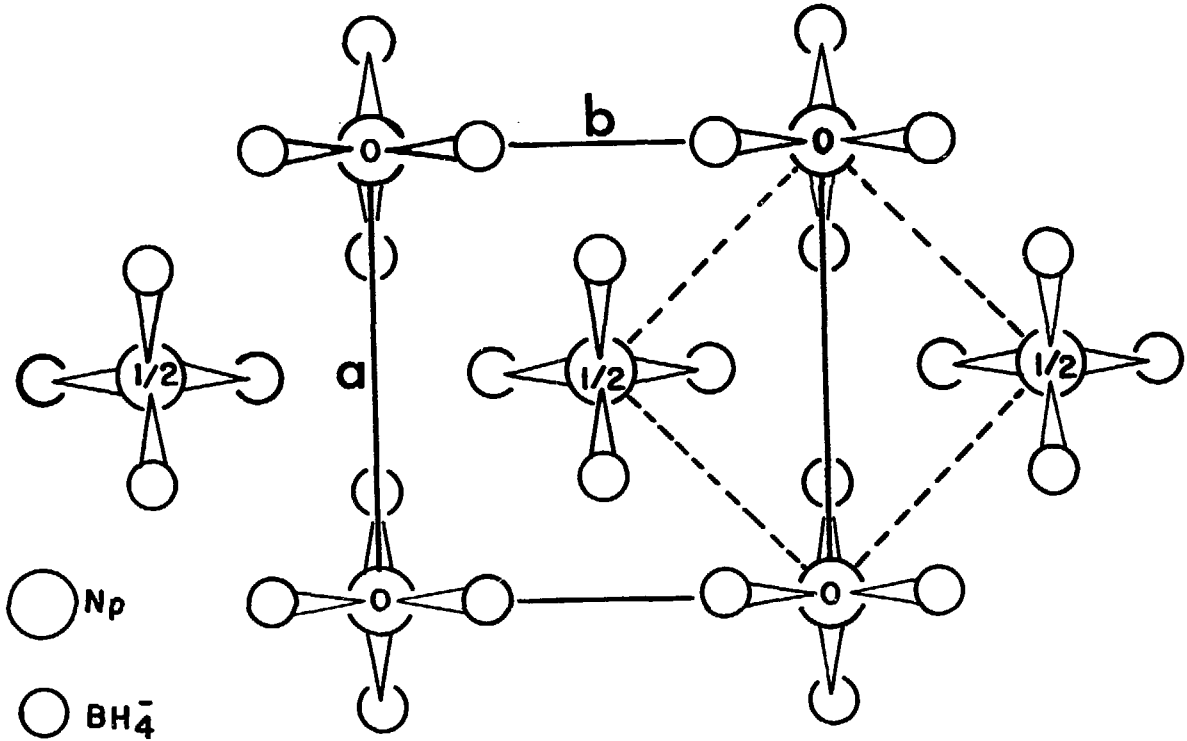

XBL 796-10085

Figure 3.

second molecule were moved to z = 0 and inverted, this structure would be identical with that of the Zr and Hf compounds, apart from a deviation of about 0.6% from cubic lattice dimensions. The boron positions are hardly changed in this transformation, but the packing of their terminal hydrogen atoms is significantly different in the two structures.

Volatilities of the Metal Tetrakis-Borohydrides

The crystal structures of the seven metal tetrakis-borohydrides fall into three types, $P4_32_12$ (Th, Pa, U), $P4_2/nmc$ (Np, Pu), and $P\bar{4}3\,m$ (Hf, Zr) but their molecular structures are only of two types, polymeric, C_2 symmetry (Th, Pa, U) and monomeric, T_d symmetry (Np, Pu, Hf, Zr). The primary properties of these metal borohydrides reflect the polymeric or monomeric nature of their solid-state structures. In chapter 1, it was pointed out that the polymeric compounds display very different properties than the monomeric ones, especially their volatilities.

Schlesinger and Brown[25] measured the vapor pressure of $U(BH_4)_4$ as a function of temperature and Hoekstra and Katz[26] determined those of Th, Zr, and Hf borohydrides. In order to put the vapor pressure of the $Np(BH_4)_4$-type structure on a quantitative basis, the vapor pressure of $Np(BH_4)_4$ was measured at various temperatures.

Using the data obtained from the measurements, linear plots were found for the equation $\log p_{mmHg} = -A/T + B$, where T is in degrees K, for liquid and for solid $Np(BH_4)_4$. Least squares lines were fitted to the observed points and are given in Fig. 4 along with those from other work for U,[25] Hf,[26] and Zr[26] borohydrides. Table 7 lists the values of A and B for U, Zr, Hf, and Np borohydrides and various thermodynamic

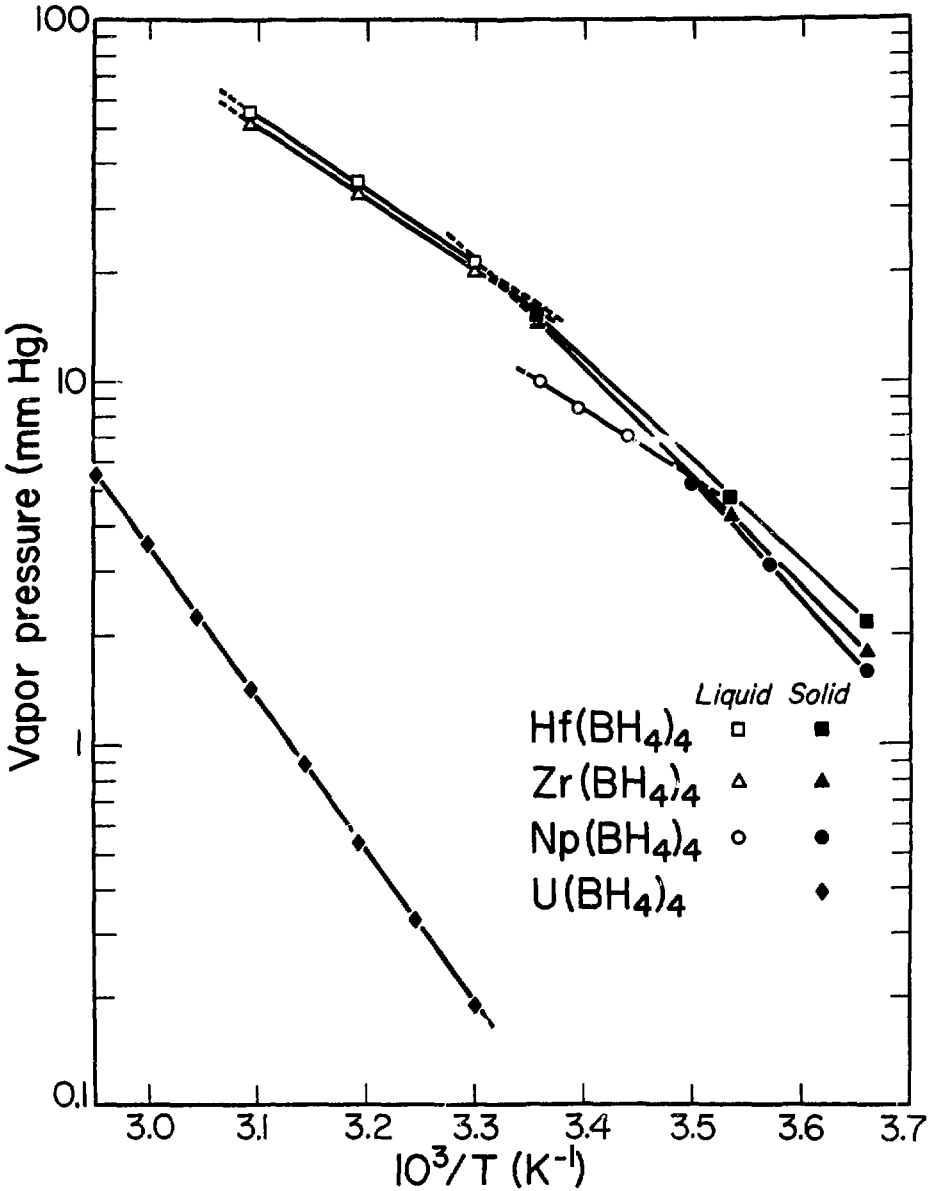

Figure 4. XBL 7911-13273

quantities calculated from the vapor pressure curves. Other physical properties are also given.

From Fig. 4 it is seen that the vapor pressure of polymeric $U(BH_4)_4$ is much lower than those of the monomeric compounds which themselves are very similar. It appears that the intermolecular bonds holding the $U(BH_4)_4$ molecules together in a polymeric structure are responsible for the low vapor pressure of the compound and the large disparity in volatilities of Th, Pa, and U borohydrides is caused by the large differences in the intermolecular-bond strengths. The small differences in the volatilities of the monomeric borohydrides are due to the rather weak van der Waals forces between molecules.

The consequences of a polymeric structure, in addition to low volatility, are high melting points accompanied by decomposition, good chemical stability toward hydrolysis and low solubility in nonpolar, non-coordinating organic solvents. The monomeric borohydrides are low melting, react violently with water, and are very soluble in solvents such as pentane. At room temperature $Pa(BH_4)_4$ is insoluble in $Zr(BH_4)_4$ but when the mixture is heated slightly above the sublimation temperature of $Pa(BH_4)_4$, the liquid turns yellow as the polymeric structure is disrupted and the Pa compound dissolves.

All of the metal tetrakis-borohydrides are monomeric in the gaseous state and therefore the intermolecular bonds in the polymeric compounds must break, changing the coordination number of the Th, Pa, or U atom from 14 to 12. The free energy for the structure transformation at 298K described by the equation

Table 7

Physical Properties of Metal Tetrakis-Borohydrides

Property	$Th(BH_4)_4$ [a]	$Pa(BH_4)_4$ [e]	$U(BH_4)_4$ [b]	$Np(BH_4)_4$ [c]	$Pu(BH_4)_4$ [e]	$Hf(BH_4)_4$ [a]	$Zr(BH_4)_4$ [a]
Color	white	orange	green	green	bluish-black	white	white
Crystallographic space group	$P4_32_12$ (tetragonal)	$P4_32_12$ (tetragonal)	$P4_32_12$ [d] (tetragonal)	$P4_2/nmc$ (tetragonal)	$P4_2/nmc$ (tetragonal)	$P\bar{4}3m$ [f] (cubic)	$P\bar{4}3m$ [g] (cubic)
Solid-state structure	polymeric	polymeric	polymeric	monomeric	monomeric	monomeric	monomeric
Solid-state density (gm/cm^3)	2.53	2.57	2.69	2.23	2.20	1.86	1.13
Melting point (°C)	203 [h]	----	126 [h]	14.2	15	29.0	28.7
Boiling point (°C) extrap.	----	----	----	153	----	118	123
Vapor pressure (mmHg/°C)	.05/130	$\sim 10^{-1}/55$	.19/30	10.0/25	$\sim 10^{1}/25$	14.9/25	15.0/25
Liquid [i] A	----	----	----	1858	----	2097	2039
Liquid [i] B	----	----	----	7.24	----	8.247	8.032
Solid [i] A	----	----	4264.6	3168	----	2844	2983
Solid [i] B	----	----	13.354	11.80	----	10.719	10.919
Heat of sublimation (kcal/mol)	21	----	19.5	14.5	----	13.0	13.6
Heat of vaporization (kcal/mol)	----	----	----	8.5	----	9.6	9.3
Heat of fusion (kcal/mol)	----	----	----	6.0	----	3.4	4.3
Entropy of sublimation (cal/mol°)	----	----	61.1	54.0	----	49.0	50.0
Entropy of vaporization (cal/mol°)	----	----	----	33.1	----	37.7	36.8
Entropy of fusion (cal/mol°)	----	----	----	20.9	----	11.3	13.2
Solubility in pentane at 25°	insol	insol	slight	high	high	high	high

[a] Reference 26. [b] Reference 25. [c] Reference 5. [d] Reference 6. [e] Reference 1. [f] Reference 9.

[g] Reference 20. [h] With decomposition. [i] Log p(mmHg) $= -A/T + B$

$U(BH_4)_4$ (solid, 14 coordinate, 4 double-, 2 triple-hydrogen-bridge bonds) → $U(BH_4)_4$ (solid, 12 coordinate, 4 triple-hydrogen-bridge bonds)

can be estimated. ΔH and ΔS values for a 12 coordinate $U(BH_4)_4$ structure were obtained by an extrapolation of the measured quantities for $Hf(BH_4)_4$ and $Np(BH_4)_4$ vs. metal ionic radius. Subtracting these derived $U(BH_4)_4$ values from the corresponding measured ones gives the heat of transformation (4.5 kcal/mol) and entropy of transformation (6.5 cal/mol°) of the 14 coordinate to the 12 coordinate structure for $U(BH_4)_4$. Using the equation $\Delta G = \Delta H - T\Delta S$, ΔG is found to be +2.6 kcal/mol. This value can be compared to the free energy of an exchange process involving the bridge and terminal hydrogen atoms in solution for $(C_5H_5)_3UBH_4$ where $G^* \approx 5$ kcal/mol at the coalescence temperature of $-140 \pm 20°$.[27] The calculated value for the spontaneous transformation from 14 to 12 coordination is ~700K.

The molecular structure parameters found in the Xray study of $Np(BH_4)_4$ will be used in the normal coordinate vibrational analysis of $Np(BH_4)_4$ discussed in the next chapter.

References

[1]Banks, R. H.; Edelstein, N. M.; Rietz, R. R.; Templeton, D. H.; Zalkin, A. J. Am. Chem. Soc. 100 1957 (1978).

[2]Ghiassee, N.; Clay, P. G.; Walton, G. N. Inorg. Nucl. Chem. Lett. 14 117 (1978).

[3]James, B. D.; Smith, B. E.; Wallbridge, M. G. H. J. Mol. Struct. 14 327 (1972).

[4]Paine, R. T.; Light, R. W.; Nelson, M. Spectrochim. Acta 35A 213 (1979).

[5]Banks, R. H.; Edelstein, N. M.; Spencer, B.; Templeton, D. H.; Zalkin, A. J. Am. Chem. Soc. 102 0000 (1980).

[6]Bernstein, E. R.; Keiderling, T. A.; Lippard, S. J.; Mayerle, J. J. J. Am. Chem. Soc. 94 2552 (1972).

[7]Bernstein, E. R.; Hamilton, W. C.; Keiderling, T. A.; La Placa, S. J.; Lippard, S. J.; Mayerle, J. J. Inorg. Chem. 11 3009 (1972).

[8]Williams, D. E. Ames Lab. Rept. IS-1052 (1964).

[9(a)]Broach, R. S.; Chuang, I. S.; Williams, J. M.; Marks, T. J. Private communication, 1979.

[(b)]Keiderling, T. A. Ph.D. Thesis. Princeton University, 1974.

[10]Doyle, P. A.; Turner, P. S. Acta Cryst. A24 390 (1968).

[11]Stewart, R. F.; Davidson, E. R.; Simpson, W. T. J. Chem. Phys. 42 3175 (1965).

[12]Ibers, J. A.; Hamilton, W. C. "International Tables for Xray Crystallography." Vol. 4. Kynoch Press. Birmingham, 1974, p. 97.

[13]Volkov, V. V.; Myakishev, K. G.; Grankina, Z. A. Russ. J. Inorg. Chem. 15 1490 (1970).

[14]Shannon, R. D.; Prewitt, C. T. Acta Cryst. B25 925 (1969).

[15]Muetterties, E. L. "Boron Hydride Chemistry." Academic Press. New York, N.Y., 1975.

[16]Davies, N.; Wallbridge, M. G. H.; Smith, B. E.; James, B. D. J. Chem. Soc. Dalton 162 (1973).

[17]Smith, B. E.; Shurvell, H. F.; James, B. D. J. Chem. Soc. Dalton 710 (1978).

[18]Keiderling, T. A.; Wozniak, W. T.; Gay, R. S.; Jurkowitz, D.; Bernstein, E. R.; Lippard, S. J.; Spiro, T. G. Inorg. Chem. 14 576 (1975).

[19(a)]Plato, V.; Hedberg, K. Inorg. Chem. 10 590 (1971).

[(b)]Spiridonov, B. P.; Mamaeva, G. I. J. Struct. Chem. 10 120 (1969).

[20]Bird, P. H.; Churchill, M. R. Chem. Comm. 403 (1967).

[21]Rietz, R. R.; Zalkin, A.; Templeton, D. H.; Edelstein, N. M.; Templeton, L. K. Inorg. Chem. 17 653 (1978).

[22]Peterson, E. R. Diss. Abst. 25 5588 (1965).

[23]Marks, T. J.; Kolb, J. R. Chem. Rev. 77 263 (1977).

[24]James, B. D.; Smith, B. E.; Shurvell, H. F. J. Mol. Struct. 33 91 (1976).

[25]Katz, J. J.; Rabinowitch, E. "The Chemistry of Uranium." McGraw-Hill Books Co., Inc. New York, N.Y., 1951, p. 553-554.

[26]Hoekstra, H. R.; Katz, J. J. J. Am. Chem. Soc. 71 2488 (1949).

[27]Marks, T. J.; Kolb, J. R. J. Am. Chem. Soc. 97 27 (1975).

Chapter 3

VIBRATIONAL ANALYSIS OF NEPTUNIUM BOROHYDRIDE

Introduction

The study of the molecular structures of metal borohydrides was found to be very important in elucidating their chemical and physical properties.[1] Analogously, vibrational spectra can give much information on molecular structures and also on the bonding and the quantum mechanical properties of molecules.[2] Vibrational studies on metal borohydrides and their organic derivatives are numerous and a short review of a few of them is presented here.

As discussed in the previous chapter, metal borohydrides exhibit hydrogen bridge bonds linking the boron and metal atoms together. Three types of ligation geometries have been observed (shown below) and each one produces a unique spectral pattern in the infrared (IR) and Raman spectra.

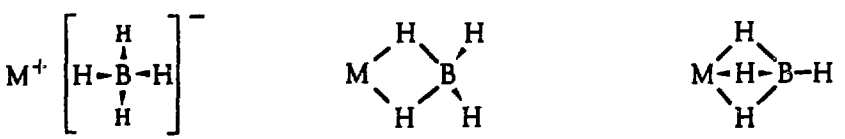

(a) (b) (c)

Simple inspection of the spectra can determine which type of bonding arrangement exists in the molecule--either (a) ionic, (b) bidentate, or (c) tridentate.

Type (a) The ionic borohydrides are those which involve an alkali metal. Their solid-state and solution IR and Raman spectra have been well studied for the tetrahedral BH_4^- anion.[3] According to symmetry selection rules, there should be only two IR active modes and these occur at 2200-2300 cm^{-1} (νBH stretching) and 1100 cm^{-1} (δHBH bending). In practice, however, more bands are observed and are attributed to overtones and combinations.[3(f)] Four bands, one of which is polarized (A_1), are seen in the Raman. Effects of the crystalline fields of alkali halides on the vibrational energy levels of the BH_4^- species have been reported by several authors.[3(e),4,5] The spectroscopic results are consistent with the structure of the borohydride ion in these compounds determined by single crystal neutron diffraction.[6]

Type (b) This is the most common bonding scheme and occurs in the bis[7]- and tris[8]-borohydrides, the polymeric actinide tetrakis-borohydrides,[9,10(a),(b)] and in mixed organometallic borohydride complexes[11] when the metal is not an actinide. Some of the first vibrational studies on these systems were of $Al(BH_4)_3$[3(a),(b),12] and $Be(BH_4)_2$[3(a),13] and useful structural information was obtained before any diffraction studies were carried out.[3(b),13(b),14] Recently cyclopentadienyl-borohydrides[15] have been prepared and from their vibrational spectra, it was concluded that for transition metals, the borohydride groups are bound in a bidentate fashion. A particularly good example of the efficacy of vibrational spectroscopy in structural analysis is the work on $C_5H_5BeBH_4$.[16] From an electron diffraction study of the compound,[17] it was not possible to distinguish between a doubly- or triply-bridged

borohydride group but results from IR and Raman spectra lead to a definite conclusion that the BH_4 group is bidentate.

The most apparent spectroscopic feature characteristic of the doubly-bridged borohydride ligand is a close doublet (60-80 cm^{-1} separation) of the symmetric and antisymmetric νBH_t stretching modes in the 2400-2600 cm^{-1} region of the IR, and a strong singlet in the Raman. Strong and broad adsorptions are observed in both effects at 1650-2150 cm^{-1} (νBH_b stretches), 1300-1500 cm^{-1} (bridge bond stretches), and 1100-1200 cm^{-1} (δHBH bends).[3(b),18]

Type (c) Triply-bridged borohydride groups are found in the metal tetrakis-borohydrides,[1,19] uranium (IV) borohydride etherates,[10] and in other mixed organoactinide borohydride complexes.[15(c),20,21] Vibrational studies have played an important part in understanding their structures and have agreed with Xray diffraction results. Marks et al.[15(c)] determined from IR spectra of compounds of the type $(C_5H_5)_3AnBH_4$ that the borohydride ligand is bonded to the actinide (An = Th, U) via triple hydrogen bridges. The same conclusions were drawn for the complexes $C_8H_8An(BH_4)_2$[20] and $An[N(Si(CH_3)_3)_2]_3BH_4$[21] from their IR spectra. An Xray crystal structure of the latter compound[21] confirmed the spectroscopic results.

The pattern of spectral bands for the tridentate structure is easily distinguishable from those of the other two types. Most noted is the νBH_t stretching region (2600-2500 cm^{-1}) where only a strong, sharp singlet is seen in each of the IR and Raman spectra. The boron bridging-hydrogen stretching region occurs around 2200-2050 cm^{-1} and

bands appear as a strong doublet (~60-80 cm^{-1} separation) in the IR. Bending modes are observed in the energy range 1150-1250 cm^{-1} in both the IR and Raman[22] spectra. Figure 1 illustrates the spectral pattern in the IR for the tetrakis borohydrides (a) and borodeuterides (b). Atomic motions contributing to the fundamental bands are given above the corresponding region.

The remaining part of this chapter will present the reults of a vibrational spectroscopic investigation on $Np(BH_4)_4$ and $Np(BD_4)_4$ whose purpose was not to obtain structural information but to quantitatively describe the vibrational energy states of a new actinide borohydride. Gaseous IR and solid-state IR and Raman spectra are given and the observed bands were assigned assuming the tetrahedral structures reported in chapter 2. From these assignments, a normal coordinate analysis was carried out to develop a simplified general valence force field (SGVFF)[23] employing a small set of force constants which could reproduce the experimental frequencies. Overtones, combinations, and isotopic impurity bands have been identified in the low temperature, solid-state IR spectra and their frequencies are compared to calculated ones using the derived force field. The vibrational and rotational partition functions and various thermodynamic quantities were calculated from the spectroscopic data and compared to experimental values found for analogous systems.

Schematic of $M(BH_4)_4$ and $M(BD_4)_4$ IR Spectra

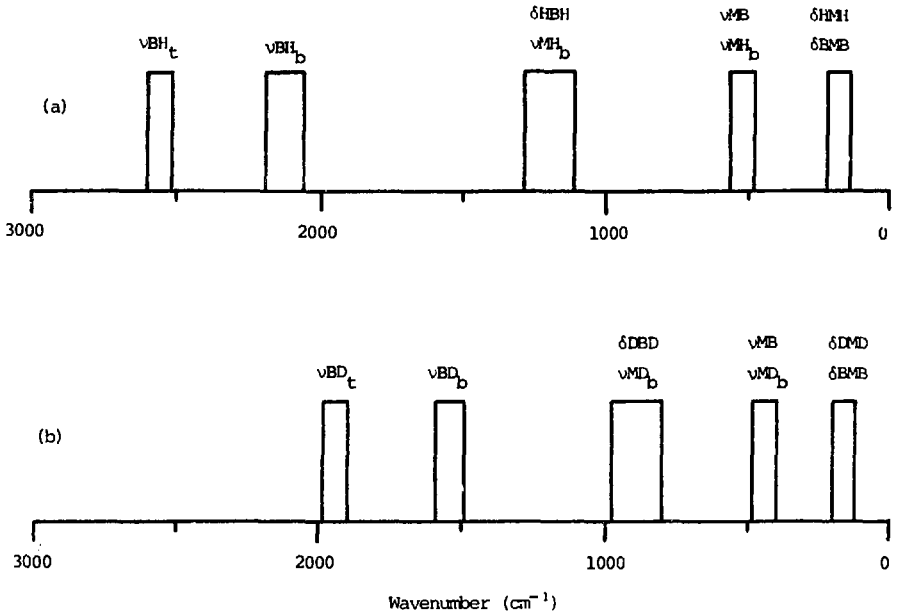

Figure 1

XBL 7912-13708

Experimental

Infrared Spectroscopy

Near infrared spectra of Np and Zr borohydrides and borodeuterides were obtained on a nitrogen purged Cary 17 spectrophotometer in the region 4000-7400 cm^{-1}. The compound was vacuum transferred into a degassed, quartz cell from its storage tube held at -10°C. The cell was then sealed off and the sample was melted and collected into the optical part of the cell. Thin single crystals of Zr borohydride measuring 1 cm x 2 cm x 25μ (and 1000μ) were vapor grown[19(a)] and then slowly cooled in a quartz optical dewar. A $Np(BH_4)_4$ single crystal (1 cm x 2 cm x 25μ) was grown by simply cooling the liquid very slowly in the optical dewar. When the sample temperature reached ~150K in about 8 hours, liquid helium was added and spectra were recorded near the lamda point, 2K. Single crystals of $Np(BD_4)_4$ (30μ thick) and $Zr(BD_4)_4$ (1000μ thick) were similarly grown and their spectra were taken at 2K.

In the region 4000-2000 cm^{-1}, a Perkin-Elmer 283 IR spectrometer was used. Gas phase spectra were taken of the sample gas contained in a 10 cm cell fitted with CsI windows. For the solid-state spectra a specially designed liquid nitrogen cryostat was built in our laboratory. It consisted of a hollow aluminum block which held two outer 2" CsI windows colinearly aligned with the sample window, a liquid nitrogen tower fixed with a copper cold finger, and a sliding evacuation-and-sample transfer tube which could be maneuvered for both

sample depositing and spectra recording operations. The borohydride compound was in the form of a very thin, translucent film made by condensing the vapor onto a cooled CsI window held by the cold finger. An evacuated and clean CsI gas phase cell of the same path length was situated in the reference beam to reduce window and trace atmospheric absorptions.

Far infrared spectra were obtained for $Np(BH_4)_4$ and $Np(BD_4)_4$ in the range 200-25 cm^{-1}. The same liquid nitrogen cryostat described above was used but it was modified for this low energy region. Each of the outer 2" CsI windows was replaced by a 2 mil-thick, 1" diameter mica disk sealed between two brass plates which were bolted to the aluminum block. Soldered to these plates were ½" O.D. brass light pipes in which the IR radiation was guided through the cell and into the detector. The light pipes were kept evacuated during the runs to eliminate atmospheric interference. Absorptions due to all materials except the sample were subtracted out during data processing. The sample vapor was condensed as a film onto a thin, wedged sapphire window held at 77K. A far infrared, 2-beam Michelson interferometer[24] was used to collect the data from which the spectra were obtained by computing the Fourier transforms of the truncated interferograms sampled at every ¼ cm^{-1}.

Raman Spectroscopy

Raman spectra were taken of $Np(BH_4)_4$ (2600-100 cm^{-1}) and $Np(BD_4)_4$ (2300-100 cm^{-1}) using a Ramanor HG, 2S spectrometer and the exciting 514.5 nm line of a Coherent Radiation Model CR-2 argon ion laser. The

scattered light was analyzed at 90° to the incident beam with a J-Y double monochromator and detected by a photon counting system.

The pyrophoric and radioactive hazards associated with neptunium-237 borohydrides required that the sample holder be wholly contained in a negative pressure, safety enclosure which hampered sample alignment and lowered detection sensitivity. This, in addition to the dark green color of the compounds, made even reasonable quality spectra difficult to obtain.

Initially the liquid compound was sealed into a 2 mm O.D. quartz tube and frozen with a flow of cold nitrogen gas. As the solid cooled, it contracted away from the inside tube surface causing much of the incident laser light to scatter from the tube before reaching the sample. Resulting transition intensities were so low that only a few of the strongest lines were observed. High intensity laser light eventually decomposed the compound.

The Raman spectra which are shown in Figs. 2 and 3 were obtained by a different method. A diagram of the cryostat is given in Fig. 4. The borohydride vapor was condensed as a thick, polycrystalline layer on a flat-sided pyrex cold finger containing liquid nitrogen. This rotatable finger fitted vacuum tight into an outer quartz tube by means of a ground glass connection. Attached to the wall of the quartz tube was a valved, sample-inlet-and-evacuation tube which aimed directly at the lower part of the cold finger. After the sample was deposited, and the cryostat was placed into the safety enclosure, the cold finger was rotated for maximum signal. Although this technique gave accept-

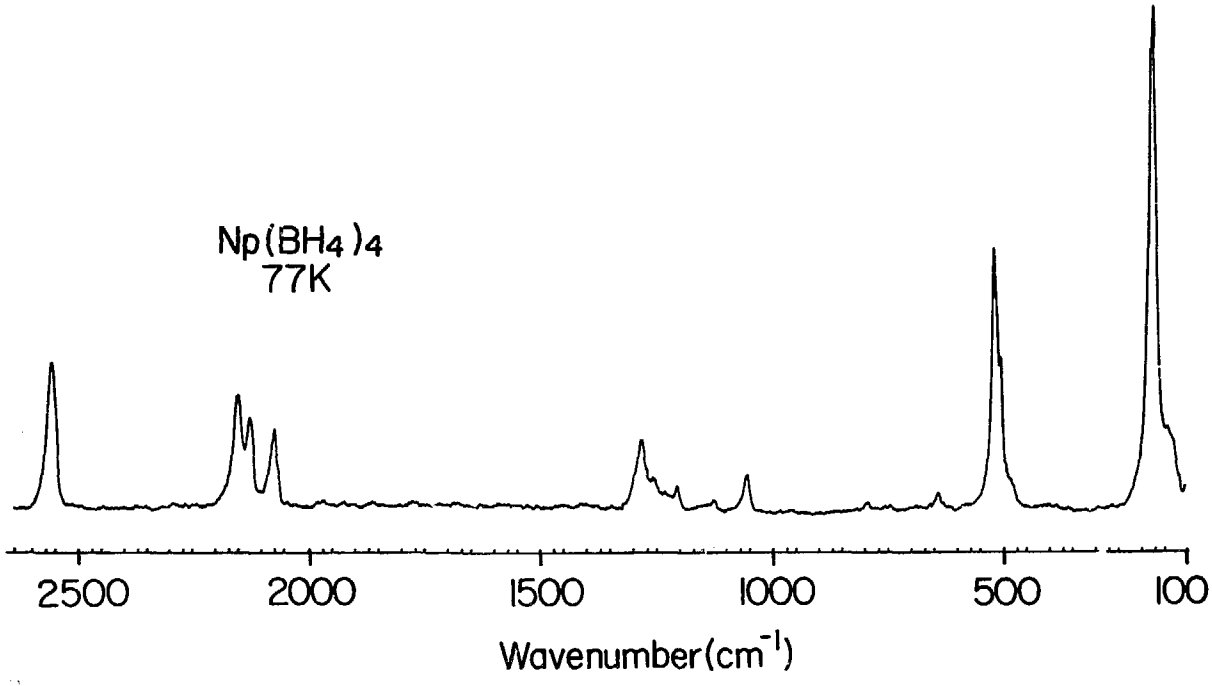

XBL 796-1878

Figure 2. Raman Spectrum of $Np(BH_4)_4$.

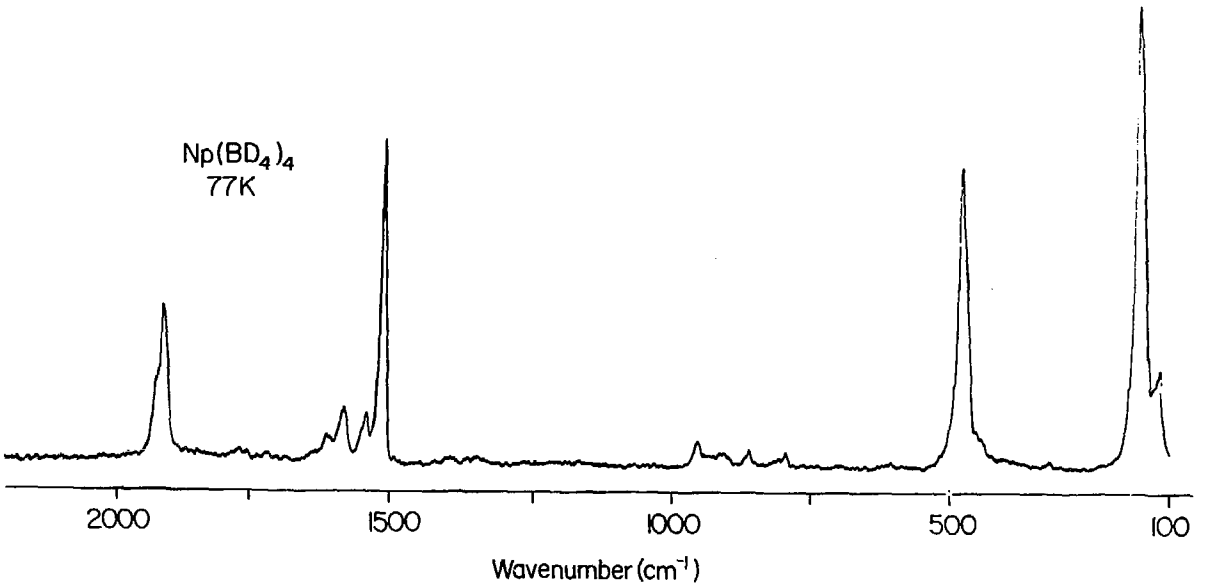

Figure 3. Raman Spectrum of $Np(BD_4)_4$.

XBL 796-1877

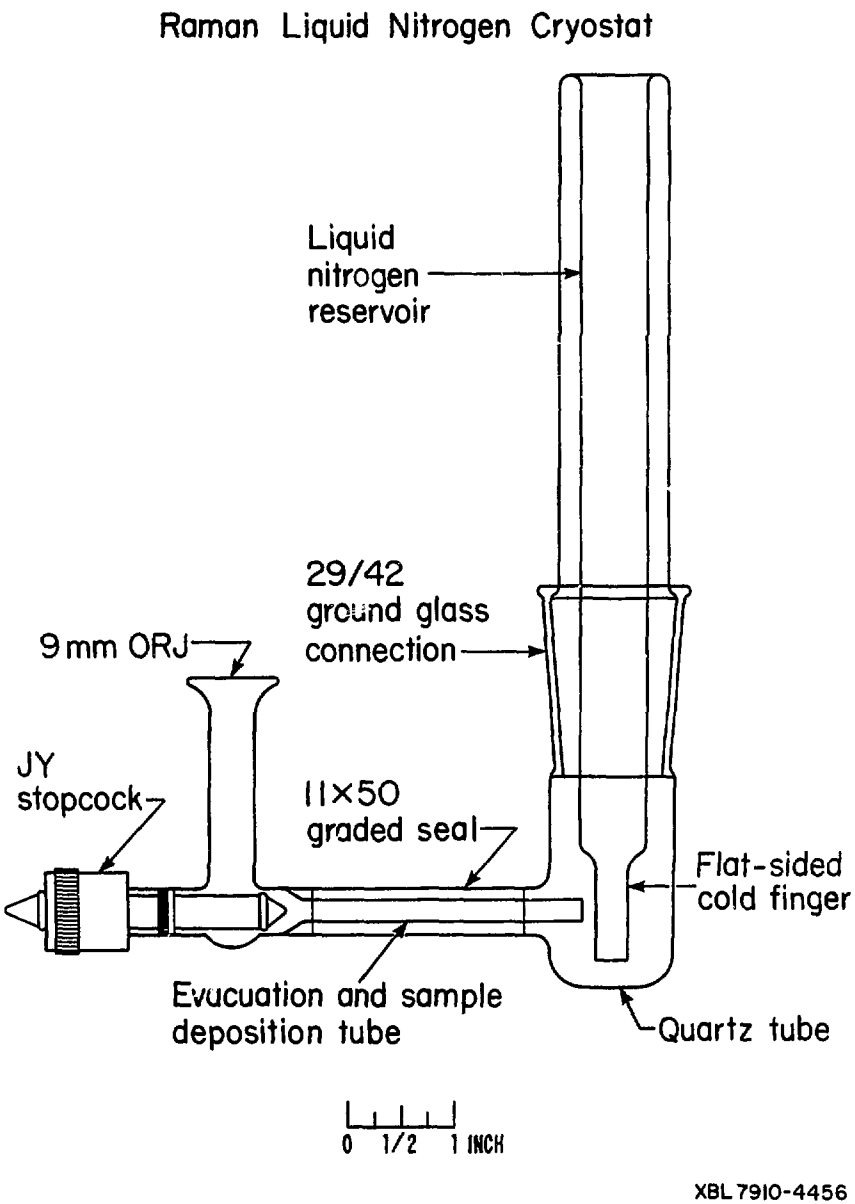
Raman Liquid Nitrogen Cryostat
Liquid nitrogen reservoir
29/42 ground glass connection
9 mm ORJ
JY stopcock
11×50 graded seal
Flat-sided cold finger
Evacuation and sample deposition tube
Quartz tube
0 1/2 1 INCH
XBL 7910-4456

Figure 4.

able intensities, it yielded very poor polarization results. The A_1 modes, however, were easily identified by comparing the frequencies and intensities of these spectral lines to those in the Raman spectra of the Zr and Hf analogs.

Assignment of Fundamentals

It might be expected that a 21-atom molecule would display a rather complicated vibrational spectrum but the high symmetry of the monomeric metal tetrakis-borohydrides causes nearly all of the numerous fundamentals to be degenerate. This property helps in making assignments and reduces the number of observable modes which need to be identified.

In this chapter a particular fundamental or overtone is denoted by the label $n\nu_a^b$, where b is the Mulliken symbol for the irreducible representation of the mode and a is the number of the mode given in numerical order beginning with 1 for the highest frequency, 2 for the second highest, etc. The n is unity and is omitted for fundamentals; it equals 2 for 1st overtones, 3 for 2nd overtones, etc. An (H) or (D) next to a frequency or assignment label indicates that isotope to which the frequency or label applies. Unless otherwise specified, the ^{11}B isotope is implied.

The 57 normal vibrational modes of a tetrahedral $M(BH_4)_4$ molecule are classified as $4A_1 + A_2 + 5E + 5T_1 + 9T_2$, where only the triply degenerate T_2 modes are IR active and the A_1 (polarized), E, and T_2 modes are Raman active. Those vibrations of A_2 or T_1 symmetry are both IR and Raman inactive.

The gas phase IR spectra of $Np(BH_4)_4$ and $Np(BD_4)_4$ are shown in Fig. 5. The low temperature, solid-state IR spectra are given in Figs. 6 and 7. Gas phase absorption bands are much broader than the corresponding solid-state ones and many of the weaker solid-state features are either absent or appear as shoulders in the gas phase spectra. In addition to narrowing, many vibrational levels undergo matrix shifts due to interaction of the borohydride molecules with the surface of the sample window.[3(e),4,5]

Complete listings of the absorption band frequencies, assignments, internal coordinate compositions, and qualitative descriptions of the spectral features for the gas phase and solid-state spectra for the region below 4000 cm^{-1} are given in Tables 1-3.

2600-2500 cm^{-1} (2000-1900 cm^{-1}) Region

The highest energy fundamental vibrations are stretches of the boron and terminal-hydrogen atom. The four $B-H_t$ bonds transform as $A_1 + T_2$ where the A_1 mode is the in-phase vibration and the T_2 modes are the degenerate set of out-of-phase stretches.

Apart from coupling to other motions occurring in the molecule, these A_1 and T_2 modes should be close in energy. One slightly broad band is seen in the Raman at 2557 cm^{-1} (H) and is assigned as $\nu_1^{A_1}$. The borodeuteride shows a peak at 1913 cm^{-1} ($\nu_1^{A_1}$) accompanied by a shoulder at 1925 ± 5 cm^{-1}. The gas phase IR spectra give strong bands at 2568 cm^{-1} (H) and 1922 cm^{-1} (d) with a shoulder at 1930 cm^{-1}(D). In the solid state, a strong, sharp singlet at 2551 cm^{-1} (H) and a sharp, intense absorption at 1912 cm^{-1} (D) adjacent to a weaker, well-resolved band at 1931 cm^{-1} are observed. Contrary to

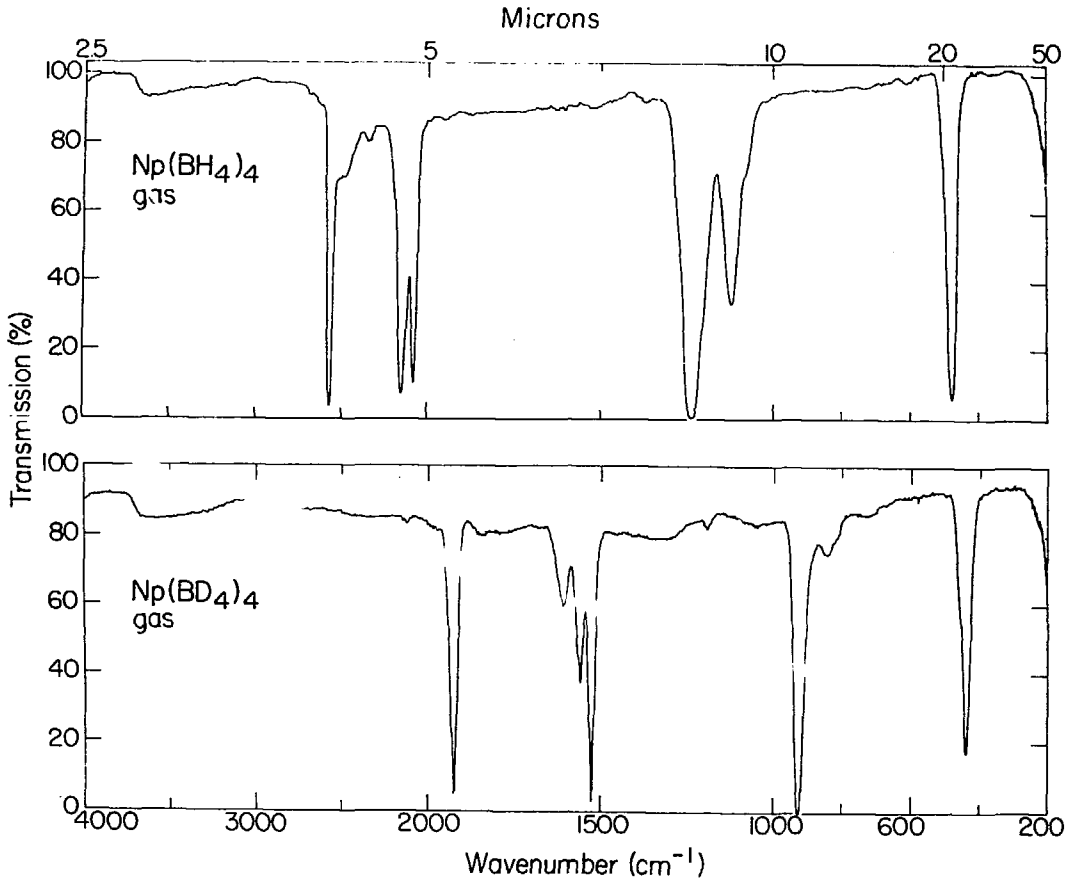

Figure 5. Gas Phase Infrared Spectra of $Np(BH_4)_4$ and $Np(BD_4)_4$. XBL798-2702

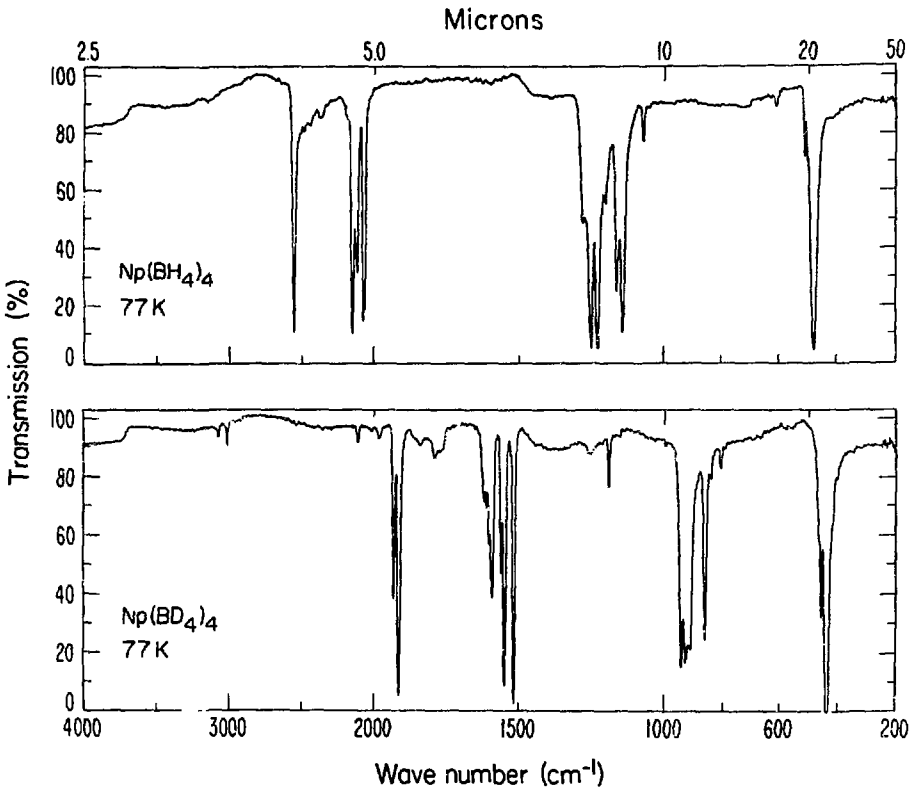

Figure 6. Solid-state Infrared Spectra.

XBL 794-9123A

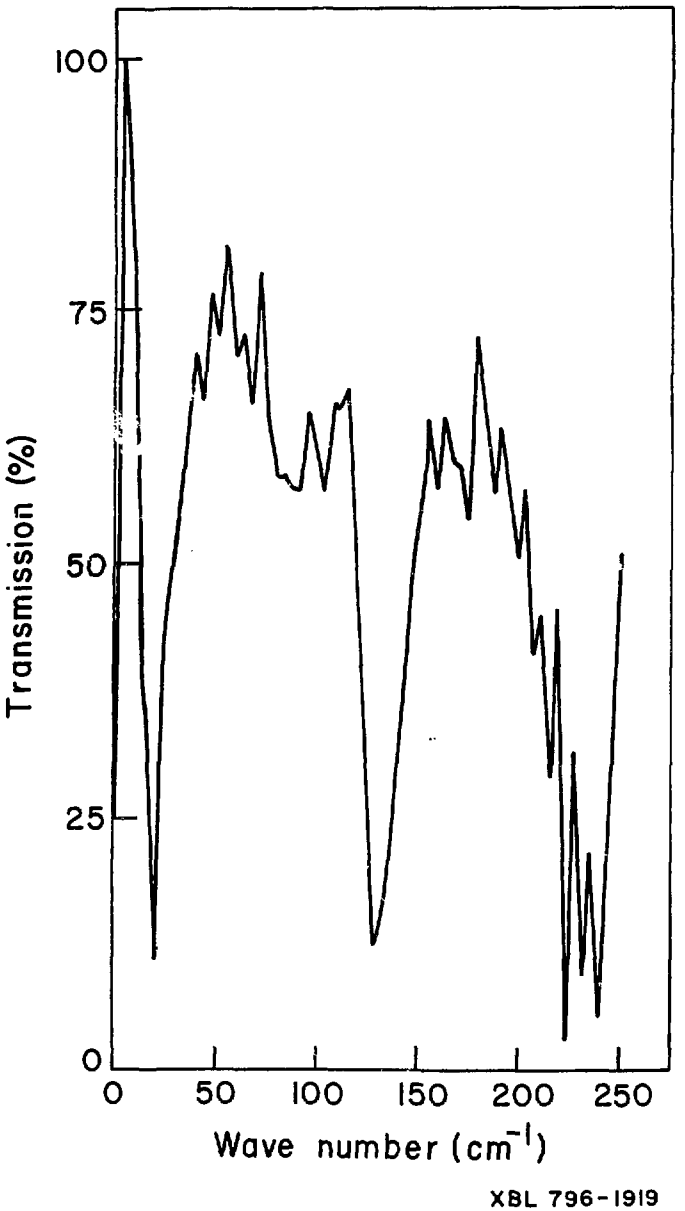

Figure 7. Far Infrared Spectrum of $Np(BH_4)_4$ at 77 K.

Table 1

Observed Bands in Gas Phase IR Spectra of $Np(BH_4)_4$ and $Np(BD_4)_4$

Energy (cm^{-1})	Assignment	Internal Coordinates	Comments
		$Np(BH_4)_4$	
2568	$\nu_1^{T_2}$	νBH_t	strong
2480	$2\nu_4^{T_2}$, $2\nu_5^{T_2}$		weak, v. broad
2350	$\nu_{4,5}^{T_2} + \nu_6^{T_2}$		weak, broad
2155	$\nu_2^{T_2}$	νBH_b	strong
2130	$\nu_{2a}^{T_2}$ [a]		shoulder on $\nu_2^{T_2}$
2084	$\nu_3^{T_2}$	νBH_b	strong, sharp
1280			shoulder on $\nu_{4,5}^{T_2}$
1240	$\nu_4^{T_2}$, $\nu_5^{T_2}$	δHBH, νMH_b	v. strong, broad
1205	$\nu_3^{E} + \nu_9^{T_2}$		shoulder on $\nu_{4,5}^{T_2}$
1122	$\nu_6^{T_2}$	δHBH	medium, broad
1080			shoulder on $\nu_6^{T_2}$
478	$\nu_8^{T_2}$	νMB, νMH_b	strong
		$Np(BD_4)_4$	
3092	$2\nu_2^{T_2}$		v. weak, broad
3030	$2\nu_3^{T_2}$		v. weak, broad
1930	$^{10}B(\nu_1^{T_2})$ [b]	$\nu^{10}BD_t$	shoulder on $\nu_1^{T_2}$
1922	$\nu_1^{T_2}$	νBD_t	strong
1605	$2\nu_3^{T_1}$ [c]		medium
1562	$^{10}B(\nu_2^{T_2})$	$\nu^{10}BD_b$	shoulder on $\nu_2^{T_2}$
1558	$\nu_2^{T_2}$ [c]	νBD_b	strong
1526	$\nu_3^{T_2}$	νBD_b	strong, sharp
1190	^1H	δHBD	weak, broad
928	$\nu_{4,5}^{T_2}$	δDBD, νMD_b	v. strong
845	$\nu_6^{T_2}$	δDBD	weak, broad

Table 1 (continued)

Energy (cm^{-1})	Assignment	Internal Coordinates	Comments
		$Np(BD_4)_4$	
810			shoulder on $\nu_6^{T_2}$
437	$\nu_7^{T_2}$	νMB, νMD_b	strong

In the table: H_t = terminal hydrogen, H_b = bridging hydrogen, v = very

[a]This feature could not be assigned with any certainty so it was given the identifying symbol, $\nu_{2a}^{T_2}$.

[b]A fundamental in parenthesis next to an impurity atom is that mode in which the impurity atom is participating.

[c]These two bands are in Fermi resonance.

Table 2

Observed Bands in 77K IR (4000-25 cm^{-1}) and Raman (2600-100 cm^{-1}) Spectra of $Np(BH_4)_4$

Energy (cm^{-1})	Assignment	Internal Coordinates	Comments
2557	$\nu_1^{A_1}$	νBH_t	medium, R.
2551	$\nu_1^{T_2}$	νBH_t	strong, sharp, IR
2490	$2\nu_4^{T_2}$		weak, IR
2445	$2\nu_5^{T_2}$		weak, IR
2378	$\nu_4^{T_2} + \nu_6^{T_2}$		weak, broad, IR
2149	$\nu_2^{A_1}$	νBH_b	medium, R
2143	$\nu_2^{T_2}$	νBH_b	strong, sharp, IR
2123	ν_1^{E}	νBH_b	medium, R
2117	$^{10}B(\nu_{2a}^{T_2})$		medium, shoulder
2110	$\nu_{2a}^{T_2}$		medium, sharp, IR
2069 (2070)[a]			strong, sharp doublet
2059 (2060)	$\nu_3^{T_2}$	νBH_b	medium, + shoulder, R
1283	$\nu_3^{A_1}$	νMH_b, δHBH[b]	medium, R
1276			medium, sharp, IR
1260	ν_2^{F}	νMH_b, δHBH	weak, R
1247 (1255)	$\nu_4^{T_2}$	νMH_b, δHBH	v. strong IR, medium, R
1225 (1230)	$\nu_5^{T_2}$	νMH_b, δHBH	v. strong IR, medium, R
1199 (1205)	$\nu_3^{E} + \nu_9^{T_2}$		medium IR, weak, R
1159			medium +, IR
1138 (1127)	$\nu_6^{T_2}$	δHBH, νMH_b	strong, IR, weak, R
1068			weak, IR
1053	ν_3^{E}	δHBH	medium, R
639	$\nu_8^{T_2} + \nu_5^{E}$		weak, R
611	$\nu_8^{T_2} + \nu_9^{T_2}$		weak, IR
517	$\nu_4^{A_1}$	νMB	strong, R
509 (506)	$\nu_7^{T_2}$?		weak, sharp, IR, medium, R

Table 2 (continued)

Energy (cm^{-1})	Assignment	Internal Coordinates	Comments
475 (~480)	$\nu_8^{T_2}$	νMB	v. strong, IR, shoulder, R
168	ν_5^{E}	δHMH	v. strong, sharp, R
130 (141)	$\nu_9^{T_2}$	δHMH	strong, IR, medium R

[a] T_2 modes also seen in the Raman are shown next to the IR value in parenthesis.

[b] The more important internal coordinates are to the left of the lesser important ones.

Table 3

Observed Bands in 77K IR (4000-25 cm^{-1}) and Raman (2300-100 cm^{-1}) Spectra of $Np(BD_4)_4$

Energy (cm^{-1})	Assignment	Internal Coordinates	Comments
3092	$^{10}B(2\nu_2{}^{T_2})$		v. weak, IR
3074	$2\nu_2{}^{T_2}$		weak, sharp, IR
3012	$2\nu_3{}^{T_2}$		weak, sharp, IR
2110	$^{1}H(\nu_3{}^{T_2}(H))$	νBH_b	weak, IR
1979			weak, broad, IR
1931	$^{10}B(\nu_1{}^{T_2})$	$\nu^{10}BD_t$	medium, sharp, IR
1925	$^{10}B(\nu_1{}^{A_1})$	$\nu^{10}BD_t$	shoulder, R
1913	$\nu_1{}^{A_1}$	νBD_t	medium +, R
1912	$\nu_1{}^{T_2}$	νBD_t	strong, sharp, IR
1842	$2\nu_4{}^{T_2}$		weak, sl. broad, IR
~1780 (~1780)	$\nu_4{}^{T_2} + \nu_6{}^{T_2}$		weak, v. broad, IR, R
1619	$\nu_1{}^{E}$	νBD_b	weak, R
1621, 1614, 1604, 1598	^{10}B, $^{1}H(2\nu_3{}^{T_1})$?		medium, sharp, IR
1593 (1592)	$2\nu_3{}^{T_1}{}^{a}$		medium +, sharp, IR, R
1560	$^{10}B(\nu_2{}^{T_2})$	$\nu^{10}BD_b$	medium, sharp, IR
1548 (1549)	$\nu_2{}^{T_2}{}^{a}$	νBD_b	strong, sharp IR, medium R
1517	$\nu_2{}^{A_1}$	νBD_b	strong, sharp, R
1516	$\nu_3{}^{T_2}$	νBD_b	v. strong, sharp, IR
1251	$^{1}H(\nu_4{}^{T_2}(H))$	νMH_b, δHBD	weak, v. broad, IR
1191	$^{1}H(\nu_{4,5}{}^{T_2}(H))$	νMH_b, δHBD	weak +, sharp, IR
955	$\nu_3{}^{A_1}$	νMD_b, δDBD	weak +, R
941			strong, sharp, IR
926	$\nu_4{}^{T_2}$	νMD_b, δDBD	strong, IR
917	$\nu_5{}^{T_2}$	νMD_b, δDBD	strong, IR
910	$\nu_3{}^{E} + \nu_9{}^{T_2}$		strong, IR

Table 3 (continued)

Energy (cm^{-1})	Assignment	Internal Coordinates	Comments
905	ν_2^E	δDBD, νMD_b	weak, sl. broad, R
860 (863)	$\nu_6^{T_2}$	δDBD	strong, sharp, IR, weak, R
838			weak, IR
802			weak, IR
795	ν_3^E	δDBD	weak, R
475	$\nu_4^{A_1}$	νMB	strong, R
457	$^{10}B(\nu_7^{T_2})$	$\nu M^{10}B$	medium, sharp IR
437 (440)	$\nu_7^{T_2}$	νMB	v. strong, IR, shoulder, R
406	$\nu_8^{T_2}$?	νMD_b, δDBD	v. weak, IR
154	ν_5^E	δDMD	v. strong, sharp
112 (121)	$\nu_9^{T_2}$	δDMD	strong, IR, medium, R

[a]These two bands are in Fermi resonance.

previous assignments for these high frequency features of other metal borodeuterides,[25] the bands at 1925 and 1931 cm^{-1} are due to the ^{10}B isotope and not to a ^{1}H impurity.[26] The strong IR bands at 2551 cm^{-1} (H) and 1912 cm^{-1} (D) are therefore assigned an $\nu_1{}^{T_2}$.

In terms of energy, these modes are well separated from all others and are practically pure νBH_t (νBD_t) stretches with $\nu H/\nu D = 1.33$, indicating substantial hydrogen motion along with slight amounts of boron motion. As is observed in other metal borohydrides,[12(b),25] these vibrational states exhibit small matrix shifts to lower energies.

2200-2000 cm^{-1} (1600-1500 cm^{-1}) Region

Similar to the above region, normal modes in this energy range are nearly pure stretches arising from one set of equivalent internal coordinates. The twelve boron bridging-hydrogen bonds (BH_b) transform as $A_1 + E + T_1 + 2T_2$ giving four allowed Raman and 2 IR bands. In the gas phase, the IR spectrum shows two strong absorptions at 2155 and 2084 cm^{-1} (H) which experience matrix shifts to lower energies and in the solid, appear at 2143 and 2069 cm^{-1}. These can be assigned as $\nu_2{}^{T_2}$ and $\nu_3{}^{T_2}$, respectively. It is seen that $\nu_2{}^{T_2}$ (H) is broader than $\nu_3{}^{T_2}$ (H) due to the presence of a weak shoulder at 2130 cm^{-1} ($\nu_{2a}^{T_2}$) which is well defined in the solid at 2110 cm^{-1}. Also $\nu_3{}^{T_2}$ (H) undergoes changes from the gas to the solid state and splits into a very close doublet with a separation of 10 cm^{-1}.

The Raman spectrum of $Np(BH_4)_4$ displays three bands instead of the predicted four at 2149, 2123, and 2070 cm^{-1} since $\nu_2{}^{A_1}$ at 2149 cm^{-1}

overlaps with the out-of-phase $\nu_2^{T_2}$ modes seen in the IR at 2143 cm^{-1}. The medium-intensity 2070 cm^{-1} Raman line, exhibiting a shoulder at 2060 cm^{-1}, corresponds to $\nu_3^{T_2}$, the doublet at 2069, 2059 cm^{-1} in the IR. Since no IR coincidence is observed for the Raman feature at 2123 cm^{-1}, its assignment as ν_1^{E} is straightforward.

Unlike the case of $Np(BH_4)_4$, this region for the borodeuteride is complicated by the presence of a mysterious, third IR band and a fourth Raman band. This apparent anomaly is also noted in the spectra of Zr,[22,25] Hf,[22,27] and U[28] borodeuterides and an explanation for its existence has yet to be confirmed. Gas phase IR transitions occur at 1605, 1558, and 1526 cm^{-1} and shift slightly to 1593, 1548, and 1516 cm^{-1} in the solid. They also sharpen and considerable fine structure becomes apparent, especially on the 1593 cm^{-1} band. Comparing both energies and intensities of these bands with those of other borodeuterides,[25,28] the very intense spike at 1516 cm^{-1} is assigned as $\nu_3^{T_2}$ (D) with $\nu H/\nu D = 1.36$, consistent that expected for a νBH_b (νBD_b) stretch.

Identification of $\nu_2^{T_2}$ (D) is not immediately obvious now and the isotopic frequency ratios are not sufficiently sensitive to be useful. The four Raman bands are at 1619, 1592, 1549, and 1517 cm^{-1}. The strong, sharp peak at 1517 cm^{-1} is easily assigned as $\nu_2^{A_1}$[25,27] which is nearly coincident with its out-of-phase partner, $\nu_3^{T_2}$ (D), at 1516 cm^{-1}. Having $\nu H/\nu D = 1.31$ and no strong IR coincidence, the rather weak Raman transition at 1619 cm^{-1} is tentatively assigned as ν_1^{E} (D). Being practically of the same energies with the 1593 and 1548 cm^{-1} IR

bands, the remaining two Raman lines at 1592 and 1594 cm^{-1} are identified as T_2 species, one of which is $\nu_2^{T_2}$ (D). Isotopic frequency ratios make both equally-likely candidates although intensity considerations favor 1548 cm^{-1} (1549 cm^{-1}) as the fundamental.

As will be seen later, the νBH_b (νBD_b) fundamentals give rise to intense overtones and it is their presence in the borodeuteride, solid-state IR spectrum (Fig. 6) that allows the identification of $\nu_2^{T_2}$ (D). Above 3000 cm^{-1} are two weak but sharp peaks at 3012 and 3047 cm^{-1} (D), the former being $2\nu_3^{T_2}$ ($2 \times \nu_3^{T_2} = 3032$ cm^{-1}).[29] The other νBD_b fundamental, $\nu_2^{T_2}$, being similar in internal coordinate composition to $\nu_3^{T_2}$, will give the overtone seen at 3074 cm^{-1} while the other nonfundamental T_2 species (1593 or 1548 cm^{-1}) will not. Assuming equal degrees of anharmonicity in $\nu_2^{T_2}$ and $\nu_3^{T_2}$, the frequency for $\nu_2^{T_2}$ can be calculated as

$$\nu_2^{T_2} = 1/2\ (2\nu_2^{T_2} - 2\nu_3^{T_2}) + \nu_3^{T_2}$$

$$\nu_2^{T_2} = 1/2\ (3074-3012)\ cm^{-1} + 1516\ cm^{-1}$$

$$\nu_2^{T_2} = 1547\ cm^{-1}.$$

This value agrees very well with the observed ones, 1548 cm^{-1} (IR) and 1549 cm^{-1} (Raman). The origin of the other T_2 species at 1592 cm^{-1} (1593 cm^{-1}) will be discussed later.

<u>1300-1050 cm^{-1} (950-800 cm^{-1}) Region</u>

This region of fundamental activity is due to metal hydrogen-bridge stretches and internal-BH_4 bending motions. Each symmetrically equiva-

lent set of internal coordinates, $12MH_b$, $12H_bBH_b$, and $12H_tBH_b$ transforms as $A_1 + E + T_1 + 2T_2$. They are also similar in energy and give complicated normal coordinates.

Since the pattern of spectra lines in this area depends so strongly on the geometry of the MH_3B unit[1,18,30] and to a somewhat lesser degree on bond strengths involving the central metal, substantial differences are observed in the spectra[31,32] of the tetrahedral actinide borohydrides and Zr, Hf $(BH_4)_4$.

Three IR and six Raman fundamentals are expected here. As seen in the gas phase spectrum of $Np(BH_4)_4$, there is a strong, broad band at 1240 cm^{-1}, a weaker one at 1122 cm^{-1}, and a number of shoulders visible on both. For the borodeuteride these same modes are at 928 and 845 cm^{-1}, respectively, with the latter decreasing in intensity. Spectra of monomeric $U(BH_4)_4$[28,32,33] and $U(BD_4)_4$[28] are very similar and show bands at 1237 and 1121 cm^{-1} (H) but only one is reported for $U(BD_4)_4$ at 924 cm^{-1}. The three IR fundamentals are not distinguishable in the gas phase where the broadness of the levels may have caused overlap of two fundamentals which are close in energy.

More in line with symmetry predictions, the isostructural zirconium and hafnium borohydrides[22] exhibit three gas phase IR bands which were assigned as $\nu_4^{T_2}$, $\nu_5^{T_2}$, and $\nu_6^{T_2}$. For comparison, these are given below.

$Zr(BH_4)_4$:	1288	1218	1034 cm^{-1}	$Zr(BD_4)_4$:	1020	922	812 cm^{-1}
$Hf(BH_4)_4$:	1300	1228	1020 cm^{-1}	$Hf(BD_4)_4$:	945	923	830 cm^{-1}
Assignment:	$\nu_4^{T_2}$?	$\nu_5^{T_2}$	$\nu_6^{T_2}$	Assignment:	$\nu_4^{T_2}$?	$\nu_5^{T_2}$	$\nu_6^{T_2}$

The $\nu_4{}^{T_2}$ assignments are not well substantiated especially in the boro-deuterides where the bands were observed to be very weak.

Assignment of 1240 cm^{-1} (H) and 928 cm^{-1} (D) for the neptunium compounds as $\nu_4{}^{T_2}$ or $\nu_5{}^{T_2}$ is somewhat arbitrary but choosing 1122 cm^{-1} (H) 845 cm^{-1} (D) as $\nu_6{}^{T_2}$ seems correct. The isotopic frequency ratios are 1.34 and 1.33 for $\nu_{4,5}{}^{T_2}$ and $\nu_6{}^{T_2}$ respectively and are considered reasonable for these kinds of normal modes. Turning to the low temperature IR and Raman spectra will help in locating the remaining fundamentals.

Differences in the solid state IR spectra between $An(BH_4)_4$ and Zr, $Hf(BH_4)_4$ are even more pronounced as the gas bands split into many sharper ones and the shoulders become clearly resolved. With so many spectral features seen here, choosing the correct ones as the fundamentals is impossible with the present data. However, any reasonable choice will be sufficiently satisfactory for the calculations which follow.

The broad 1240 cm^{-1} (H) gas phase absorption band experiences no observable matrix shift and in the solid divides into a strong, symmetrical doublet at 1247 and 1225 cm^{-1}. Although the weaker absorption at 1276 cm^{-1} seems to correspond well to that at 1286 cm^{-1} in $Zr(BH_4)_4$ as $\nu_4{}^{T_2}$, its low intensity does not favor this and with the lack of other information, $\nu_4{}^{T_2}$ is assigned to 1247 cm^{-1} and $\nu_5{}^{T_2}$ to 1225 cm^{-1}. Matrix effects are most strongly observed for $\nu_6{}^{T_2}$ which increases in energy and splits into two peaks at 1159 and 1138 cm^{-1} where the most intense and least shifted one is rather arbitrarily assigned as $\nu_6{}^{T_2}$.

A similar situation is seen for $Np(BD_4)_4$. The strong, gas phase absorption at 928 cm^{-1} becomes several equally intense bands at 941, 926, 917, and 910 cm^{-1} with the least shifted ones, 926 and 917 cm^{-1} being labelled as $\nu_4{}^{T_2}$ and $\nu_5{}^{T_2}$, respectively. The very weak feature in the gas spectra at 845 cm^{-1} sharpens in the solid and moves to higher energy, 860 cm^{-1}, but unlike the borohydride case, does not split. It is assigned as $\nu_6{}^{T_2}$.

Overtones of these T_2 fundamentals are observed in the IR spectra just as those of the νBD_b region are, but unfortunately, can offer no help in selecting fundamental transitions since they are very broad.

In the Raman spectra, the $\nu_3{}^{A_1}$ modes occur at 1283 cm^{-1} (H) and 955 cm^{-1} (D) yielding $\nu H/\nu D = 1.34$. E modes are easily spotted at 1260 cm^{-1} (H), 905 cm^{-1} (D) and 1053 cm^{-1} (H), 795 cm^{-1} (D) and conform to those of the Zr and Hf compounds. These are assigned as $\nu_2{}^{E}$ and $\nu_3{}^{E}$, respectively. A Raman line at 1230 cm^{-1} (H) identifies with 1225 cm^{-1} as $\nu_5{}^{T_2}$. For the borodeuteride, a weak peak at 863 cm^{-1} is close to the IR value of 860 cm^{-1} for $\nu_6{}^{T_2}$.

<u>600-450 cm^{-1} (450-400 cm^{-1}) Region</u>

At this point in the search, $1A_1$, 2E, and $3T_2$ fundamentals need to be located, of which four Raman and two IR bands are expected in this spectral region. νMB stretches transform as $A_1 + T_2$ and so for these two modes, $\nu H/\nu D$ ratios should be near unity. For the other E and T_2 modes, the most significant contributions are from νHBH and νMH_b coordinates and therefore should give large $\nu H/\nu D$ ratios ≈ 1.3. Confusion as to the labelling of the two T_2 modes has arisen in the past[27] since it

was not realized that the large difference in $\nu H/\nu D$ ratios caused the corresponding borodeuteride mode of $\nu_8{}^{T_2}$ (H) to be $\nu_7{}^{T_2}$ (D) and not $\nu_8{}^{T_2}$ (D). Had potential energy distributions been calculated, the problem would not have existed. The situation was further complicated by the very low intensities of $\nu_7{}^{T_2}$ (H) and $\nu_4{}^{E}$ (H,D) in the Zr and Hf compounds.

The νMB stretching modes are located easily with the aid of their low $\nu H/\nu D$ ratios. Strong IR bands at 475 cm^{-1} (H) and 437 cm^{-1} (D) give $\nu H/\nu D = 1.087$ and are assigned as $\nu_8{}^{T_2}$ (H) and $\nu_7{}^{T_2}$ (D). Their in-phase counterparts, $\nu_4{}^{A_1}$ (H,D), are observed at 517 cm^{-1} (H) and 475 cm^{-1} (D) in the Raman with $\nu H/\nu D = 1.088$. The T_2 fundamentals are present only weakly as shoulders near the bases of the $\nu_4{}^{A_1}$ bands. Accompanying much boron motion are ^{10}B effects and these are clearly visible in the low temperature IR spectrum at 457 cm^{-1} (D).

Once more spectral differences appear between the actinide and Hf, Zr compounds. The obvious distinction is seen in both gas phase and solid-state IR spectra of the borodeuterides in which a medium intensity band occurs at ~400 cm^{-1} in each of the Zr, $Hf(BD_4)_4$ spectra but not in those of $U(BD_4)_4$ or $Np(BD_4)_4$. Authors[25,27] have assigned that mode as $\nu_8{}^{T_2}$ (D) lying below the intense $\nu_7{}^{T_2}$ (D) fundamental by about 80 cm^{-1}. Strangely, the corresponding Zr, $Hf(BH_4)_4$ peaks are only very weakly observed around 570 cm^{-1} and there is doubt that they are seen at all. It was pointed out[19(a),22] that the great intensity of the 400 cm^{-1} bands may be due to a Fermi resonance interaction with

another T_2 species having an energy similar to $\nu_8^{T_2}$ (D) such that resonance is seen only in the borodeuterides. Candidates which have the correct $\nu H/\nu D$ ratios were given in the papers but they either included A_2 or T_1 modes or unreasonable difference combinations.

From a comparison of the $\nu H/\nu D$ ratios in the actinide compounds, where the interaction is absent, to those in Zr, $Hf(BH_4)_4$ and Zr, $Hf(BD_4)_4$, it appears that resonance is occurring in the Zr and Hf compounds between the two fundamentals $\nu_7^{T_2}$ (D) and $\nu_8^{T_2}$ (D). The $\nu H/\nu D$ ratio for the Np compounds is 1.087 and is the same for those of uranium. A similar ratio is expected for the Zr and Hf compounds if no resonance is operating and a smaller value if there is resonance, since interacting states repel each other. The $\nu H/\nu D$ ratios are calculated to be 1.043 for Zr and 1.026 for Hf, indicating perhaps that the mixing of wavefunctions is more complete in the Hf case.

The assignment of 398 cm^{-1} ($Hf(BD_4)_4$) and 418 cm^{-1} ($Zr(BD_4)_4$) as $\nu_8^{T_2}$ (D) may still be correct since two T_2 fundamentals close in energy can interact. In fact, this assignment is more reasonable than the others previously mentioned because if the unperturbed $\nu_7^{T_2}$ (D) and $\nu_8^{T_2}$ (D) are close in energy, the corresponding borohydride fundamentals will not be and therefore cannot interact. It is concluded that the $\nu_7^{T_2}$ (H) and $\nu_8^{T_2}$ (D) are inherently very weakly IR active and only the latter is experimentally observed for Zr, $Hf(BD_4)_4$ through the effects of Fermi resonance with $\nu_7^{T_2}$ (D). The lack of an observed state other than $\nu_7^{T_2}$ (D) for $Np(BD_4)_4$ in the 450-370 cm^{-1} range precludes an assignment for $\nu_8^{T_2}$ (D).

The last fundamental in this region is ν_4^E. In the Raman spectra of Zr and Hf compounds, very weak lines were assigned as ν_4^E at 533 cm^{-1} (H), 435 cm^{-1} (D) for Zr and tentative assignments were made for Hf at 570 cm^{-1} (H), 430 cm^{-1} (D). In the Np Raman spectra no bands near those of Zr and Hf were noted. There is a very weak peak at 639 cm^{-1} (H) and another on the low energy side of $\nu_4^{A_1}$ (H) at 506 cm^{-1} with an IR coincidence at 509 cm^{-1} but no firm assignments can be made since borodeuteride correspondences are lacking. The rather strong 506 cm^{-1} (H) Raman band cannot be in resonance with $\nu_4^{A_1}$ at 517 cm^{-1} and thus an equally intense borodeuteride counterpart is expected at 380-400 cm^{-1}, but none is seen. It is tentatively identified as a T_2 species and even though it is possible for a weak IR T_2 band to be strong in the Raman effect, it cannot be assigned as $\nu_7^{T_2}$ (H) with any degree of certainty. So like $\nu_7^{T_2}$ (H), no assignment of ν_4^E can be made at this time.

<u>200-25 cm^{-1} Region</u>

The last two modes in the lowest energy regime are $\nu_9^{T_2}$ and ν_5^E which are comprised of δHMH and to a lesser extent δBMB bends. The Raman spectra show very strong bands at 163 cm^{-1} (H) and 154 cm^{-1} (D). Weaker ones are observed at 141 cm^{-1} (H) and 121 cm^{-1} (D). A priori, either of a pair could be the E or T_2 fundamental since both species are symmetry allowed in the Raman. Both bands have approximately the same νH/νD ratio and the Teller-Redlich isotopic product rules[2] (see Table 4) are not very useful here as assignments are missing from each of the E and T_2 symmetry blocks.

Very similar Raman spectra were found for the Zr[25,34] and Hf[27] compounds and the intense lines were assigned as the E modes. Substantiating their assignments were the observations of $\nu_9^{T_2}$ in the IR for the borohydrides only; the borodeuteride transitions occurred too near or below the lower limit of the IR spectrometer to be observed.

Although these assignments could reasonably be carried over to the Np case, it was decided that far IR spectra would be needed to confirm the analogy since in other regions of the spectra, there have been very noticeable differences between Hf, Zr and the Np compounds. The IR spectrum of $Np(BH_4)_4$ in the region below 200 cm^{-1} is shown in Fig. 7. A similar one was taken of $Np(BD_4)_4$ but is not shown. Absorption bands were seen at 130 cm^{-1} (H) and 112 cm^{-1} (D) and are no doubt $\nu_9^{T_2}$. Although slightly higher values were obtained from the Raman spectra, 140 cm^{-1} (H) and 121 cm^{-1} (D), there is no problem in assigning the intense Raman lines at 168 cm^{-1} (H) and 154 cm^{-1} (D) as ν_5^E, thus justifying the earlier analogy.

Teller-Redlich Isotopic Product Rules

The theoretical ratios[2,23] for the product of frequencies are given in Table 4 and can sometimes detect gross errors in a set of assignments. These ratios are rigorously correct for zero-order frequencies which, as will be discussed later, can be very different from the observed ones due to anharmonicity. Usually observed frequencies give ratios slightly smaller than predicted theoretically.[35]

Table 4

Teller-Redlich Isotopic Product Rules

H → D Isotope Change

Symmetry Block	Formula	Ratio ^{10}B	Ratio ^{11}B
A_1	$\prod_{i=1}^{4} \frac{\omega_{i_H}}{\omega_{i_D}} = \left(\frac{m_D}{m_H}\right)^{3/2}$	2.82	2.82
A_2	$\frac{\omega_H}{\omega_D} = \left(\frac{m_D}{m_H}\right)^{1/2}$	1.41	1.41
E	$\prod_{i=1}^{5} \frac{\omega_{i_H}}{\omega_{i_D}} = \left(\frac{m_D}{m_H}\right)^{2}$	3.99	3.99
T_1	$\prod_{i=1}^{5} \frac{\omega_{i_H}}{\omega_{i_D}} = \left(\frac{m_D}{m_H}\right)^{5/2} \left(\frac{I_D}{I_H}\right)^{1/2}$	6.49	6.44
T_2	$\prod_{i=1}^{9} \frac{\omega_{i_H}}{\omega_{i_D}} = \left(\frac{m_D}{m_H}\right)^{7/2} \left(\frac{M_D}{M_H}\right)^{1/2}$	11.59	11.58
	$^{10}B \rightarrow {}^{11}B$ Isotope Change	H	D
A_1	$\prod_{i=1}^{4} \frac{\omega_{i_{10}}}{\omega_{i_{11}}} = \left(\frac{m_{11}}{m_{10}}\right)^{1/2}$	1.049	1.049
E	$\prod_{i=1}^{5} \frac{\omega_{i_{10}}}{\omega_{i_{11}}} = \left(\frac{m_{11}}{m_{10}}\right)^{1/2}$	1.049	1.049

Table 4 (continued)

Symmetry Block	Formula	Ratio H	Ratio D
T_1	$\prod_{i=1}^{5} \frac{\omega_{i_{10}}}{\omega_{i_{11}}} = \left(\frac{m_{11}}{m_{10}}\right)^{1/2} \left(\frac{I_{11}}{I_{10}}\right)^{1/2}$	1.083	1.075
T_2	$\prod_{i=1}^{9} \frac{\omega_{i_{10}}}{\omega_{i_{11}}} = \left(\frac{m_{11}}{m_{10}}\right) \left(\frac{M_{11}}{M_{10}}\right)^{1/2}$	1.1070	1.1066
	Zr,Hf → Np Mass Change*	Zr	Hf
T_2	$\prod_{i=1}^{9} \frac{\omega_{i_{Zr,Hf}}}{\omega_{i_{Np}}} = \left(\frac{m_{Np}}{m_{Zr,Hf}}\right)^{1/2} \left(\frac{M_{Np}}{M_{Zr,Hf}}\right)^{1/2}$	2.26 (H) 2.21 (D)	1.29 (H) 1.28 (D)

In the table: m = isotope mass, M = molecular mass, I = moment of inertia.

*The ^{11}B isotope is used here.

A complete list of assignments for the A_1 block was obtained from the spectra and the experimental Teller-Redlich ratio is 2.77 which compares favorably to the theoretical value of 2.82. Because the E and T_2 symmetry blocks are still incomplete, a reasonable value of 1.33 for the $\nu H/\nu D$ ratios of ν_4^E and $\nu_7^{T_2}$ (H), ($\nu_8^{T_2}$ (D)) is used. Experimental ratios now come out to be 10.1 and 3.51 for the T_2 and E blocks respectively. Theoretical ratios are 11.58 and 3.99. Inversely, the theoretical values can give information on missing fundamentals. It seems certain that from Zr, $Hf(BD_4)_4$ spectra, the missing $\nu_8^{T_2}$ (D) for $Np(BD_4)_4$ would occur at 380 ± 15 cm^{-1}. Using this value and the theoretical ratio of 11.58, $\nu_7^{T_2}$ (H) = 550 cm^{-1} which agrees well to the tentative $\nu_7^{T_2}$ (H) assignment of 570 cm^{-1} for $Hf(BH_4)_4$.

Normal Coordinate Analysis

The Program

After having tentatively assigned 32 of 36 fundamental modes, a normal coordinate analysis seemed feasible. The program NORCRD used to calculate frequencies and normal coordinates was devised by Gwinn[36] and later expanded to include least squares fitting, group theory, and other calculations by D. Reuter.[37] Especially well suited for electronic computers, the program sets up the normal coordinate problem in terms of mass-weighted Cartesian coordinates. Since the 3N Cartesian coordinates are all independent, the question of redundancy never arises.

In this coordinate system, the kinetic energy matrix is simply a unit matrix while the potential energy can be written as

$$2V = \sum_{ijkl} \frac{\partial q_k}{\partial x_i} \frac{\partial q_l}{\partial x_j} F_{kl} dx_i dx_j$$

where q_k, q_l are any generalized coordinates x_i, x_j are Cartesian coordinates; and F_{kl} are the force constants in terms of bond distances and angles. The orthogonal transformation which diagonalizes $\underset{\sim}{V}$ is just the transformation from mass-weighted Cartesian coordinates to normal coordinates. Only after the diagonalization process are rotation and translation separated from the normal vibrations.

Using a nonlinear least squares routine, NORCRD finds the best-fit values for an input set of force constants by minimizing the difference between the observed and calculated vibrational frequencies for all isotopes simultaneously. All of the symmetry information about a calculated normal mode is contained in its eigenvector and the program insures that each calculated frequency which is adjusted to agree with an observed one is of the same symmetry type.

In addition to many other physical quantities which the program can calculate,[37] those of moment of inertia, the first derivative of the dipole moment with respect to the normal coordinates, and the normal coordinates in terms of Cartesian coordinates were included in this study.

The molecular structure parameters used in the calculations were taken from the results of the low temperature Xray structure investigation on $Np(BH_4)_4$ and are given in Table 5. For the majority of the calculations, the T_d staggered ($\omega = 60°$) configuration[38] was used but the other T_d eclipsed ($\omega = 0°$) structure was also tried.

Table 5

Molecular Structure Parameters for $Np(BH_4)_4$

Distances (Å)	
Np - B	2.455
B - H_t	1.000
B - H_b	1.170
Np - H_b	2.341 (calc)

Angles (deg)	
H_t - B - H_b	109.47
H_b - B - H_b	109.47
B - Np - B	109.47
Np - H_b - B	81.37 (calc)

Masses (amu)	
^{237}Np	237.048
^{10}B	10.0129
^{11}B	11.00931
H	1.007825
D	2.0140

Internal coordinate sets used in this analysis are the $4BH_t$, $12BH_b$, $12MH_b$, 4MB bonds; $12H_tBH_b$, $12H_bBH_b$, $12H_bMH_b$ (triads of H_b's related by C_3) angles; and $36H_bBMB$ torsions. Variations in these sets were considered during the fitting process. The fundamental frequencies which were input into the program are listed in Tables 2, 3, and 7 and each was given unit weight.

The Least Squares Fit

Primary Force Constants. For a molecule of this type there are 86 independent force constants allowed by symmetry.[45] Since there are not nearly this many observed spectral data, an approximate force field was derived using a limited number of the more important force constants. During the course of least squares fitting, only four or five constants could be fit simultaneously per run. By fitting a different group of four or five constants each time until all have been adjusted, a steady-state condition was reached and then a conclusion as to the quality of the field could be made. Throughout all runs, the torsion constant was held fixed since the dependences of all other frequencies besides the unobserved ν^{A_2} on this constant are negligible.

Initially some of the values of the force constants were taken from the results of the $Hf(BH_4)_4$ study[19(a),27] and others were guesses. Fits using no interaction constants were tried first and then interaction constants were added later to achieve better agreement. To a large degree, the quality of a force field was determined by the standard deviation (SD) it produced and is defined as

$$SD = \left(\sum_i \frac{(\nu_{calc} - \nu_{obs})_i^2}{N - M} \right)^{\frac{1}{2}}$$

where N is the total number of frequencies for all isotopes, M is the number of force constants allowed to vary, and i is the number of observations.

The νBH_t constant converged rapidly and was not significantly affected by other changes in the potential function so it was held fixed during subsequent runs. Likewise the νBH_b constant was easily fit but interactions between it and other constants were observed and the anomalously poor agreement of $\nu_2^{T_2}$ (D) with the calculated value made the adjustment of the νBH_b constant frequently necessary.

Attempts to add a set of 12 δBH_bM bends to the 4 νMB coordinates resulted in very low values of the bending constant while the stretching constant remained significant. No improvement in the fits was obtained and those using only the bends gave very large SD's. Therefore the bends were dropped.

Difficulty was encountered in fitting the δHBH bends. The δH_tBH_b and δH_bBH_b force constants are highly correlated and reaching convergence took many iterations, if it occurred at all, when the two were simultaneously varied. No problem in convergence was noted when only one was allowed to vary at a time in the least squares fit. Trials with both internal coordinate sets combined into one representing 24 δHBH_b bends gave significant discrepancies between observed and calculated frequencies and were no longer considered.

The low energy modes proved to be a problem in that ν_5^E calculated lower than $\nu_9^{T_2}$ in disagreement with experiment. Since $\nu_4^{A_1}$ was also

affected by the δHMH constant, satisfactory agreement could not be attained by simply reducing the force constant value. In one test, the 12 δHMH coordinates were replaced by 6 δBMB angles but no improvement was seen. Even when the two sets were used together, the δBMB constant diminished practically to zero and eventually was deleted. The other symmetry-equivalent set of 12 δHMH bends described by Keiderling et al.[27] as δHMH (tor), where the H_b atoms are related by C_2, has a very large A_2 component and affects ν^{A_2} to a similar degree as our torsion. Its influence on the other frequencies is negligible and consequently does not help in fitting ν_5^E or $\nu_9^{T_2}$.

At this point the νBH_t frequencies, $\nu_1^{A_1}$ and $\nu_1^{T_2}$ fit well, with observed and calculated frequencies agreeing to better than 0.5%. Both pairs of νBH_b and νBD_b modes have calculated separations larger than are observed especially in the borodeuteride. The $\nu_4^{T_2}$ and $\nu_5^{T_2}$ modes calculate too high in the borohydride but too low in the borodeuteride. However, considering how sensitive these frequencies are to bridge geometry, the agreement is satisfactory. From the IR spectra, it was seen that $\nu_6^{T_2}$ experiences a large matrix shift to higher frequency so the low calculated value is not unexpected and agrees surprisingly well with the unperturbed gas phase frequency. The A_1 modes gave excellent agreement to the Teller-Redlich rules and in general fit the best, although $\nu_3^{A_1}$, which depends essentially on νMH_b and δHBH, calculated low without interaction permitted between the two internal coordinate sets. The calculated E modes were fairly satisfactory, with the greatest per cent deviation occurring in ν_5^E.

Employing a set of only 8 primary force constants, the SD = 20 cm^{-1} for 32 observed frequencies.

Interaction Constants. A few well-chosen interaction constants in the potential function can greatly improve the overall agreement between observed and calculated frequencies and give a more realistic description of the normal coordinates. The number of interaction constants greatly exceeds that of primary or diagonal ones and it would be unwise to try them all. Knowing some of their properties is worthwhile and three of them are given below.

(a) Symmetry considerations are helpful in choosing an interaction constant. A mode will be influenced by an interaction constant only if its symmetry species is common to both sets of internal coordinates involved in the constant.

(b) The modes which are most affected by an interaction constant have as their major components at least one of two internal coordinate sets constituting the constant.

(c) The pair of internal coordinates which interact strongly will be close together in energy.

For complex molecules, it is not possible, a priori, to know whether a frequency will increase or decrease when an interaction constant is introduced. In this work, in more than 50% of the cases, the frequency decreased.

The choice of the first interaction constant, $\nu BH_b:\nu BH_b$, where stretches in one BH_4^- group could only interact with those in the same

BH_4^- group made use of all three of the above properties. This type of interaction is labelled an "intra" for intragroup interaction. It was found that the motion of a BH_b bond did not significantly couple to the motion of another such bond located in another borohydride group. In fact this is generally true for all internal coordinates and is the basic assumption of the SGVFF model.[23] Being similar in energy, the interaction is appreciable and its inclusion made a definite improvement to the quality of the fit. The $\nu_2^{T_2}$, $\nu_3^{T_2}$ separation decreased as desired, but as will be discussed later, the calculated $\nu_2^{T_2}$ (D) is still too high. The $\nu_2^{A_1}$ and ν_1^{E} modes also improved and the SD dropped to 16 cm^{-1}.

Similarly the νMH_b modes improved with the addition of a νMH_b:νMH_b interaction constant and the SD dropped to 12 cm^{-1}.

The three types of binary combinations using the δH_tBH_b and δH_bBH_b coordinates did not lower the SD significantly since very likely the problem of poor agreement does not lie in their interaction but more probably in the accurate location of the fundamentals and in the molecular structure parameters. There was difficulty in obtaining convergence and in the end, these constants were eliminated.

Including a νMB:νMB interaction did help somewhat but later was replaced by a more effective constant involving the νMB stretching coordinates. The lowest frequency modes did not get better using a δHMH:δHMH interaction constant. An unsymmetrical interaction constant employing the above two low energy coordinates, νMB:δHMH, was then considered since,

by property (a), would only affect the A_1 and T_2 modes and it was hoped that $\nu_9^{T_2}$ would decrease while ν_5^E would remain unchanged. The interaction constant converged to a large but negative value, decreasing the SD to 11 cm^{-1} and improving the calculated $\nu_4^{A_1}$ frequency. Unfortunately, it caused not the reduction of $\nu_9^{T_2}$ but a slight increase. Some relief, however, was found in the low energy modes by the use of a $\nu MH_b:\delta HMH$ interaction which converged rapidly to the value in Table 6.

For the 1200 cm^{-1} (H) and 900 cm^{-1} (D) regions, the only interaction constant tried which assumed a reasonably large value was the $\nu BH_b:\delta H_bBH_b$ constant and the final SD = 10 cm^{-1} for the SGVFF given in Table 6.

Although the staggered orientation of bridging hydrogen atoms is the most stable from a steric point of view,[1,39] the results of Smith et al.[25,38] and Plato and Hedberg[19(c)] on $Zr(BH_4)_4$ prompted an investigation on the eclipsed, tetrahedral structure of $Np(BH_4)_4$. As far as the computer program was concerned, all that needed to be changed were the Cartesian coordinates of the new H_b atom positions and the numbering of the δHMH bending coordinates. The SGVFF given in Table 6 was applied to the eclipsed structure and the resulting frequencies are shown in Table 8. The major differences in the two structures are in the δHBH and δHMH bending modes, as expected. The ν_5^E frequencies are calculated very low while those in the 1200 cm^{-1} (H) and 900 cm^{-1} (D) region of the spectra increased. Allowing the force constants to vary in a number of fits improved the bending frequencies only moderately and

Table 6

Best-Fit Force Constants for Neptunium Borohydride

Primary Force Constants		Interaction Force Constants	
Internal Coordinates	Value	Internal Coordinates	Value
νBH_t	3.51 md/Å	νBH_b : νBH_b (intra)	.04 md/Å
νBH_b	2.36	νMH_b : νMH_b	.02
νMH_b	.37	νMB : δH_bMH_b	-.09 md/rad
νMB	1.28	νBH_b : δH_bBH_b (intra)	.04
δH_tBH_b	.28 mdÅ/rad^2	νMH_b : δH_bMH_b	.04
δH_bBH_b	.36		
δH_bMH_b (C_3)	.26		
ϵH_bBMB	.18*		

*The torsion force constant is essentially undetermined since the A_2 mode is not observed. It was set at .18 and kept constant during all fits.

ν_5^E always calculated less than 100 cm^{-1}. Since the SD was never below 17 cm^{-1} in any of the runs, the eclipsed structure was finally disregarded.

The observed and calculated frequencies using the best-fit force constants in Table 6 are listed in Table 7. The agreement in the A_1 symmetry block is very good for both isotopes while that in the others is satisfactory. For reasons unknown, the low energy modes do not agree as well as the higher ones, a result also found in the analyses of Zr[25] and Hf[27] borohydrides. Of course, by including a greater number of force constants, the fit can be made better but it was the purpose of this study to explain the spectra with a small number of constants. It is completely senseless to expect an exact fit to a set of anharmonic frequencies of a quantum mechanical system as complex as $Np(BH_4)_4$ using a classical harmonic oscillator model. That such a good fit was obtained seems almost fortuitous.

The final force fields derived for $Zr(BH_4)_4$, $Hf(BH_4)_4$, and $Np(BH_4)_4$ are slightly different in composition and one must be cautious in making close comparisons of the force constants. It is seen that all the primary constants are very similar especially the νBH_t force constants. In general the stretching constants are ten times the bending constants and the bending constants are about ten times the interaction constants. The νMH_b force constants in all three studies were unusually low while the νMB constants turned out to be large and may be indicative of significant M-B bonding in these molecules.

The allowed fundamentals which were not observed in the spectra are calculated at reasonable energies. Going back to the spectra and looking

Table 7

Fundamental Vibrations (cm^{-1}) of $Np(BH_4)_4$ and $Np(BD_4)_4$

Normal Mode	$Np(BH_4)_4$ Observed	$Np(BH_4)_4$ Calculated	$Np(BD_4)_4$ Observed	$Np(BD_4)_4$ Calculated
$\nu_1\ ^{T_2}$	2551	2557	1912	1911
$\nu_2\ ^{T_2}$	2143	2144	1548	1603
$\nu_3\ ^{T_2}$	2069	2078	1516	1485
$\nu_4\ ^{T_2}$	1247	1266	926	897
$\nu_5\ ^{T_2}$	1225	1223	917	895
$\nu_6\ ^{T_2}$	1138	1104	860	824
$\nu_7\ ^{T_2}$	——	575	437	447
$\nu_8\ ^{T_2}$	475	488	——	415
$\nu_9\ ^{T_2}$	130	156	112	139
$\nu_1\ ^{A_1}$	2557	2554	1913	1905
$\nu_2\ ^{A_1}$	2149	2147	1517	1523
$\nu_3\ ^{A_1}$	1283	1284	955	953
$\nu_4\ ^{A_1}$	517	517	475	466
$\nu_1\ ^{E}$	2123	2117	1619	1589
$\nu_2\ ^{E}$	1260	1270	905	899
$\nu_3\ ^{E}$	1053	1089	795	807
$\nu_4\ ^{E}$	——	571	——	413
$\nu_5\ ^{E}$	168	142	154	125
$\nu_1\ ^{T_1}$	——	2116	——	1587
$\nu_2\ ^{T_1}$	——	1256	——	889
$\nu_3\ ^{T_1}$	——	1084	——	810
$\nu_4\ ^{T_1}$	——	565	——	405
$\nu_5\ ^{T_1}$	——	405	——	288
$\nu\ ^{A_2}$	——	288	——	204

Table 8

Calculated Frequencies for the Eclipsed ($\omega = 0°$) Structure

Mode	$Np(^{11}BH_4)_4$	$Np(^{11}BD_4)_4$
$\nu_1^{T_2}$	2556.9	1910.9
$\nu_2^{T_2}$	2110.2	1584.3
$\nu_3^{T_2}$	2066.5	1476.8
$\nu_4^{T_2}$	1289.2	915.1
$\nu_5^{T_2}$	1223.2	895.1
$\nu_6^{T_2}$	1121.5	825.8
$\nu_7^{T_2}$	587.7	448.3
$\nu_8^{T_2}$	486.3	425.7
$\nu_9^{T_2}$	147.1	130.7
$\nu_1^{A_1}$	2555.8	1908.7
$\nu_2^{A_1}$	2076.5	1480.3
$\nu_3^{A_1}$	1333.5	972.3
$\nu_4^{A_1}$	499.0	455.1
ν_1^{E}	2106.8	1581.7
ν_2^{E}	1287.5	915.0
ν_3^{E}	1126.4	829.2
ν_4^{E}	584.8	423.4
ν_5^{E}	96.8	85.2
$\nu_1^{T_1}$	2107.4	1582.4
$\nu_2^{T_1}$	1259.3	891.4
$\nu_3^{T_1}$	1081.8	805.4
$\nu_4^{T_1}$	577.3	416.5
$\nu_5^{T_1}$	519.6	367.7
ν^{A_2}	288.2	203.9

for transitions near the calculated values gives no positive results, however. The symmetry forbidden T_1 modes were also calculated and identified by the program and since the A_1, E, and T_2 modes were calculated rather accurately, it does not seem likely that the frequencies for the T_1 modes are in serious error. The $\nu_3^{T_1}$ mode was observed for $Zr(BH_4)_4$ by inelastic neutron scattering[39] at 594 cm^{-1} and the corresponding 565 cm^{-1} value for that in $Np(BH_4)_4$ is quite reasonable in light of the overall trend found in this analysis where even for the non T_2 modes, $\nu(Np) < \nu(Zr)$. Further assurance is given by the Teller-Redlich product rules. The ratio for the calculated frequencies from Table 7 is 5.0 and is not considered too unreasonable when compared to the theoretical value of 6.4 using the values of the moments of inertia computed by the program. Using the same arguments, the values of ν^{A_2} simply obtained by setting the torsion constant to 0.18 are again probably not too bad considering the value of ν^{A_2} for $Zr(BH_4)_4$ of 302 cm^{-1} observed by Tomkinson and Waddington.[39] It is comforting to know that the calculated $\nu H/\nu D$ ratio of 1.41 for ν^{A_2} agrees exactly with the theoretical value.

Assignment of Nonfundamental IR Bands

4000-200 cm^{-1} Region

Now that a better understanding of $Np(BH_4)_4$ and $Np(BD_4)_4$ fundamentals was supplied by the normal coordinate analysis, an effort in identifying the nonfundamental transitions seen in the low temperature IR spectra was carried out. These extra features are either impurity, overtone

or combination bands. Since overtones and combinations are rarely seen in the ordinary Raman effect, just those which are IR allowed will be discussed here. Only overtones of T_1 and T_2 fundamentals are IR active and the active combination bands comprised of observable parent fundamentals are $A_1 + T_2$, $E + T_2$, and $T_2 + T_2$. Difference bands are also allowed but due to intensity arguments, they are not considered in this work.[2] Although the T_1 modes are not directly observable, it was found that their overtone activity is important and the calculated values from Table 7 are used but with caution. They are also involved in numerous combinations: $A_2 + T_1$, $E + T_1$, $T_1 + T_1$, and $T_1 + T_2$.

It is perhaps worth mentioning at this point of the possibility of $Np(BH_4)_4$ exhibiting electronic transitions in this spectral region. Unlike Zr^{4+} and Hf^{4+}, Np^{4+}([Rn]$5f^3$) has unpaired electrons which can undergo transitions within the ^4I manifold.[40] In a tetrahedral crystalline field, two transitions can take place between the ground Γ_6 state[41] and the two excited Γ_8 levels of the $^4I_{9/2}$ manifold.[42] In contrast to vibrational states, the electronic states should show only very weak H → D shifts and not necessarily to lower energies.

The only possible candidate for a $\Gamma_6 \rightarrow \Gamma_8$ transition, is the weak but sharp 1199 cm^{-1} (H), 1191 (D) peaks. However, this is readily ruled out since this 1191 cm^{-1} band is also seen in $Zr(BD_4)_4$ at 1188 cm^{-1}[25] and is of the same shape and relative intensity and is explained as a ^1H impurity of the very strong 1200 cm^{-1} region of the borohydride spectrum.[43] The 1199 cm^{-1} (H) band is seen weakly in the Raman at ~1205 cm^{-1}

and is tentatively assigned as $\nu_3^E + \nu_9^{T_2} = 1183\ cm^{-1}$ or $1194\ cm^{-1}$ if the Raman value of $\nu_9^{T_2}$ is used. For the deuteride, this combination yields $907\ cm^{-1}$ and may be buried in the strong absorption there.

Pure transitions of this kind are forbidden by parity and only through configuration interaction with the higher d states can forced transitions be observed. Therefore electronic transitions in very thin samples are expected to be extremely weak. Vibronic bands could have appreciable intensity but their identification as such is not possible at this time.

From the gas phase IR spectra of mixed isotopic molecules of the formula $ZrB_4H_xD_{16-x}$[43] and $NpB_4H_xD_{16-x}$,[44] the other ^1H impurity bands listed in Tables 1 and 3 are easily assigned.

Locating ^{10}B bands is not as easy since their isotopic shifts are inherently smaller and there is always some of each boron isotope in every sample. Besides knowing the $^{10}B/^{11}B$ abundance ratio and the atomic masses, calculations using the previously derived SGVFF on various isotopically substituted molecules are the only handles on the problem of locating ^{10}B impurity bands.

The program NORCRD is very well suited for calculations of this kind. Davies et al.[22] determined that 44% of all metal tetrakis-borohydride molecules contain four ^{11}B atoms, 40% contain one ^{10}B atom, and 14% have two of each isotope. Calculations of the fundamental frequencies for the molecules $Np(^{10}BH_4)_x(^{11}BH_4)_{4-x}$ and $Np(^{10}BD_4)_x(^{11}BD_4)_{4-x}$, where x = 0, 1, 2, 4 assuming the SGVFF of Table 6 were performed and

the results are given in Tables 9-13. Although molecules in which x = 4 are exceedingly rare, their calculated frequencies were invaluable in assigning the new, lower symmetry modes.

Tables 10 and 11 (x = 1) were particularly useful. The IR band at 1931 cm^{-1} (D) (see Fig. 6) is nicely predicted by the calculations. Even though the corresponding band in the borohydride spectrum should occur at 2564 cm^{-1} and be observable, it is evidently too close to $\nu_1^{T_2}$ in the wavenumber range where the resolution is half of that below 2000 cm^{-1}. A separation of 11 cm^{-1} between $\nu_2^{T_2}$ (D) and $^{10}B(\nu_2^{T_2}(D))$ is predicted and observed. However, no ^{10}B band on $\nu_3^{T_2}$ (D) is expected or seen due to the small calculated separation of 1.6 cm^{-1}. None of the "extra" bands in the δHBH bending region at 1300-1050 cm^{-1} (H) and 950-800 cm^{-1} (D) is due to ^{10}B since there is very little boron motion. This is also noted in the Zr and Hf borohydride spectra[22] and the calculations agree.

Distinct ^{10}B effects are clearly visible in the νMB stretching region. Unfortunately the calculations indicate smaller shifts than are observed. Both the borohydride and borodeuteride fundamentals at 475 cm^{-1} (H) and 437 cm^{-1} (D) reveal subbands of reasonable intensity and energy but that in the borohydride spectrum at 509 cm^{-1} is too high in frequency to be $^{10}B(\nu_8^{T_2})$ with a $\nu^{10}/\nu^{11} > 1.050$. The 457 cm^{-1} (D) peak gives a satisfactory frequency ratio of 1.046 but is predicted at only 444 cm^{-1} (x = 1) and 449 cm^{-1} (x = 4). This brings up again the question as to whether 509 cm^{-1} (H) could be $\nu_7^{T_2}$ (H).

Table 9

Calculated Frequencies for $Np(^{10,11}B^{1,2}H_4)_4$

Symmetry	$Np(^{11}BH_4)_4$	$Np(^{10}BH_4)_4$	$Np(^{11}BD_4)_4$	$Np(^{10}BD_4)_4$
$\nu_1^{T_2}$	2557.0	2570.8	1911.1	1932.4
$\nu_2^{T_2}$	2143.8	2155.7	1602.9	1620.5
$\nu_3^{T_2}$	2078.4	2081.1	1485.2	1487.4
$\nu_4^{T_2}$	1266.3	1266.5	897.3	900.6
$\nu_5^{T_2}$	1223.2	1227.6	895.0	897.5
$\nu_6^{T_2}$	1104.4	1111.3	823.7	830.5
$\nu_7^{T_2}$	574.8	576.0	447.3	459.2
$\nu_8^{T_2}$	488.4	505.8	414.6	415.8
$\nu_9^{T_2}$	156.1	160.7	139.3	142.3
$\nu_1^{A_1}$	2554.2	2567.5	1905.1	1925.5
$\nu_2^{A_1}$	2146.6	2147.4	1523.4	1524.1
$\nu_3^{A_1}$	1284.3	1290.8	953.0	961.2
$\nu_4^{A_1}$	517.0	536.4	466.0	479.1
ν_1^{E}	2117.3	2130.0	1588.5	1606.8
ν_2^{E}	1270.0	1270.1	899.0	899.1
ν_3^{E}	1088.6	1094.7	807.2	813.2
ν_4^{E}	571.2	572.7	412.6	413.9
ν_5^{E}	142.1	146.9	125.1	128.3
$\nu_1^{T_1}$	2115.9	2128.5	1587.1	1605.2
$\nu_2^{T_1}$	1255.6	1255.6	888.8	889.0
$\nu_3^{T_1}$	1084.1	1091.3	810.2	817.1
$\nu_4^{T_1}$	565.0	565.9	404.5	405.2
$\nu_5^{T_1}$	404.7	405.0	287.8	288.0
ν^{A_2}	288.2	288.2	203.9	203.9

Table 10

Calculated Frequencies for $Np(^{11}BH_4)_3{}^{10}BH_4$

Symmetry in T_d	$Np(^{11}BH_4)_3{}^{10}BH_4$		
	A_1	A_2	E
$\nu_1{}^{T_2}$	2570.1		2557.0
$\nu_2{}^{T_2}$	2143.9		2149.6
$\nu_3{}^{T_2}$	2080.2		2078.5
$\nu_4{}^{T_2}$	1266.3		1266.4
$\nu_5{}^{T_2}$	1226.5		1223.2
$\nu_6{}^{T_2}$	1104.4		1107.6
$\nu_7{}^{T_2}$	574.8		575.3
$\nu_8{}^{T_2}$	498.7		488.4
$\nu_9{}^{T_2}$	156.2		158.0
$\nu_1{}^{A_1}$	2554.8		
$\nu_2{}^{A_1}$	2146.8		
$\nu_3{}^{A_1}$	1286.0		
$\nu_4{}^{A_1}$	524.6		
$\nu_1{}^{E}$			2123.1
$\nu_2{}^{E}$			1270.1
$\nu_3{}^{E}$			1090.6
$\nu_4{}^{E}$			571.6
$\nu_5{}^{E}$			143.2
$\nu_1{}^{T_1}$		2115.9	2116.7
$\nu_2{}^{T_1}$		1255.6	1255.6
$\nu_3{}^{T_1}$		1084.1	1085.7
$\nu_4{}^{T_1}$		565.0	565.3
$\nu_5{}^{T_1}$		404.7	404.8
ν^{A_2}		288.2	

Table 10 (continued)

Correlation Table

T_d	$\longrightarrow$ C_{3v}
A_1	A_1
A_2	A_2
E	E
T_1	A_2+ E
T_2	A_1+ E

In the new point group, C_{3v}, the A_1 and E modes are IR and Raman active. A_2 is both IR and Raman inactive.

Table 11

Calculated Frequencies for $Np(^{11}BD_4)_3{}^{10}BD_4$

Symmetry in T_d	$Np(^{11}BD_4)_3{}^{10}BD_4$		
	A_1	A_2	E
$\nu_1{}^{T_2}$	1931.0		1911.1
$\nu_2{}^{T_2}$	1602.9		1614.4
$\nu_3{}^{T_2}$	1486.8		1485.2
$\nu_4{}^{T_2}$	899.1		897.4
$\nu_5{}^{T_2}$	897.1		895.1
$\nu_6{}^{T_2}$	823.7		827.0
$\nu_7{}^{T_2}$	454.3		447.3
$\nu_8{}^{T_2}$	414.7		415.1
$\nu_9{}^{T_2}$	139.3		140.5
$\nu_1{}^{A_1}$	1906.3		
$\nu_2{}^{A_1}$	1523.6		
$\nu_3{}^{A_1}$	955.2		
$\nu_4{}^{A_1}$	471.2		
$\nu_1{}^{E}$			1594.2
$\nu_2{}^{E}$			899.0
$\nu_3{}^{E}$			807.9
$\nu_4{}^{E}$			412.8
$\nu_5{}^{E}$			125.9
$\nu_1{}^{T_1}$		1587.1	1587.9
$\nu_2{}^{T_1}$		888.8	888.9
$\nu_3{}^{T_1}$		810.2	812.9
$\nu_4{}^{T_1}$		404.5	404.8
$\nu_5{}^{T_1}$		287.8	287.9
ν^{A_2}		203.9	

Table 12

Calculated Frequencies for $Np(^{11}BH_4)_2(^{10}BH_4)_2$

Symmetry in T_d	$Np(^{11}BH_4)_2(^{10}BH_4)_2$ A_1	A_2	B_1	B_2
$\nu_1^{T_2}$	2569.3		2570.8	2557.0
$\nu_2^{T_2}$	2151.1		2148.1	2153.5
$\nu_3^{T_2}$	2079.7		2080.9	2078.6
$\nu_4^{T_2}$	1266.4		1266.4	1266.4
$\nu_5^{T_2}$	1225.3		1227.6	1223.2
$\nu_6^{T_2}$	1108.5		1106.7	1110.0
$\nu_7^{T_2}$	575.5		575.1	575.7
$\nu_8^{T_2}$	494.5		505.7	488.4
$\nu_9^{T_2}$	158.8		157.3	159.6
$\nu_1^{A_1}$	2555.5			
$\nu_2^{A_1}$	2147.0			
$\nu_3^{A_1}$	1287.6			
$\nu_4^{A_1}$	529.3			
ν_1^{E}	2122.3	2129.3		
ν_2^{E}	1270.1	1270.1		
ν_3^{E}	1091.0	1093.5		
ν_4^{E}	571.8	572.0		
ν_5^{E}	144.2	144.6		
$\nu_1^{T_1}$		2116.6	2124.1	2118.3
$\nu_2^{T_1}$		1255.6	1255.6	1255.6
$\nu_3^{T_1}$		1085.8	1088.9	1085.5
$\nu_4^{T_1}$		565.4	565.7	565.2
$\nu_5^{T_1}$		404.8	404.9	404.8
ν^{A_2}		288.2		

Table 12 (continued)

Correlation Table

$T_d \longrightarrow$	C_{2v}
A_1	A_1
A_2	A_2
E	$A_1 + A_2$
T_1	$A_2 + B_1 + B_2$
T_2	$A_1 + B_1 + B_2$

In the new point group, C_{2v}, all but A_2 are IR active; all all are Raman active.

Table 13

Calculated Frequencies for $Np(^{11}BD_4)_2(^{10}BD_4)_2$

Symmetry in T_d	$Np(^{11}BD_4)_2(^{10}BD_4)_2$			
	A_1	A_2	B_1	B_2
$\nu_1^{T_2}$	1929.5		1932.4	1911.1
$\nu_2^{T_2}$	1616.0		1612.4	1618.3
$\nu_3^{T_2}$	1486.3		1487.4	1485.3
$\nu_4^{T_2}$	898.0		900.5	897.6
$\nu_5^{T_2}$	897.0		897.2	895.1
$\nu_6^{T_2}$	827.7		826.2	829.3
$\nu_7^{T_2}$	451.4		459.2	447.3
$\nu_8^{T_2}$	415.4		415.0	415.4
$\nu_9^{T_2}$	141.0		140.1	141.5
$\nu_1^{A_1}$	1907.6			
$\nu_2^{A_1}$	1523.8			
$\nu_3^{A_1}$	957.3			
$\nu_4^{A_1}$	474.4			
ν_1^{E}	1593.3	1606.0		
ν_2^{E}	899.1	899.1		
ν_3^{E}	809.6	808.2		
ν_4^{E}	413.1	413.2		
ν_5^{E}	126.6	126.8		
$\nu_1^{T_1}$		1587.8	1595.6	1589.4
$\nu_2^{T_1}$		888.9	888.9	888.9
$\nu_3^{T_1}$		815.6	814.6	811.4
$\nu_4^{T_1}$		404.9	405.1	404.7
$\nu_5^{T_1}$		287.9	287.9	287.8
ν^{A_2}		203.9		

To further explore the utility of these calculations, the frequencies of the molecules $Np(^{11}B^{1,2}H_4)_3(^{11}B^{1,2}H_3)^{2,1}H_{t,b}$ (e.g., $Np(^{11}B^2H_4)_3(^{11}B^2H_3)^1H_t = Np(^{11}BD_4)_3(^{11}BD_3)H_t$) investigated. Statistically, singly contaminated molecules with the impurity atom in the bridging position should be three times more abundant than those with a terminal impurity atom and their spectral features should be more easily seen. Unfortunately, the symmetry of the more abundant molecule is C_s and all 57 modes are nondegenerate and IR allowed, making an analysis of them intractable. The symmetry of the less abundant molecule is higher, C_{3v}, but its effects are seen only for the more highly contaminated samples. The calculated frequencies for both types of molecules are given in Tables 14-16.

Other conclusions relating to the spectra are difficult to draw since transition intensities and concentrations of the impure species are unknown. The program used in this analysis can compute the first derivative of the dipole moment with respect to the normal coordinates with an input set of partial charges on the atom. Infrared intensities are proportional to the square of these quantities.[45]

Approximate partial charge calculations were performed on metal borohydrides by Sanderson[46] and James[47] and using the values of partial charges: Np = +.772, B = +.095, H = -.072, intensities were calculated for $Np(^{11}B^{1,2}H_4)_4$. They were in mediocre agreement with experiment and there were a few major disparities which essentially showed the intensity calculations to be useless. The simple charge distribution,

Table 14

Calculated Frequencies for $Np(^{11}BD_4)_3{}^{11}BD_3H_t$

Symmetry in T_d	$Np(^{11}BD_4)_3{}^{11}BD_3H_t$ A_1	A_2	E
$\nu_1{}^{T_2}$	2552.0		1911.1
$\nu_2{}^{T_2}$	1603.0		1603.7
$\nu_3{}^{T_2}$	1499.7		1485.2
$\nu_4{}^{T_2}$	901.6		898.3
$\nu_5{}^{T_2}$	897.1		895.1
$\nu_6{}^{T_2}$	823.7		857.5
$\nu_7{}^{T_2}$	454.8		456.8
$\nu_8{}^{T_2}$	414.7		446.5
$\nu_9{}^{T_2}$	139.3		142.7
$\nu_1{}^{A_1}$	1906.6		
$\nu_2{}^{A_1}$	1527.3		
$\nu_3{}^{A_1}$	957.3		
$\nu_4{}^{A_1}$	472.3		
$\nu_1{}^{E}$			1589.3
$\nu_2{}^{E}$			1020.3
$\nu_3{}^{E}$			808.3
$\nu_4{}^{E}$			413.4
$\nu_5{}^{E}$			126.8
$\nu_1{}^{T_1}$		1587.1	1587.6
$\nu_2{}^{T_1}$		888.8	892.7
$\nu_3{}^{T_1}$		810.2	817.2
$\nu_4{}^{T_1}$		404.5	407.7
$\nu_5{}^{T_1}$		287.8	287.9
ν^{A_2}		203.9	

The point group of this molecule is C_{3v}.

Table 15

Calculated Frequencies for $Np(^{11}BH_4)_3{}^{11}BH_3D_t$

Symmetry in T_d	$Np(^{11}BH_4)_3{}^{11}BH_3D_t$ A_1	A_2	E
$\nu_1{}^{T_2}$	2554.9		2557.0
$\nu_2{}^{T_2}$	2144.2		2143.7
$\nu_3{}^{T_2}$	1865.6		2078.4
$\nu_4{}^{T_2}$	1266.3		1261.4
$\nu_5{}^{T_2}$	1216.3		1223.2
$\nu_6{}^{T_2}$	1104.4		1098.2
$\nu_7{}^{T_2}$	574.8		572.9
$\nu_8{}^{T_2}$	473.6		479.8
$\nu_9{}^{T_2}$	156.1		153.2
$\nu_1{}^{A_1}$	2153.0		
$\nu_2{}^{A_1}$	2105.7		
$\nu_3{}^{A_1}$	1281.0		
$\nu_4{}^{A_1}$	513.8		
$\nu_1{}^{E}$			2117.2
$\nu_2{}^{E}$			1268.9
$\nu_3{}^{E}$			1086.6
$\nu_4{}^{E}$			568.1
$\nu_5{}^{E}$			139.0
$\nu_1{}^{T_1}$		2115.9	2115.7
$\nu_2{}^{T_1}$		1255.6	1229.3
$\nu_3{}^{T_1}$		1084.1	1006.3
$\nu_4{}^{T_1}$		565.0	498.5
$\nu_5{}^{T_1}$		404.7	404.6
ν^{A_2}		288.2	

Table 16

Calculated Frequencies for $Np(^{11}BH_4)_3{}^{11}BH_3D_b$ and $Np(^{11}BD_4)_3{}^{11}BD_3H_b$

Symmetry in T_d	$Np(^{11}BH_4)_3{}^{11}BH_3D_b$		$Np(^{11}BD_4)_3{}^{11}BD_3H_b$	
	A'	A''	A'	A''
$\nu_1{}^{T_2}$	2557.0, 2556.0	2557.0	2125.5, 1911.1	1911.1
$\nu_2{}^{T_2}$	2143.8, 2133.3	2143.7	1898.3, 1602.9	1603.7
$\nu_3{}^{T_2}$	2078.4, 1574.5	2078.4	1507.2, 1485.3	1485.3
$\nu_4{}^{T_2}$	1266.3, 1260.8	1260.2	898.6, 897.3	898.4
$\nu_5{}^{T_2}$	1223.2, 1110.7	1221.0	896.8, 985.1	895.1
$\nu_6{}^{T_2}$	1104.3, 1092.4	1098.2	835.9, 823.7	846.1
$\nu_7{}^{T_2}$	574.8, 573.0	573.3	455.6, 447.3	447.4
$\nu_8{}^{T_2}$	488.4, 470.3	488.4	433.9, 414.6	426.5
$\nu_9{}^{T_2}$	156.1, 154.9	155.2	140.4, 139.3	139.9
$\nu_1{}^{A_1}$	2553.9		1906.7	
$\nu_2{}^{A_1}$	2145.6		1535.2	
$\nu_3{}^{A_1}$	1281.0		1161.1	
$\nu_4{}^{A_1}$	505.0		472.7	
$\nu_1{}^{E}$	2116.8	2117.1	1597.3	1589.8
$\nu_2{}^{E}$	1268.8	1268.8	945.2	1060.0
$\nu_3{}^{E}$	1085.4	1086.8	808.2	808.2
$\nu_4{}^{E}$	568.1	568.9	413.4	413.4
$\nu_5{}^{E}$	141.0	141.5	125.8	125.5
$\nu_1{}^{T_1}$	2090.2	2115.9, 2115.8	1587.9	1587.5, 1587.1
$\nu_2{}^{T_1}$	1237.5	1255.6, 1223.3	891.0	891.8, 888.8
$\nu_3{}^{T_1}$	998.7	1084.1, 972.0	815.3	817.5, 810.2
$\nu_4{}^{T_1}$	521.3	565.0, 544.5	407.2	406.9, 404.5
$\nu_5{}^{T_1}$	404.5	404.7, 367.4	287.8	307.3, 287.8
ν^{A_2}		274.1		

Table 16 (continued)

Correlation Table

T_d	$\longrightarrow$ C_s
A_1	A'
A_2	A"
E	A'+ A"
T_1	A'+ 2A"
T_2	2A'+ A"

In the new point group, C_s, both A' and A" modes are IR and Raman active.

as given above, does not describe the real situation in $Np(BH_4)_4$. For a clear understanding of the spectra, isotopically pure samples would have to be examined.

The identity of the troublesome 1593 cm^{-1} (D) IR absorption remains to be solved. It is apparent from Table 7 that while the agreement between the observed and calculated frequencies for $\nu_2^{T_2}$ (H) is very good, that for the borodeuteride is surprisingly poor. The fact that the 1593 cm^{-1} (D) band is so intense for a nonfundamental transition and $\nu_2^{T_2}$ (D) is so far removed from its calculated value suggests that Fermi resonance is operating. Identical effects in this same energy region only for the borodeuterides are also observed in $Zr(BD_4)_4$,[22,25] $Hf(BD_4)_4$,[19(a),27] $U(BD_4)_4$,[28] and $Al(BD_4)_3$.[12(b)] A possible explanation was given for $Zr(BD_4)_4$[22] as the first harmonic of a very weak, unassigned transition at 812 cm^{-1} (D) in Fermi resonance with $\nu_2^{T_2}$ (D) at 1603 cm^{-1}. This may be possible but still does not help since the origin of the 812 cm^{-1} band was never given and may have been caused by an impurity. Later the same authors[24] tentatively assigned the third band as the T_1 mode, $\nu_1^{T_1}$, allowed in their T symmetry model but made no mention of the obvious perturbation of $\nu_2^{T_2}$ (D) they reported earlier. In that same paper, they rejected their earlier explanation of Ref. 22.

In this work, the 1593 cm^{-1} band is assigned as the T_2 component of $2\nu_3^{T_1}$ (D) (of symmetry species $A_1 + E + T_2$) in resonance with $\nu_2^{T_2}$ (D) causing a mixing of wavefunctions and a change in intensities and energies. The calculated value of $2\nu_3^{T_1}$ is perhaps a bit high but anharmonicity, which must be present, could put it at the correct energy.

The nature of the high frequency subbands is interesting but must remain a mystery for now.

7400-4000 cm^{-1} Region

The near IR spectra of Zr and Np borohydrides are shown in Fig. 8 and listings of the observed bands are given in Tables 17-18. For polyatomic molecules, making assignments of the observed bands in the non-fundamental region is difficult since there are many possible symmetry allowed combinations and overtones. The effects of anharmonicity cause the non uniform spacing of vibrational levels as the quantum number, v, increases. Therefore the energy of an overtone or combination band will not be an exact multiple of the fundamental frequency or exactly the sum of the parent terms of a combination. Identification of such transitions is not a simple task as the degrees of anharmonicity are ordinarily unknown. The subject of anharmonicity is very complex in the case of polyatomic molecules but for diatomics it is better understood.[48] As was found in the normal coordinate analysis, the 2500 cm^{-1} (1900 cm^{-1}) region is practically pure νBH_t (νBD_t) stretches. This result and the νBD_t normal mode pictured in Fig. A1 suggest that a diatomic molecule approximation would be a useful model in describing this portion of the borohydride molecule.

The overtones of the νBH_t modes are seen at the high energy end of the spectra in Fig. 8 with the ^{10}B modes clearly visible. From the spectrum of a 1 mm thick $Zr(BH_4)_4$ crystal, transitions up to the 2nd harmonic of this fundamental were observed.

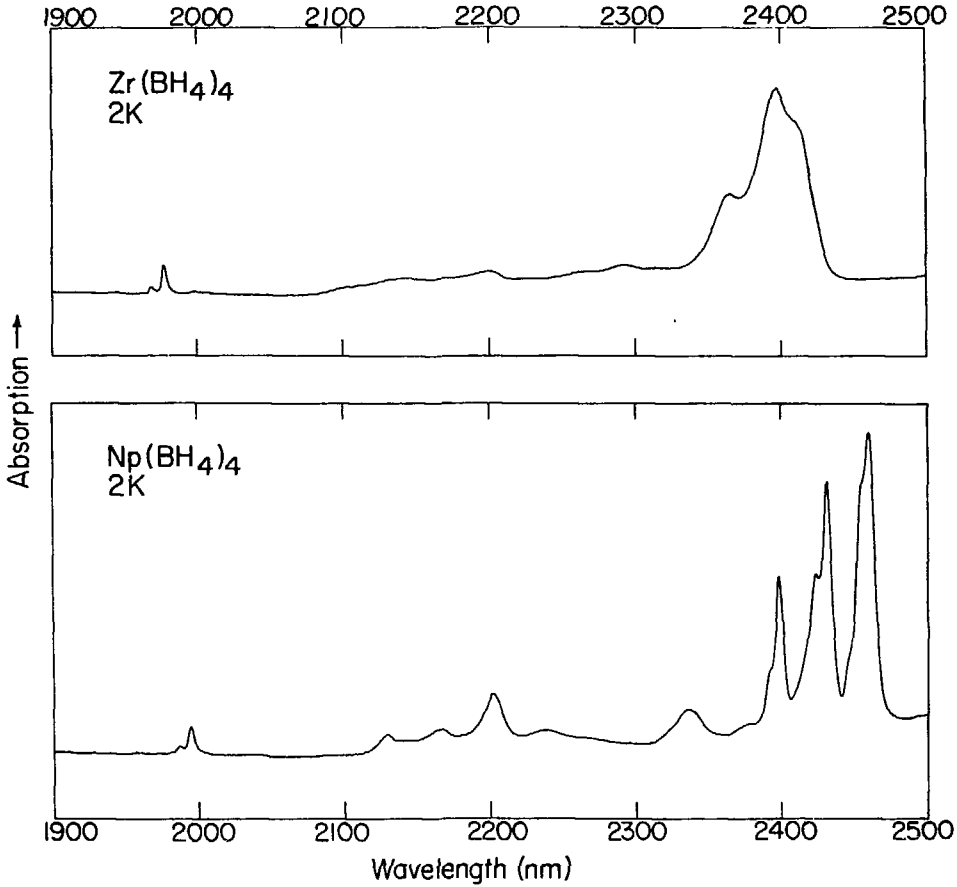

Figure 8. Near IR Spectra of $Zr(BH_4)_4$ and $Np(BH_4)_4$. XBL 798-2703

Table 17

Observed IR Bands (7400-4000 cm^{-1}) of $Np(BH_4)_4$ at 2K

Wavelength (nm)	Energy (cm^{-1})	Assignment	Comments
2460	4064	$2\nu_3^{T_2}$	v. strong
2457	4070	$^{10}B(2\nu_3^{T_2})$?	shoulder on $2\nu_3^{T_2}$
2447	4086	$\nu_2^{T_2} + \nu_3^{T_2}$	weak shoulder
2431	4113	$2\nu_{2a}^{T_2*}$	strong, sharp
2423	4126	$2\nu_1^{T_1}$	medium, sharp
2398	4169	$2\nu_2^{T_2}$	medium, sharp
2392	4180	$^{10}B(2\nu_2^{T_2})$	shoulder on $2\nu_2^{T_2}$
2378	4205	$\nu_3^{T_2} + \nu_6^{T_2} + \nu_3^{E}$	broad, v. weak
2335	4281	$2\nu_6^{T_2} + \nu_3^{T_2}$	broad, weak
2237	4469	$\nu_1^{T_2} + 2\nu_3^{T_2}$	v. broad, v. weak
2201	4542	$\nu_3^{T_2} + 2\nu_4^{T_2}$	broad, weak +
2165	4618	$\nu_2^{T_2} + 2\nu_4^{T_2}$	broad, weak
2129	4696	$\nu_2^{T_2} + 2\nu_3^{A_1}$	broad, weak
1994	5013	$2\nu_1^{T_2}$	weak, sharp
1986	5033	$^{10}B(2\nu_1^{T_2})$	weak
1654	6046	$3\nu_3^{T_2}$	broad
1353	7389	$3\nu_1^{T_2}$	weak

*See Table 1, footnote a.

Table 18

Observed IR Bands (7500-4000 cm^{-1}) of $Zr(BH_4)_4$ at [illegible]

Wavelength (nm)	Energy (cm^{-1})	Assignment	Comments
2407	4153	$2\nu_3^{T_2}$	shoulder, intense
2395	4174	$2\nu_1^{T_1}$ [a]	strong
2363	4230	$2\nu_2^{T_2}$	medium, broad
2290	4366	$\nu_3^{T_2} + \nu_6^{T_2} + \nu_3^{E}$	v. weak, broad
2261	4422	$\nu_3^{T_2} + 2\nu_6^{T_2}$	v. weak, broad
1976	5053	$2\nu_1^{T_2}$	weak +, sharp
1968	5080	$^{10}B(2\nu_1^{T_2})$	weak
1946 [b]	5138		medium
1634	6117	$3\nu_3^{T_2}$	v. intense, sharp
1621	6167	$3\nu_1^{T_1}$	shoulder on 3 ^{T}
1592	6279	$3\nu_2^{T_2}$	weak
1579	6332		medium, broad
1341	7458	$3\nu_1^{T_2}$	medium, sharp
1335	7487	$^{10}B(3\nu_1^{T_2})$	weak

[a] The calculated value for $\nu_1^{T_1}$ was taken from Ref. 27 for $Hf(BH_4)_4$ which is *believed to be more accurate than that from Ref. 25.*

[b] This band and the others listed below it are taken from the spectrum of the 1 mm pathlength crystal.

The energy level expression for a diatomic molecule with one anharmonicity constant, $\omega_e X_e$, is

$$E_V(cm^{-1}) = (V+\tfrac{1}{2})\omega_e - (V+\tfrac{1}{2})^2\omega_e X_e \quad , \qquad (1)$$

where ω_e is the zero-order frequency. Using the values of $n\nu_1^{T_2}$ (n = 1, 2, 3) for $Zr(BH_4)_4$ from Table 18, $\omega_e X_e$ is calculated to be 44 cm^{-1} which is typical for diatomics involving a hydrogen atom.[48] Similar calculations for $Np(BH_4)_4$ yield $\omega_e X_e$ = 45 cm^{-1}.

The borodeuterides do not show any overtones of this mode (see Fig. 6) but a sufficiently thick sample undoubtedly would. Therefore an anharmonicity constant cannot be calculated from the spectra. An approximate value can be obtained using the relation[48]

$$\frac{(\omega_e X_e)_D}{(\omega_e X_e)_H} = \frac{\mu_H}{\mu_D} \qquad (2)$$

where μ is the reduced mass. A value of $(\omega_e X_e)_D$ = 24 cm^{-1} is obtained for $Zr(BD_4)_4$ and $Np(BD_4)_4$.

From Eq. (1), a formula for the zero-order frequency is easily derived by letting $E_{V=1} = \nu_1$ and V = 1.

One gets

$$\omega_e = \nu_1 + 2\omega_e X_e \quad , \qquad (3)$$

where ν_1 is the observed fundamental frequency. In terms of ω_e and $\omega_e X_e$, the frequency of any overtone can be calculated from Eq. (1)

as
$$\nu_V = V\omega_e - V(V+1)\omega_e X_e \tag{4}$$

or from the fundamental frequency and anharmonicity constant

$$\nu_V = V\nu_1 + V(1-V)\omega_e X_e \tag{5}$$

Using Eq. (3), the harmonic frequencies are

Zr compounds: $\omega_{e1}{}^{T_2}$ (H) = 2657 cm^{-1} and $\omega_{e1}{}^{T_2}$ (D) = 1968 cm^{-1}

Np compounds: $\omega_{e1}{}^{T_2}$ (H) = 2641 cm^{-1} and $\omega_{e1}{}^{T_2}$ (D) = 1960 cm^{-1}

As a simple test of the accuracy of the diatomic approximations, the frequency of $^{10}B(2\nu_1{}^{T_2})$ can be calculated and compared to experiment. For $Zr(BH_4)_4$, the calculated separation between $2\nu_1{}^{T_2}$ and $^{10}B(2\nu_1{}^{T_2})$ is 24 cm^{-1} which is very close to the observed value. Similarly for $Np(BH_4)_4$, $^{10}B(\omega_{e1}{}^{T_2})$ = 2653 cm^{-1} and therefore $^{10}B(2\nu_1{}^{T_2})$ = 5013 + 24 = 5037 cm^{-1}. Using Eq. (4), the value of 5036 cm^{-1} is found in good agreement with the observed values of 5033 cm^{-1} in Table 17. According to Eq. (2), the anharmonicity constant is also dependent on the reduced mass. After correction $\omega_e X_e$ for ^{10}B, a better calculated value of $^{10}B(2\nu_1{}^{T_2})$ is 5034 cm^{-1}.

The next region of interest is the 2100-2250 nm region. Looking at the T_1 and T_2 frequencies in Table 7, it appears that no first or second harmonic has the correct energy. Third harmonics of the 1200 cm^{-1} region are possibilities but intensities of higher-order overtones decrease rapidly with v and it seems that the relative intensities of the observed bands may be too high. Overtones of $\nu_4{}^{T_2}$, $\nu_5{}^{T_2}$ (H) are seen

in the 4000-200 cm^{-1} spectra at 2490 and 2445 cm^{-1}. Since the modes in the 1200 cm^{-1} region are primarily δHBH bends, the diatomic approximation is no longer valid. Using linear extrapolations, the energies of the third harmonics are found to lie outside the 2100-2250 nm region. The frequencies for $4\nu_6^{T_2}$ and $4\nu_3^{T_1}$ are in the range but these are discarded on the grounds that not even their 1st harmonics are observed. The only probable origins left are the ternary combinations and some possible ones are given in Tables 17 and 18 where only energy and symmetry considerations were used.

The last group of bands are the most intense ones between 2350 and 2470 nm (4250 and 4050 cm^{-1}). Simple division by two suggests that the three bands are due to overtones of the three νBH_b stretching modes ($2T_2$, $1T_1$) seen at 2150-2060 cm^{-1} in $Np(BH_4)_4$ and 2180-2100 cm^{-1} in $Zr(BH_4)_4$.

As discussed previously overtones of the νBD_b modes appear as weak, sharp bands in the 4000-200 cm^{-1} spectra but only two bands are visible unlike the three predicted. In the borodeuterides, Fermi resonance is operating and perhaps the perturbation of $\nu_2^{T_2}$ (D) (and therefore $2\nu_2^{T_2}$ (D)) has caused the overlap of $2\nu_2^{T_2}$ and $2\nu_1^{T_1}$.

The diatomic molecule approximation was tried for these modes but as the normal coordinate calculations have shown, there is significant coupling between the νBH_b modes and other vibrations. With a non zero force constant between the M and H_b atoms, the BH_b bonds are not diatomic and deviations between theory and experiment are expected.

The borodeuteride overtones were easily identified in Fig. 6 and from them a value for $(\omega_e X_e)_D$ is calculated to be 10.5 cm^{-1} as the average for $\nu_2^{T_2}$ and $\nu_3^{T_2}$. From Eq. (2), $(\omega_e X_e)_H$ = 19 cm^{-1} for $Np(BH_4)_4$. Using Eq. (5), $2\nu_3^{T_2}(H)$ is calculated to be 4100 (4080) cm^{-1} for the 2069 (2059) cm^{-1} fundamental. Similarly $2\nu_2^{T_2}$ (H) = 4248 cm^{-1}. It is obvious that the two calculated values do not agree very well with the observed data. The diatomic model is not satisfactory in this case as the borohydride anharmonicity constant seems to be larger than is predicted and those for $\nu_3^{T_2}$ and $\nu_2^{T_2}$ appear to differ greatly.

It seems reasonable, based on the frequencies for $\nu_2^{T_2}$ (H), $\nu_3^{T_2}$ (H), and $\nu_1^{T_1}$ $(H)_{calc}$, that one might assign the 4064, 4113, and 4169 cm^{-1} observed bands as $2\nu_3^{T_2}$, $2\nu_1^{T_1}$, and $2\nu_2^{T_2}$, respectively. The 4113 cm^{-1} band has a peak nearby at 4126 cm^{-1} and if $2\nu_1^{T_1}$ is assigned as 4113 cm^{-1}, its 4126 cm^{-1} neighbor is too intense for a ^{10}B mode since at least two ^{10}B atoms per molecule are needed to produce the 13 cm^{-1} shift (see Table 12) and those molecules are only 14% abundant. A more reasonable explanation may be that 4113 cm^{-1} is $2\nu_{2a}^{T_2}$ (H) and 4126 cm^{-1} is $2\nu_1^{T_1}$ where the 13 cm^{-1} separation between the overtones agrees with the 6 cm^{-1} separation between the fundamentals.

The lowest frequency absorption $(2\nu_3^{T_2})$ has on its high-frequency side two shoulders at 4070 and 4086 cm^{-1}. From earlier ^{10}B calculations, $^{10}B(\nu_3^{T_2}) = \nu_3^{T_2} + 2$ cm^{-1}, indicating that the overtones should be separated by about 4 cm^{-1}. This suggests that 4070 cm^{-1} is the ^{10}B band by its high intensity is worrisome. For $2\nu_2^{T_2}$, the ^{10}B overtone is

calculated to be about 10-12 cm^{-1} higher than the ^{11}B overtone and this agrees well with the 4180 cm^{-1} shoulder both in terms of energy and intensity.

The overtones seen for $Zr(BH_4)_4$ are not as well resolved but three bands are visible. By analogy with assignments for $Np(BH_4)_4$, $2\nu_3{}^{T_2}$ is the low frequency shoulder at 4153 cm^{-1} and the broad band at 4230 cm^{-1} is $2\nu_2{}^{T_2}$. However, the "observed" value for $\nu_1{}^{T_1}$ of $Zr(BH_4)_4$ by Smith et al.[25] contradicts this explanation and suggests that 4230 cm^{-1} is $2\nu_1{}^{T_1}$ and 4174 cm^{-1} is $2\nu_2{}^{T_2}$. It is believed that their value of 2199 cm^{-1} for $\nu_1{}^{T_1}$ is too high and if the calculated value for $\nu_1{}^{T_1}$ obtained in the $Hf(BH_4)_4$ study[27] of 2122 cm^{-1} is used, agreement is found with the present results on $Np(BH_4)_4$ given in Tables 17 and 18. Carrying over the 2122 cm^{-1} value for $\nu_1{}^{T_1}$ for $Zr(BH_4)_4$ is probably accurate since change in metal mass does not significantly affect the T_1 modes for Zr and Hf.

The IR spectrum of $Zr(BD_4)_4$ is shown in Fig. 9 and a listing of the observed bands is given in Table 19. The very low intensities of the bands compared to those of the borohydride is due to the fact that since deuteride fundamentals are so low in frequency, it takes higher-order overtones and combinations to get into the 4000-4800 cm^{-1} region. The resulting number of possible candidates for the bands is too high for a choice to be made with any degree of certainty.

Using the $(\omega_e X_e)_D$ value found earlier, no harmonic of $\nu_1{}^{T_2}$ is predicted anywhere in the areas where bands are seen. The second harmonic of $\nu_3{}^{T_2}$ is probably the 4545 cm^{-1} band showing small ^{10}B effects

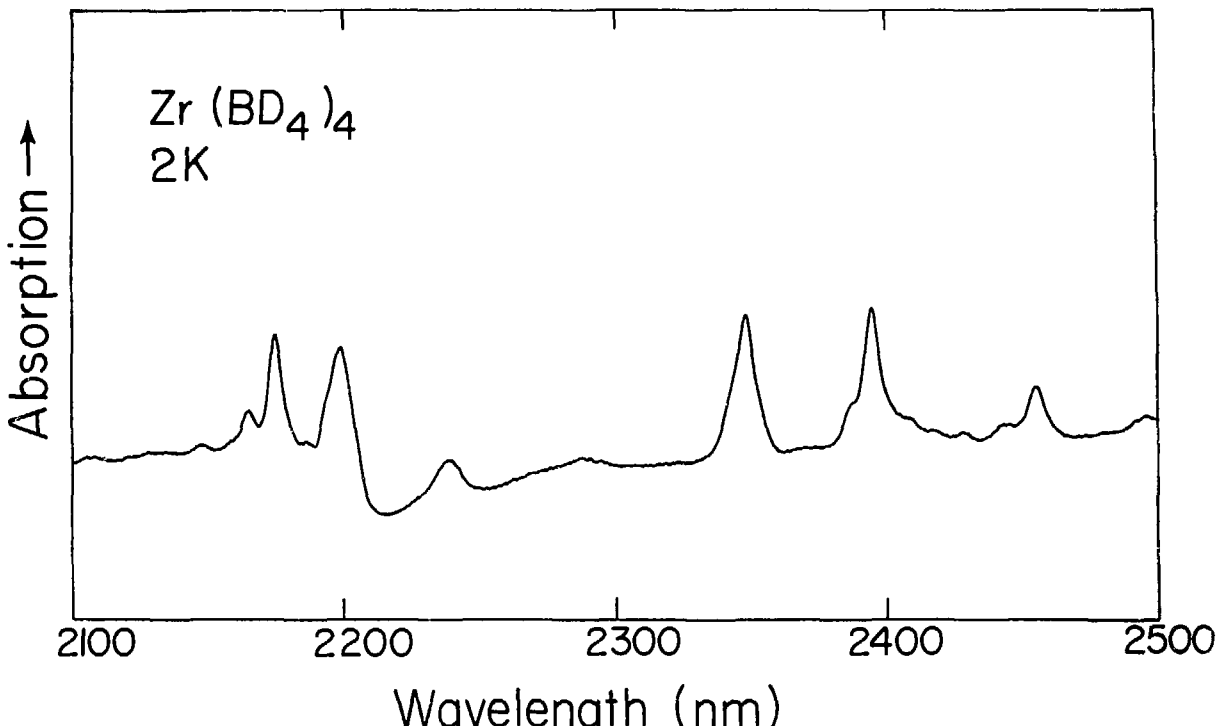

Figure 9. Near IR Spectrum of $Zr(BD_4)_4$.

XBL 798-2701

Table 19

Observed IR Bands (4800-4000 cm^{-1}) of $Zr(BD_4)_4$ at 2K

Wavelength (nm)	Energy (cm^{-1})	Assignment	Comments
2455	4072	$\nu_2^{T_2} + 3\nu_6^{T_2}$	medium
2394	4176	$\nu_3^{T_2} + 2\nu_5^{T_2} + \nu_6^{T_2}$	strong
2347	4259	$\nu_2^{A_1} + 3\nu_5^{T_2}$	strong
2238	4486	$\nu_1^{T_2} + 2\nu_6^{T_2} + \nu_5^{T_2}$	weak +, broad
2199	4545	$3\nu_3^{T_2}$	strong
2175	4597	$\nu_2^{A_1} + 2\nu_3^{T_2}$	strong
2165	4617	$2\nu_2^{A_1} + \nu_3^{T_2}$	weak +
2148	4655	$3\nu_2^{T_2}$	weak

as a high-frequency shoulder. The other νBD_b second harmonic (the first harmonic was not seen in the 4000-200 cm^{-1} spectrum) calculates to be about 150 cm^{-1} above $3\nu_3{}^{T_2}$ and is assigned to the weak absorption at 2148 nm (4655 cm^{-1}).

The remaining bands are assigned rather arbitrarily to combinations which were allowed and had a calculated energy in reasonable agreement with those observed. The assignments are given in Table 19.

No spectrum could be obtained on such a large sample needed for $Np(BD_4)_4$ but it is assumed that its spectrum is very similar to that of $Zr(BD_4)_4$.

Other Calculations

Pictures of A_1 Normal Modes

The eigenvectors expressed in Cartesian coordinates were calculated by the program and from these, pictures of the normal modes were drawn. In Appendix A the four A_1 normal modes for $Np(BD_4)_4$ are shown where the displacement vectors were multiplied by five times their actual length for clarity. $Np(BD_4)_4$ was chosen in order to make the boron vectors long enough to be visible.

Partition Function and Thermodynamic Quantities

In statistical mechanics,[49] the partition function of a system is defined as

$$Q = \sum q_n e^{-\varepsilon_n/kT}$$, where q_n is the statis-

tical weight of the nth energy level of energy ε_n. From the partition function all thermodynamic quantities can be derived.

The total partition function for our case is $Q = Q_t Q_i$, where Q_t is the translational partition function and Q_i is the internal partition function. For calculations of entropy and heat capacity, $Q_i = Q_r Q_v$, where Q_r and Q_v are the rotational and vibrational partition functions. At ordinary temperatures, only the ground electronic state is assumed to be populated.

Assuming $Np(BH_4)_4$ to be an ideal gas, the expression for the entropy of translation is[50]

$$S_t = R(\tfrac{3}{2}\ell nM + \tfrac{5}{2}\ell nT) - 2.315 \text{ cal/deg},$$

where M is the molecular weight and T is the absolute temperature. The entropy of translation is therefore $S_t^\circ = 42.97$ cal/deg for $Np(BH_4)_4$ at 298.15K.

The heat capacity $C_{p_t}^\circ = 5/2R = 4.97$ cal/deg.

The vibrational entropy and heat capacity can be calculated from Q_v. For a single harmonic oscillator, the vibrational energy is the sum

$$E = \sum_v \omega V \quad ,$$

where ω is the frequency and v is the vibrational quantum number. From the definition of Q, Q_v can be written down immediately as

$$Q_v = \sum_v e^{-\omega v hc/kT}$$

For a polyatomic molecule with 3N-6 normal vibrations, Q_v becomes

$$Q_v = \sum_{v_1}\sum_{v_2}\cdots\sum_{v_{3N-6}} e^{-(\omega_1 v_1+\omega_2 v_2+\ldots+\omega_{3N-6}v_{3N-6})hc/kT}$$

$$Q_v = \prod_i \left(\sum_{v_i} e^{-\omega_i v_i hc/kT}\right) \quad , i = 1, 2, 3, \ldots, 3N-6.$$

This expression can be made easier to evaluate by using the dengeracies to reduce the number of factors. The substitution, $X_i = \omega_i hc/kT$, is also helpful.

$$Q_v = \prod_i \left(\sum_{v_i} e^{-X_i v_i}\right)^{q_i} \quad i = 1, 2, 3, \ldots, 24$$

for $Np(BH_4)_4$

The infinite sum over V_i can be written in closed form as

$$\sum_{v_i} e^{-X_i v_i} = \frac{1}{1-e^{-X_i}}$$

so that

$$Q_v = \prod_i (1-e^{-X_i})^{q_i} \text{ and } \ln Q_v = -\sum_i q_i \ln(1-e^{-X_i})$$

Since $$S_v = RT\frac{d\ln Q_v}{dT} + R\ln Q_v \text{ and} \qquad (6)$$

$$C_{p_v} = R \frac{d}{dT}\left[T^2 \frac{d\ln Q_v}{dT}\right] , \qquad (7)$$

one obtains

$$S_v = R\sum_i q_i \ln(1-e^{-X_i}) + R\sum_i \frac{q_i X_i e^{-X_i}}{1-e^{-X_i}} \quad \text{and}$$

$$C_{p_v} = R\sum_i \frac{q_i X_i^2 e^{-X_i}}{(1-e^{-X_i})^2}$$

The vibrational partition functions can be calculated using the fundamental frequencies and their degeneracies found in this vibrational study of $Np(BH_4)_4$.

It was very profitable to write a simple computer program and using the information in Table 7, the following quantities were calculated for T = 298.15K

$$Q_v = 184.21$$
$$C^o_{p_v} = 34.01 \text{ cal/deg.}$$
$$S^o_v = 25.83 \text{ cal/deg.}$$

The last contribution is that due to the rotational partition function which is more complex than either the translational or vibrational partition functions. It involves not only rotation of the molecule as a whole but in the case of $M(BH_4)_4$ molecules, includes internal rotation whether hindered or not. The rotational barrier of one BH_4^- group in $Zr(BH_4)_4$ has been determined; however, it is very possible that the bar-

rier in other metal tetrakis-borohydrides could be very different and the values would not be transferable. In similar compounds of the type $M(CH_3)_4$, barriers to internal rotation vary significantly with the size of the central atom.[51,52] Since an accurate value of a barrier of rotation is lacking for $Np(BH_4)_4$, it will be assumed to be free initially and then the potential found in $Zr(BH_4)_4$ will be introduced as a rough correction.

For spherical tops, all these moments of inertia are equal and therefore all three rotational constants are equal. The energy expression for the rotational levels is

$$F(J) = BJ(J+1),$$

where B is the rotational constant, $\frac{h}{8\pi^2 cI}$, and J is the rotational quantum number. The rotational partition function for the rigid molecule is

$$Q_r = \sum_{J=0}^{\infty} (2J+1)e^{-BJ(J+1)hc/kT}$$

Kassel[53] has derived a formula for Q_r which is suitable for numerical evaluation. Q_r is now

$$Q_r = e^{Bhc/4kT}\left[\frac{\pi}{B^3}\left(\frac{kT}{hc}\right)^3\right]^{\frac{1}{2}} \qquad (8)$$

Using the value of $I = 4.20 \times 10^{-38}$ gm-cm^2 for $Np(BH_4)_4$,

$$Q_r = 3.08 \times 10^5$$

The rotational entropy S_r is obtained from Eq. (6) by replacing Q_v by Q_r:

$$S_r = RT \frac{d\ln Q_r}{dT} + R\ln Q_r$$

At room temperature and for small rotational constants, the exponential factor in Eq. (8) is very close to unity and need not be considered further in Q_r. The rotational entropy is[2]

$$S_r = \frac{R}{2}\left\{3\ln T - 3\ln B - 2\ln\sigma + \ln\left[\pi\left(\frac{k}{hc}\right)^3\right] + 3\right\}$$

For tetrahedral molecules, the symmetry number, σ, is equal to 12. So S_r^o for $Np(BH_4)_4$ is

$$S_r^o = 23.16 \text{ cal/deg.}$$

At temperatures considered in these calculations, it is a good approximation to assume that each degree of rotational freedom contributes $\frac{1}{2}R$ to the heat capacity at constant pressure. This gives

$$C_{p_r}^o = \frac{3}{2}R = 2.98 \text{ cal/deg.}$$

Thus far, the molecule is rigid with no internal rotation occurring.

The total entropy and heat capacity for the ideal gas at 298.15K is

$$S^\circ = S^\circ_t + S^\circ_v + S^\circ_r = 91.96 \text{ cal/deg.}$$

$$C^\circ_p = C^\circ_{p_t} + C^\circ_{p_v} + C^\circ_{p_r} = 41.96 \text{ cal/deg.}$$

The free internal rotation partition function was derived by Pitzer and Gwinn.[54] The quantum mechanical expression for the energy levels of a system of linked free rotation is

$$E_K = \frac{h^2K^2}{8\pi^2 I_r}$$, where I_r is the reduced moment of inertia and K is the rotational quantum number. The partition function, Q_{f_r}, is

$$Q_{f_r} = \frac{1}{n} \sum_{K=-\infty}^{+\infty} e^{-K^2h^2/8\pi^2 I_r kT}$$

$$Q_{f_r} = \frac{2.7935}{n} (10^{38} I_r T)^{\frac{1}{2}}$$

Here n is the number of equivalent orientations of the rotation (n = 3 for BH_4^-) and $I_r = I_1I_2/(I_1+I_2)$ where I_1 and I_2 are the moments of inertia for the two symmetrical, coaxial tops.

In $Np(BH_4)_4$, there are 4 equivalent tops and each contributes one factor to Q_{f_r}. The total Q_{f_r} is

$$Q_{f_r} = 2.725 \times 10^{-3} T^2$$

$$Q_{f_r} = 242.20 \text{ at } 298.15K$$

Substituting Q_{f_r} into Eq. (7), the heat capacity becomes

$$C^{\circ}_{p_{f_r}} = 2R = 3.97 \text{ cal/deg.}$$

The entropy of free internal rotation is obtained by substituting Q_{f_r} into Eq. (6) and is[2]

$$S_{f_r} = 2R(\ln T + \ln I_r - 2\ln n + 90.667)$$

$$S^{\circ}_{f_r} = 15.34 \text{ cal/deg.}$$

In the case of hindered internal rotation, the energy expression for the rotational levels is very complex but Pitzer and Brewer[55] have developed tables of thermodynamic functions in terms of the difference between the function for restricted rotation and for free rotation. The contribution of hindered internal rotation, when the barrier potential energy is $V = \frac{1}{2}V_o(1-\cos n\phi)$, to the thermodynamic properties is given as functions of two variables, V_o/RT and $1/Q_{f_r}$.

From the tables[55] it is apparent that the size of the contributions are not strongly dependent on relatively small (< 50%) changes in V_o. For lack of a better value, the barrier potential energy of V_o = 3420 cal/mol for $Zr(BH_4)_4$[39] is used to obtain the value for the contributions to the heat capacity and entropy due to hindered rotation at 298.15K. They are

$$C^{o}_{p_{h_r}} = 8.56 \text{ cal/deg.}$$

$$S^{o}_{h_r} = 8.80 \text{ cal/deg.}$$

In using the tables, the Q_{f_r} used is that for one top and the total contribution for all four tops is obtained by multiplying the single-top value by four.

Table 20 gives total sums of all contributions and these calculations are compared to the experimental and calculated values for $Pb(CH_3)_4$,[56] $Sn(CH_3)_4$,[57] $Ge(CH_3)_4$,[57] $Si(CH_3)_4$,[57,58] $C(CH_3)_4$,[59] and $Hf(BH_4)_4$.[60]

Conclusion

From infrared and Raman spectra most of the fundamentals were assigned for $Np(BH_4)_4$ and $Np(BD_4)_4$. These were used in a normal coordinate analysis and a simple force field was derived using 8 primary and 5 interaction constants. The overall agreement with experiment was satisfactory but rather large discrepancies were found in the low energy modes. Matrix isolated spectra would have helped in obtaining better agreement. Spectra of samples containing pure ^{10}B and ^{11}B isotopes would greatly simplify the identification of nonfundamental bands while also reducing the general complexity of the vibrational problem. Calculated frequencies of theoretically ^{10}B- and ^{1}H-contaminated molecules in addition to those of the ^{11}B-containing molecules formed the foundation upon which the assignment of impurity, overtone, and combination bands were based. Hopefully the results obtained from this work will be of use in future spectral studies on actinide borohydrides.

Using the method of statistical thermodynamics, the entropy and heat capacity for gaseous $Np(BH_4)_4$ were calculated from the spectral information obtained from the vibrational analysis. A comparison of the calculations to those of similar compounds confirms both the utility and accuracy of such a study. Since $M(CH_3)_4$ type molecules have slightly fewer atoms, their heat capacities and entropies are expected to be lower, with the greatest deviation existing in the vibrational contribution. A closer examination, however, must await experimental values and more accurate, low frequency infrared data.

Table 20

Entropies and Heat Capacities of $Hf(BH_4)_4$, $Np(BH_4)_4$ and $M(CH_3)_4$

Heat Capacities [a]

$Hf(BH_4)_4$		$Np(BH_4)_4$		$Pb(CH_3)_4$	$Sn(CH_3)_4$	$Ge(CH_3)_4$	$Si(CH_3)_4$	$C(CH_3)_4$
FIR	HIR	FIR	HIR	FIR	FIR	FIR	FIR	
45.09	49.77	45.93	50.52	34.42	33.34	31.98	33.39	-----

Entropies

$Hf(BH_4)_4$		$Np(BH_4)_4$		$Pb(CH_3)_4$	$Sn(CH_3)_4$	$Ge(CH_3)_4$	$Si(CH_3)_4$	$C(CH_3)_4$
FIR	HIR	FIR	HIR	FIR	FIR	FIR	FIR	FIR
102.51	96.04	107.30	100.76	100.5	96.11	91.99	88.25	80.12
				100.48 [b]			86.04 [b]	71.71 [c]

In the table: FIR = free internal rotation, HIR = hindered internal rotation. All values for C_p^o and S^o are for the ideal gas at 298.15K.

[a] All C_p^o values are calculated.

[b] Experimental values.

[c] Experimental value at 282.6K. Ref. 59(b).

References and Footnotes

[1]Banks, R. H.; Edelstein, N. M.; Spencer, B.; Templeton, D. H.; Zalkin, A. J. Am. Chem. Soc. 102 0000 (1980).

[2]Herzberg, G. "Infrared and Raman Spectra." D. Van Nostrand Co., Inc. Princeton, N.J., 1945.

[3](a)Price, W. C.; Longuet-Higgins, H. C.; Rice, B.; Young, T. F. J. Chem. Phys. 17 217 (1949).

(b)Price, W. C. J. Chem. Phys. 17 1044 (1949).

(c)Emery, A. R.; Taylor, R. C. J. Chem. Phys. 28 1029 (1958).

(d)Taylor, R. C.; Schultz, D. R.; Emery, A. R. J. Am. Chem. Soc. 80 27 (1958).

(e)Coker, E. H.; Hofer, D. E. J. Chem. Phys. 48 2713 (1968).

(f)Coker, E. H.; Hofer, D. E. J. Chem. Phys. 53 1652 (1970).

(g)Harvey, K. B.; McQuaker, N. R. J. Chem. Phys. 55 4396 (1971).

(h)Harvey, K. B.; McQuaker, N. R. Can. J. Chem. 49 3272 (1971).

(i)Harvey, K. B.; McQuaker, N. R. Can. J. Chem. 49 3282 (1971).

[4]Price, W. C.; Sherman, W. F.; Wilkinson, G. R. Spectrochim. Acta 16 663 (1960).

[5]Ketelaar, J. A. A.; Schutte, C. H. J. Spectrochim. Acta 17 1240 (1961).

[6]Peterson, E. R. Diss. Abstracts 25 5588 (1965).

[7](a)Marynick, D. S.; Lipscomb, W. N. J. Am. Chem. Soc. 93 2322 (1971).

(b)Marynick, D. S.; Lipscomb, W. N. Inorg. Chem. 11 820 (1972).

[8]Almenningen, A.; Gunderson, G.; Haaland, A. Acta Chem. Scand. 22 328 (1968).

[9]Bernstein, E. R.; Hamilton, W. C.; Keiderling, T. A.; LaPlaca, S. J.; Lippard, S. J.; Mayerle, J. J. Inorg. Chem. 11 3009 (1972).

[10(a)]Rietz, R. R.; Zalkin, A.; Templeton, D. H.; Edelstein, N. M.; Templeton, L. K. Inorg. Chem. 17 653 (1978).

[(b)]Rietz, R. R.; Edelstein, N. M.; Ruben, H. W.; Templeton, D. H.; Zalkin, A. Inorg. Chem. 17 658 (1978).

[(c)]Zalkin, A.; Rietz, R. R.; Templeton, D. H.; Edelstein, N. M. Inorg. Chem. 17 661 (1978).

[11(a)]Lippard, S. J.; Melmed, K. M. Inorg. Chem. 6 2223 (1967).

[(b)]Lippard, S. J.; Melmed, K. M. J. Am. Chem. Soc. 89 3929 (1967).

[(c)]Bailey, N. A.; Bird, P. H.; Wallbridge, M. G. H. Inorg. Chem. 7 1575 (1968).

[(d)]Davidson, J. M. Chem. Ind. (London) 2021 (1964).

[(e)]Cariati, F.; Naldini, L. Gazz. Chim. Ital. 95 3 (1965).

[12(a)]Emery, A. R.; Taylor, R. C. Spectrochim. Acta 16 1455 (1960).

[(b)]Coe, D. A.; Nibler, J. W. Spectrochim. Acta 29A 1789 (1973).

[13(a)]Nibler, J. W.; Shriver, D. F.; Cook, T. H. J. Chem. Phys. 54 5257 (1971).

[(b)]Nibler, J. W. J. Am. Chem. Soc. 94 3349 (1972).

[14]Longuet-Higgins, H. C. J. Chem. Soc. 139 (1946).

[15(a)]Nanda, R. K.; Wallbridge, M. G. H. Inorg. Chem. 3 1798 (1964).

[(b)]Smith, B. E.; James, B. D.; Dilts, J. A. J. Inorg. Nucl. Chem. 38 1973 (1976).

[(c)]Marks, T. J.; Kennelly, W. J.; Kolb, J. R.; Shimp, L. A. Inorg. Chem. 11 2540 (1972).

[(d)]King, R. B. Z. Naturforsch. 18(b) 157 (1963).

[(e)]Anand, S. P.; Multani, R. K.; Jain, B. D. J. Organometal. Chem. 26 115 (1971).

[16]Coe, D. A.; Nibler, J. W.; Cook, T. H.; Drew, D.; Morgan, G. L. J. Chem. Phys. 63 4842 (1975).

[17]Drew, D. A.; Gunderson, G.; Haaland, A. Acta Chem. Scand. 26 3351 (1972).

[18]Marks, T. J.; Kolb, J. R. Chem. Revs. 77 263 (1977).

[19](a)Keiderling, T. A. Ph.D. Thesis, Princeton University, 1974.

(b)Bird, P. H.; Churchill, M. R. Chem. Comm. 403 (1967).

(c)Plato, V.; Hedberg, K. Inorg. Chem. 10 590 (1971).

(d)Broach, R. S.; Chuang, I. S.; Williams, J. M.; Marks, T. J. Private communication, 1979.

[20](a)Le Vanda, C.; Solar, J. P.; Streitwieser, A., Jr. Submitted to J. Am. Chem. Soc. 1979.

(b)Solar, J. P.; Streitwieser, A., Jr.; Edelstein, N. M. In "Lanthanides and Actinides, ACS Symposium Series," Edelstein, N. M. Ed.; American Chemical Society: Washington, D. C., 1980; in press.

[21]Turner, H. W.; Andersen, R. A.; Zalkin, A.; Templeton, D. H. Inorg. Chem. 18 1221 (1979).

[22]Davies, N.; Wallbridge, M. G. H.; Smith, B. E.; James, B. D. J. Chem. Soc. Dalton 162 (1973).

[23]Califano, S. "Vibrational States." John Wiley and Sons, Ltd. New York, N.Y., 1976. p. 248.

[24]Joyce, R. R.; Richards, P. L. Phys. Rev. 179 375 (1969).

[25]Smith, B. E.; Shurvell, H. F.; James, B. D. J. Chem. Soc. Dalton 710 (1978).

[26]Since the change in reduced mass for a $^{10}B \rightarrow {}^{11}B$ exchange in the borohydride is approximately half that in the borodeuteride, ^{10}B effects are not easily seen in the borohydride.

[27]Keiderling, T. A.; Wozniak, W. T.; Gay, R. S.; Jurkowitz, D.; Bernstein, E. R.; Lippard, S. J.; Spiro, T. G. Inorg. Chem. 14 576 (1975).

[28]Paine, R. T.; Light, R. W.; Nelson, M. Spectrochim. Acta 35A 213 (1979).

[29]The corresponding $\nu_3{}^{T_2}$ band of $Zr(BD_4)_4$ at 1539 cm^{-1} gives an overtone of 3058 cm^{-1} ($2 \times \nu_3{}^{T_2} = 3078\ cm^{-1}$). Ref. 25.

[30]The validity of this statement is also based on normal coordinate calculations using different molecular geometries.

[31]Banks, R. H.; Edelstein, N. M.; Rietz, R. R.; Templeton, D. H.; Zalkin, A. J. Am. Chem. Soc. 100 1957 (1978).

[32]Ghiassee, N.; Clay, P. G.; Walton, G. N. Inorg. Nucl. Chem. Lett. 14 117 (1978).

[33]James, B. D.; Smith, B. E.; Wallbridge, M. G. H. J. Mol. Struct. 14 327 (1972).

[34]Smith, B. E.; James, B. D. Inorg. Nucl. Chem. Lett. 7 857 (1971).

[35]Ref. 2, p. 232.

[36]Gwinn, W. D. J. Chem. Phys. 55 477 (1971).

[37]Reuter, D.; Gwinn, W. D. To be submitted to QCPE in 1980.

[38]James, B. D.; Smith, B. E.; Shurvell, H. F. J. Mol. Struct. 33 91 (1976).

[39]Tomkinson, J.; Waddington, T. C. J. Chem. Soc. Faraday II 1245 (1976).

[40](a)Meredith, R. E.; Jenney, J. A. J. Chem. Phys. 39 3127 (1963).

(b)Conway, J. G. J. Chem. Phys. 41 904 (1964).

[41]The ground electronic state of $Np(BH_4)_4$ was found to be Γ_6 by EPR spectroscopy. Banks, Edelstein, unpublished results.

[42]Lea, K. R.; Leask, M. J. M.; Wolf, W. P. J. Phys. Chem. Solids 23 1381 (1962).

[43]Davies, N.; Saunders, D.; Wallbridge, M. G. H. J. Chem. Soc. (A) 2915 (1970).

[44]Unpublished results in our laboratory, 1978.

[45]Wilson, E. B.; Decius, J. C.; Cross, P. C. "Molecular Vibration," McGraw-Hill, N.Y., 1955.

[46]Sanderson, R. T. J. Chem. Ed. 29 539 (1952); 31 2 (1954); 31 238 (1954).

[47]James, B. D. Ph.D. Thesis, University of Sheffield, 1967.

[48]Herzberg, G. "Spectra of Diatomic Molecules." D. Van Nostrand and Co., Inc. New York, 1950.

[49]Hill, T. J. "Introduction to Statistical Thermodynamics." Addison-Wesley. Reading, Mass., 1950.

[50]Pitzer, K. S.; Brewer, L. "Thermodynamics." McGraw-Hill Book Co. New York, 1961.

[51]Ref. 2, p. 520.

[52]French, F. A.; Rasmussen, R. S. J. Chem. Phys. 14 389 (1946).

[53]Kassel, L. S. J. Chem. Phys. 1 576 (1933).

[54]Pitzer, K. S.; Gwinn, W. D. J. Chem. Phys. 10 428 (1942).

[55]Ref. 50, p. 440-446.

[56(a)]Crowder, G. A.; Gorin, G.; Kruse, F. H.; Scott, D. W. J. Mol. Spect. 16 115 (1965).

[(b)]Good, W. D.; Scott, D. W.; Lacina, J. L.; McCullough, J. P. J. Phys. Chem. 63 1139 (1959).

[57]Lippincott, E. R.; Tobin, M. C. J. Am. Chem. Soc. 75 4141 (1953).

[58(a)]Shimizu, K.; Murata, H. J. Mol. Spect. 5 44 (1960).

[(b)]Aston, J. G.; Kennedy, R. M.; Messerly, G. H. J. Am. Chem. Soc. 63 2343 (1941).

[59(a)]Pitzer, K. S. J. Chem. Phys. 5 473 (1937).

[(b)]Aston, J. G.; Messerly, G. H. J. Am. Chem. Soc. 58 2354 (1936).

[60]The fundamental frequencies and molecular structure parameters used in the calculations were taken from Ref. 27.

APPENDIX A

Totally Symmetric (A_1)

Normal Modes of $Np(BD_4)_4$

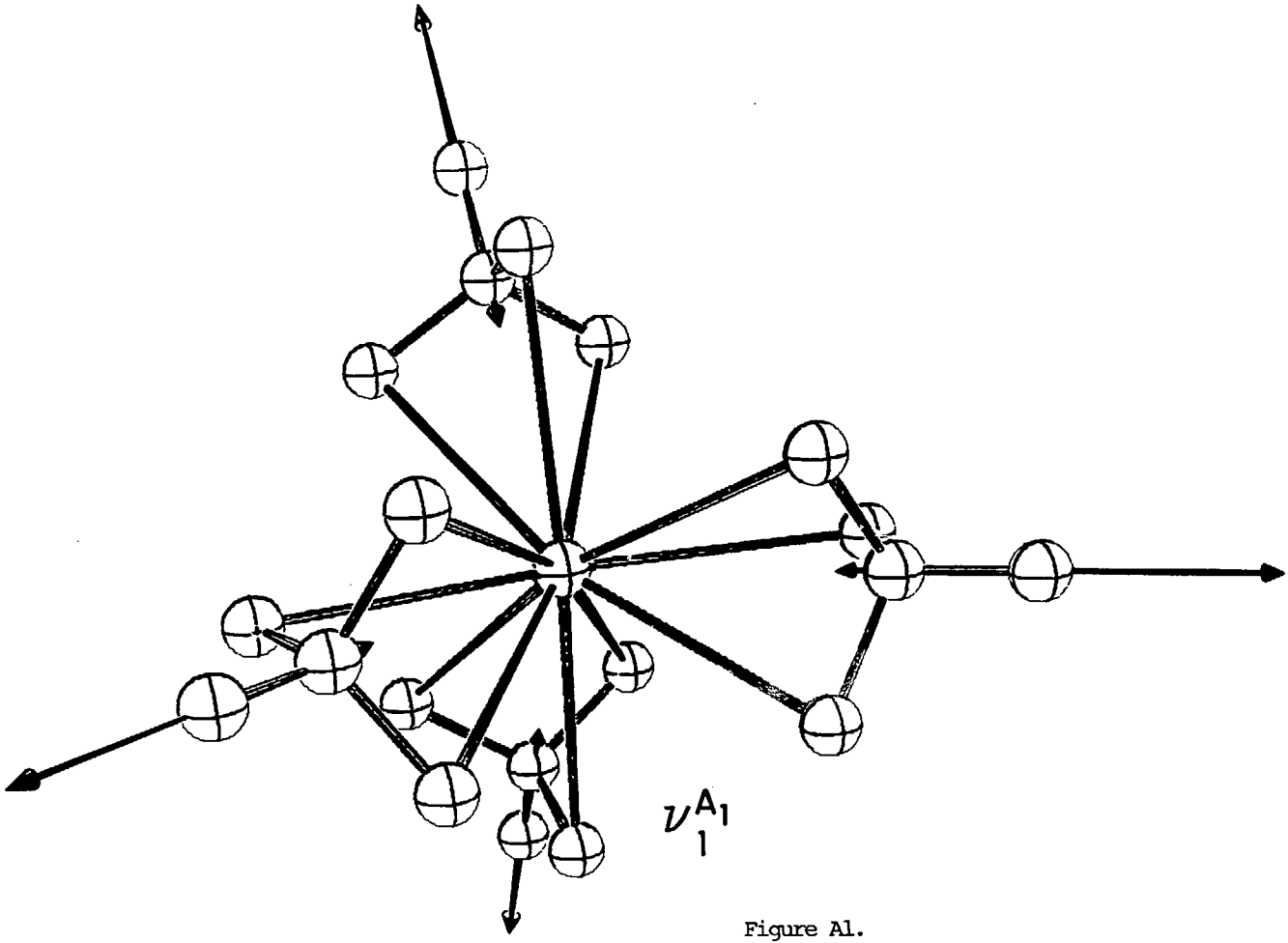

Figure A1.

XBL 7910-4458

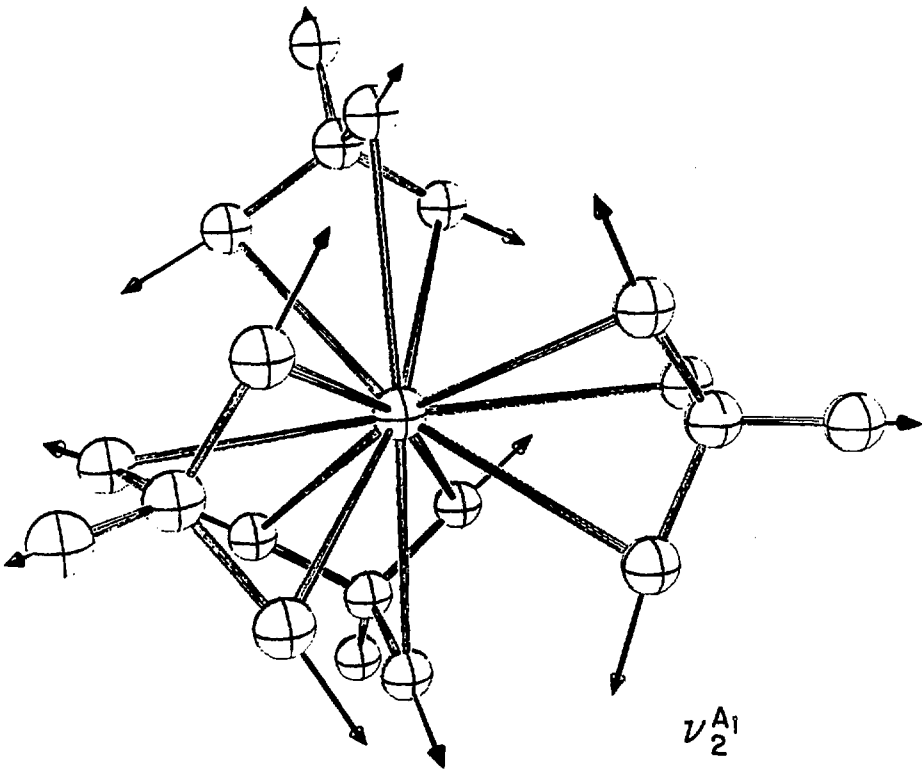

XBL 7910-4460

Figure A2.

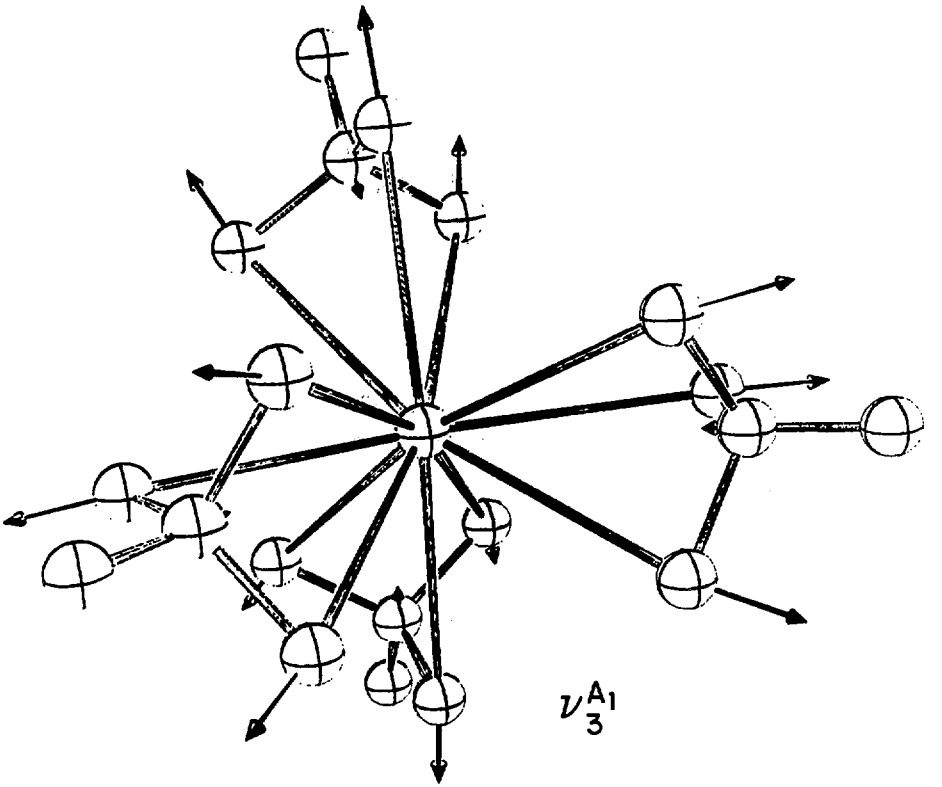

XBL 7910-4459

Figure A3.

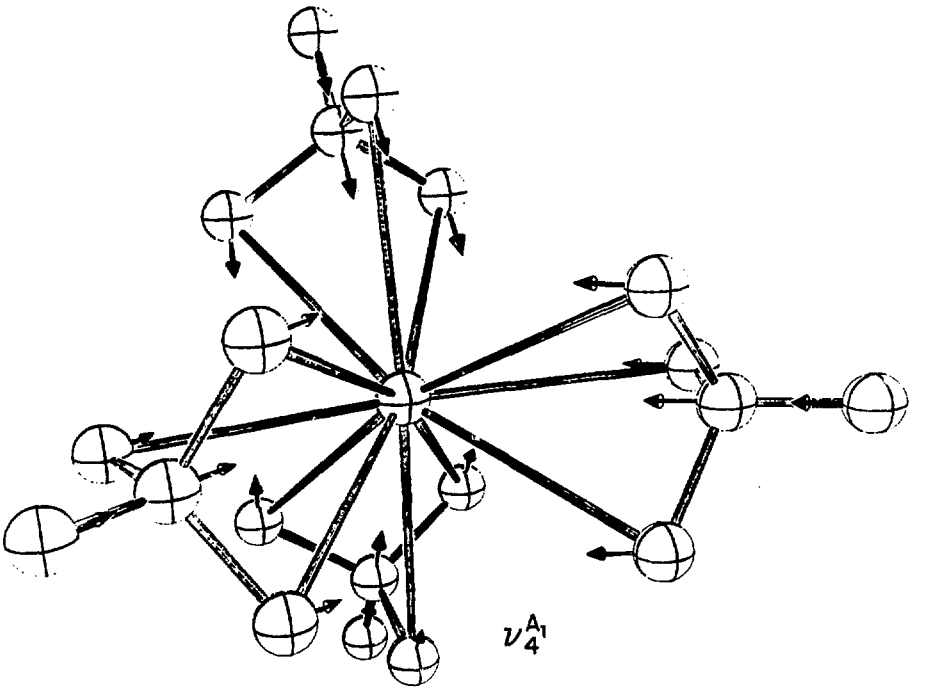

XBL 7910-4461

Figure A4.

APPENDIX B

The spectroscopic notation used in this chapter is not standard literature notation. A correlation table is given below relating that of this work to that found in the literature.

This work	Literature
$\nu_1^{A_1} - \nu_4^{A_1}$	$\nu_1 - \nu_4$
ν^{A_2}	ν_5
$\nu_1^{E} - \nu_5^{E}$	$\nu_6 - \nu_{10}$
$\nu_1^{T_1} - \nu_5^{T_1}$	$\nu_{11} - \nu_{15}$
$\nu_1^{T_2} - \nu_9^{T_2}$	$\nu_{16} - \nu_{24}$

Chapter 4

ELECTRON PARAMAGNETIC RESONANCE OF $Np(BH_4)_4$

Introduction

Electron paramagnetic resonance (EPR) spectroscopy involves transitions between the magnetic sublevels of the ground crystal field state of a paramagnetic ion situated in a host crystal.[1] While the microwave frequency is kept constant, an EPR transition can take place when the variable external magnetic field produces an energy separation between two Zeeman levels which equals the energy of the incident microwave radiation. Whether a transition is allowed or forbidden depends on the quantum numbers of the levels involved. The resulting EPR spectrum yields a series of lines which can be fitted to an appropriate Hamiltonian. Values of the Hamiltonian parameters which describe the ground state are obtained and are important in the interpretation of optical spectra (see chapter 5) because they identify the ground crystal field state.

EPR spectra of $Np(BH_4)_4$ and $Np(BD_4)_4$ in various host materials were obtained and an analysis of them is given in this chapter.

Experimental

Approximately 50-100 mg $Zr(BH_4)_4$ was vacuum transferred to the bottom of a 3 mm ID quartz EPR tube. A small amount (~ 100 μg) of $Np(BH_4)_4$ was then condensed on top of the $Zr(BH_4)_4$. Due to the small sizes of

the microwave cavities, the sample tubes were required to be no longer than 3 cm. Several initial attempts at sealing off the tubes of that length resulted in the formation of metallic mirrors at the seal-off end. These mirrors sufficiently lowered the Q values of the cavities so that no EPR signals were observed.

Since the solid $Zr(BH_4)_4/Np(BH_4)_4$ mixture remained at -196° and the tube was kept evacuated during seal off, the origin of the mirrors must have been due to the decomposition of adsorbed borohydride molecules on the inner tube surface. It was found that these adsorbed molecules bind tenaciously to the quartz surface and cannot be removed without decomposition. If the seal-off area remained above room temperature during borohydride addition, the mirrors did not form, unlike the case when the area was ordinarily cold due to the presence of liquid nitrogen below it. Prevention of mirror formation was achieved using a nichrome heater wire wrapped around the seal-off area.

After the tubes were sealed off cleanly, the solid borohydride mixture was melted to give a solution whose green color was barely perceptible. Following solidification of the liquid at one end of the tube, the other end was kept immersed $\frac{1}{4}$ in. in ice water for 15 hours. The resulting vapor-grown single crystal was homogeneous and transparent. Spectra of $Np(BD_4)_4/Zr(BD_4)_4$ mixed crystals, pure $Np(BD_4)_4$, and $Np(BH_4)_4$/methylcyclohexane were also obtained.

The EPR measurements at X and Q bands were made at 4.2K with Varian models E-101 (9GHz) and E-110 (34.5 GHz) microwave bridges. The magnetic field was produced by a rotating electromagnet with a 2-5/8" gap (12"

diameter polefaces, maximum field strength 10.8 kG) and measured with an Alpha Scientific NMR gaussmeter monitored by a frequency counter.

The K band spectra were obtained with a superheterodyne spectrometer at 1.7K in the region 24-25 GHz. A George Associates rotating-coil gaussmeter was used to measure the magnetic field.

Theory and Results

Since the EPR transition energies are in the GH_z region (.3 - 1.2 cm^{-1}), only the lowest electronic state is involved and all other J states can be neglected. The electron configuration of Np^{4+} is $[Rn]5f^3$ and the Russell-Saunders ground state is predominantly $^4I_{9/2}$.

From the single-crystal Xray study of $Np(BH_4)_4$ (see chapter 2), the Np ion is surrounded by a tetrahedral array of BH_4^- ligands. The potential exerted by this crystal field[2] can be expressed as

$$V = \sum_{nm} B_n O_n^m = B_4 (O_4^0 + 5O_4^4) + B_6 (O_6^0 - 21O_6^4) \qquad (1)$$

where B_4 and B_6 are the 4th and 6th degree crystal field parameters and the O_n^m are operator equivalents derived by Stevens.[3] A J = 9/2 state in a crystal field of the form of Eq. (1) splits into an isotropic Γ_6 Kramers doublet and two anisotropic Γ_8 quartets.

Point-charge calculations in the past have been successful in predicting the ground crystal field states of ions in crystals. The effect of the cubic crystal potential Eq. (1) on various angular momentum J states as a function of B_4/B_6 have been determined by Lea, Leask, and Wolf.[4] Their energy level diagram for J = 9/2 is given in Fig. 1 in

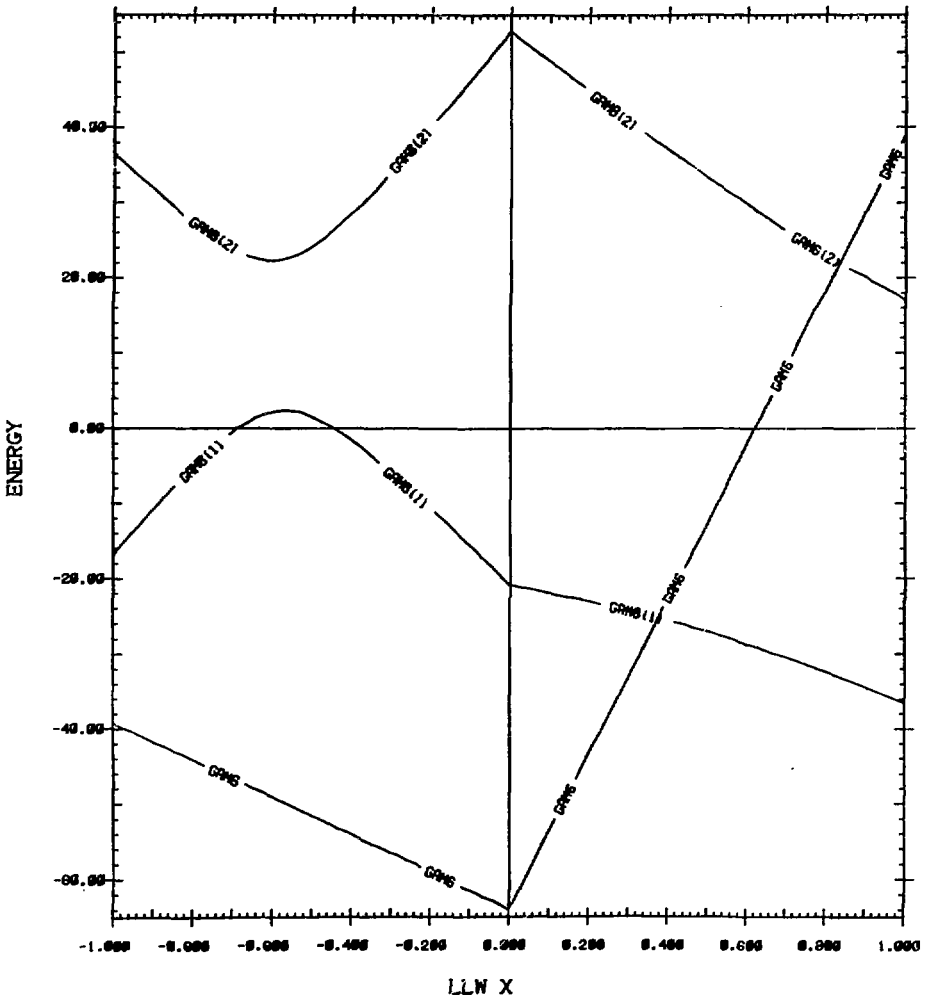

LEA,LEASK,WOLF DIAGRAM J=9/2

XBL 7812-13894

Figure 1. Energy level diagram for the Γ_6, $\Gamma_8^{(1)}$, and $\Gamma_8^{(2)}$ states for J = 9/2 manifold as a function of x, where $\frac{B_4}{B_6} = \frac{42x}{1-|x|}$.

which all values of B_4/B_6 from ∞ to $-\infty$ are represented by the parameter x, where $B_4/B_6 = \frac{42x}{1 - |x|}$ for f^3.

Using a B(4) model,[5] in which four point changes are located at the vertices of a regular tetrahedron, yields a positive B_4, negative B_6, and a Γ_8 ground state. However, isotropic resonances were observed in the EPR spectra, showing that the Γ_6 state lies lowest. Therefore the B(4) model is unsatisfactory. This same conclusion was also reached by Bernstein et al.[5] in their interpretation of the optical spectra of $U(BH_4)_4/Hf(BH_4)_4$ mixed crystals. They derived a successful H(12) model where the crystal field is generated by the twelve bridging hydrogen atoms in the coordination sphere of the actinide ion. It was assumed that the hydrogen atoms were located on the midpoints of the edges of a cube. This model gives both B_4 and B_6 positive and the correct ground state if $0 < x < .37$. The experimental results therefore show that $0 < B_4/B_6 < 24$. The observation that the resonances were isotropic to at least 1 part in 10^3 indicate that the higher-lying $\Gamma_8^{(1)}$ level does not interact greatly with the Γ_6 state and the upper limit of B_4/B_6 should be somewhat less than 24. If the crystal field parameters for $U(BH_4)_4$[5] are applied to $Np(BH_4)_4$, a B_4/B_6 ratio of +12.6 is obtained.

The EPR spectrum of $Np(BD_4)_4/Zr(BD_4)_4$ at K band is shown in Fig. 2 and those of $Np(BH_4)_4/Zr(BH_4)_4$ at X and Q bands are given in Fig. 3. Listings of the resonance field values are given in Tables 1 and 2.

Calculations of Hamiltonian Parameters

In cases where EPR transitions are induced between a few levels which are isolated from all others, it is convenient to assign to the

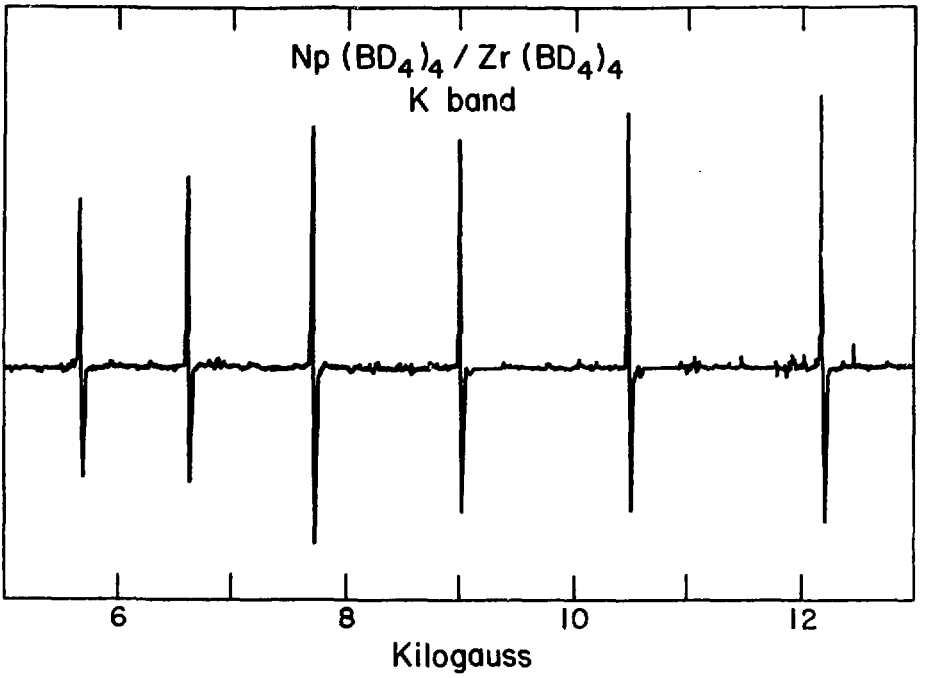

XBL 7910-4457

Figure 2. EPR Spectrum of $Np(BD_4)_4/Zr(BD_4)_4$.

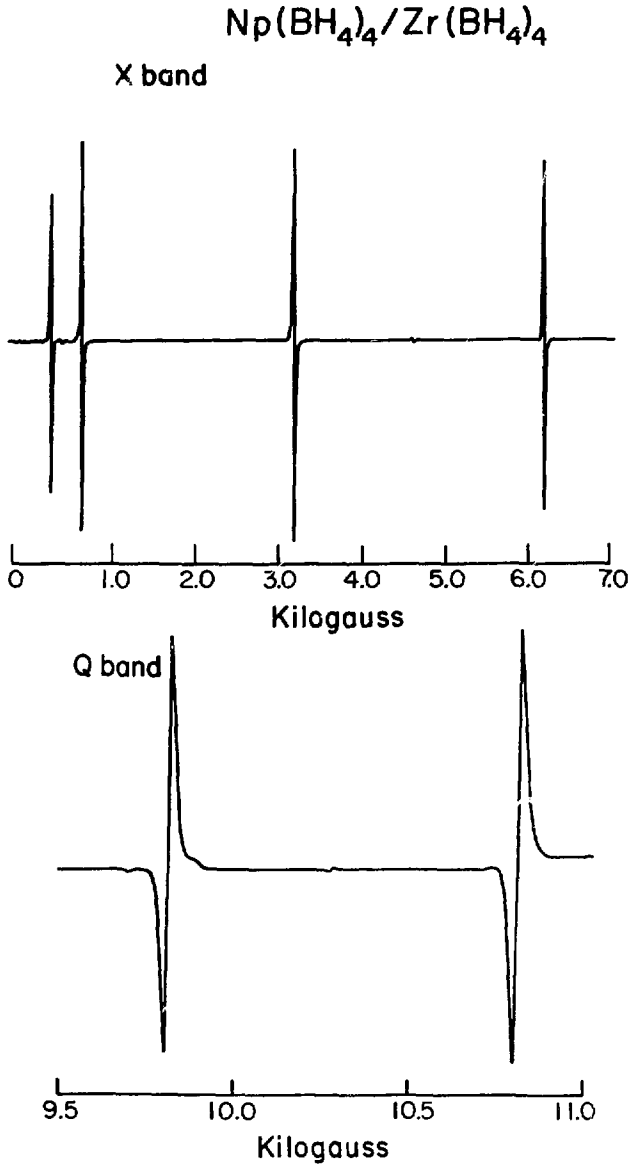

XBL 7911-13254

Figure 3. EPR Spectra of $Np(BH_4)_4/Zr(BH_4)_4$.

Table 1

Observed X and Q Band Resonances of $Np(BH_4)_4$

Transition Type	X Band (ν = 9.3928 GHz)	Q Band (ν = 34.933 GHz)
Allowed	400.8 754.4 3242.3 6266.5	9790.3 10820.3
Forbidden	508.3 4829.0	10270.0

Table 2

Observed and Calculated Field Values (gauss) at K Band

$Np(BH_4)_4$ ν = 25.986 GHz		$Np(BH_4)_4$ ν = 24.238 GHz	
Observed	Calculated	Observed	Calculated
6355.6	6355.8	5683.1	5683.1
7295.0	7294.3	6596.0	6595.8
8406.0	8405.7	7695.0	7694.3
9700.0	9700.2	8991.0	8991.4
11177.0	11178.1	10487.6	10487.1
12829.6	12828.7	12167.9	12167.6

system as an effective spin S' such that 2S' + 1 equals the number of levels. For the Γ_6 doublet, $S' = \frac{1}{2}$ and there will be one transition from $S' = \frac{-1}{2}$ to $S' = \frac{1}{2}$. If the nuclear spin I is included, this electron spin transition is split into 2I + 1 hyperfine levels. For ^{237}Np, I = 5/2. The spin Hamiltonian describing the system consists of three terms and can be written as

$$\mathcal{H} = A\vec{I} \cdot \vec{S}' + g\beta\vec{H} \cdot \vec{S}' - g_I\beta\vec{H} \cdot \vec{I} \qquad (2)$$

where A is the hyperfine coupling constant, β is the Bohr magneton, and g is the g value.

The EPR data for the hydride and deuteride were fitted to the spin Hamiltonian, Eq. (2) above and the results of the least squares calculations are given in Table 3. The $Np(BH_4)_4/Zr(BH_4)_4$ spectra displayed relatively broad resonances compared to those of $Np(BD_4)_4/Zr(BD_4)_4$ and a reliable g_I value could not be obtained from the hydride data. Inclusion of a nonzero g_I value in the calculations of the deuteride improved the fit even though it calculated to be very small. Similar trials on the hydride data gave poorer fits.

The large hyperfine interaction of ^{237}Np[6] and the observation of low-field transitions at X band, suggested that setting up the energy level calculations in terms of the weak magnetic field case was appropriate.[7] In this case, $\vec{I}$ and $\vec{S}'$ are strongly coupled together to form a resultant $\vec{F}$, where $\vec{F} = \vec{I} + \vec{S}'$. In the absence of a magnetic field, there are two states, F = 2 and F = 3 which are separated by 3A. When the magnetic

Table 3

Electron Paramagnetic Resonance of $^{237}Np(BH_4)_4$ and $^{237}Np(BD_4)_4$

$$\mathcal{H} = A\vec{I}\cdot\vec{S}' + g\beta\vec{H}\cdot\vec{S}' - g_I\beta\vec{H}\cdot\vec{I} \quad \begin{cases} I = 5/2 \\ S' = 1/2 \end{cases}$$

Spin Hamiltonian Parameters

	$\lvert A\rvert$ (cm^{-1})	g	g_I
$Np(BH_4)_4$	.1140 ± .001	1.894 ± .002	∿0
$Np(BD_4)_4$	.1140 ± .001	1.892 ± .002	.0062 ± .002

field is turned on, each of these two states split into $(2F+1)|m_F\rangle$ Zeeman levels as shown in Fig. 4, where $A > 0$. The arrows in the figure represent the observed allowed transitions in accordance with the selection rules $\Delta F = 0, \pm 1$; $\Delta m_F = \pm 1$. In addition, three forbidden transitions were also seen with $\Delta F = \pm 1$; $\Delta m_F = 0$, but were much less intense (see Table 1 and Fig. 3).

In the weak magnetic field case where the hyperfine interaction is comparable to the microwave energy, the spacings of the resonance lines is very irregular as can be seen in the X band data in Figs. 3 and 4. The predicted six-line spectrum is not even observed. At low magnetic fields, the energy levels are nonlinear functions of H due to large off-diagonal matrix elements of $A\,\vec{I} \cdot \vec{J}$ and this term is the dominant one in the spin Hamiltonian. Only F and its Z-component, m_F, are good quantum numbers with I and S' being nominal at best. In the K and Q band regions however, the magnetic field can more successfuly compete with the hyperfine interaction and the spacings of resonant absorption transitions are more uniform. As the strong magnetic field case is approached from the weak field limit, the field-dependent terms in Eq. (2) become more important, the energy levels become more linear, and $\vec{I}$ and $\vec{S}'$ begin to precess about $\vec{H}$ independently. Descriptions of the energy levels, therefore, are better denoted by $|I, m_I, S', m_{S'}\rangle$ basis functions since F is not longer a good quantum number.

Assuming no crystal field mixing of states, the wavefunction for the Γ_6 ground state is[4]

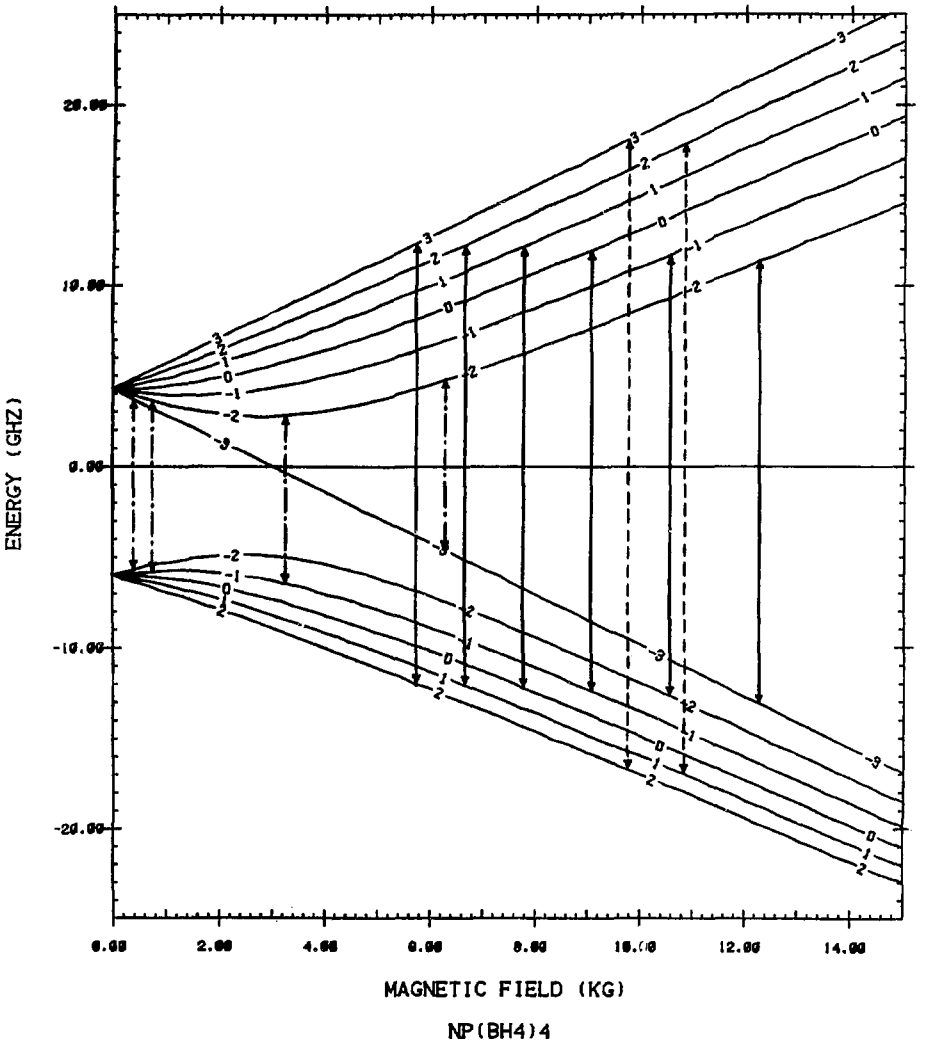

XBL 798-11097

Figure 4. Zeeman Energy Levels for $Np(BH_4)_4$. Observed allowed transitions are shown for X band —— · —— · ——, K band ———, and Q band -----.

$$\Psi_{\Gamma_6} = .6124|\pm 9/2\rangle + .7638|\pm 1/2\rangle + .2041|\mp 7/2\rangle$$

and gives a g value of 2.667. This calculated value is larger than the 1.894 value determined from the EPR spectra. Since the volatile, low melting metal borohydrides are regarded as covalent molecules in contrast to the non-volatile, high melting, ionic alkali metal borohydrides,[8] the effects of covalency[9] may be an important factor in lowering the g value. Crystal field calculations performed in the preliminary analysis of $Np(BH_4)_4$ optical spectra have included J mixing and yielded the correct g value for certain values of Hamiltonian parameters. A discussion of the calculations are given in chapter 5.

The g_I value found for $Np(BD_4)_4$ improved the fit and was used in a second-order perturbation calculation[10-12] for the energy of the higher-lying $\Gamma_8^{(1)}$ state. The deviation of the observed pseudo-nuclear g value from the calculated one is reflected in the interaction of the ground Γ_6 state and the nearest $\Gamma_8^{(1)}$ quartet. The energy of the $\Gamma_8^{(1)}$ state is

$$E(\Gamma_8^{(1)}) = \frac{2ag_J\Sigma\langle\Gamma_6|J_Z|\Gamma_8^{(1)}\rangle^2\beta}{G_N\beta_N} \qquad (3)$$

where $a = \frac{3}{11}A$, $g_J = \frac{3}{11}g$, G_N is the difference between the observed and calculated nuclear g_N values,[10,13] and β_N is the nuclear magneton. Using the $\Gamma_8^{(1)}$ wave function[4] where x = .23, the $\Gamma_8^{(1)}$ energy is 7 cm^{-1}. To test whether the 7 cm^{-1} separation would cause anisotropy in the ob-

served EPR spectra, the complete Hamiltonian for the J = 9/2 manifold was used in calculating the energy levels for all three crystal field levels and their Zeeman components. The Hamiltonian is

$$\mathcal{H} = a\,\vec{I}\cdot\vec{J} + g_J\beta\vec{H}\cdot\vec{J} - g_N\beta\vec{H}\cdot\vec{I} + B_4(O_4^0+5O_4^4) + B_6(O_6^0-21O_6^4) \qquad (4)$$

Using the B_4 and B_6 values found for $U(BH_4)_4$[5] in Eq. (4) for $Np(BH_4)_4$, gave a much larger Γ_6, $\Gamma_8^{(1)}$ separation than that obtained from Eq. (3). If the same B_4/B_6 ratio of 12.6 is used in Eq. (4), the calculated values of B_4 and B_6 which results by requiring $E(\Gamma_8^{(1)}) - E(\Gamma_6) = 7\ cm^{-1}$, turn out to be unreasonably small. This suggests that the g_I value given in Table 3 was not accurately determined.

If the $\Gamma_8^{(1)}$ state is sufficiently close to the Γ_6 ground state, the wavefunctions will mix and anisotropy will be seen in the EPR spectra as a function of the angle between the magnetic field and the crystal axes. The degree of anisotropy of the Γ_6 state was calculated as a function of the Γ_6, $\Gamma_8^{(1)}$ separation for the (001) and (111) directions by the Hamiltonian

$$\mathcal{H} = a\,\vec{I}\cdot\vec{J} + g_J\beta(H_xJ_x+H_zJ_z) - g_N\beta(H_xI_x+H_zI_z)$$

$$+ B_4(O_4^0+5O_4^4) + B_6(O_6^0-21O_6^4) \qquad (5)$$

The direction of the magnetic field was restricted to lie along the xz

plane, making an angle Θ with the z-axis. Energy levels for $\vec{H}$ along (001) were calculated with $\Theta = 0°$ and those for $\vec{H}$ along (111) were found using $\Theta = \tan^{-1}\sqrt{2}$ and $-O_4^4$ and $-O_6^4$ instead of O_4^4 and O_6^4.

Results of the above calculations showed that considerable anisotropy would be noticeable for a change of the magnetic field direction from (001) to (111) if the Γ_6, $\Gamma_8^{(1)}$ separation were less than approximately 20 cm^{-1}. Field values for transitions of all samples at X, K, and Q bands were not observed to change when the magnet was rotated. Although the orientation of the crystals were not known, it seems unlikely that the calculated 7 cm^{-1} separation is correct. The other calculations using Eq. (4) described earlier, support this conclusion. The significance of the improved fit and g_I value in Table 3 must be tested further.

It was hoped that, from the EPR data, values of B_4 and B_6 could be determined using Eq. (4). It turned out that the energy levels are too insensitive to the crystal field parameters and accurate values must be obtained from the electronic spectra discussed in the next chapter.

The observed EPR transitions shown in Figs. 2 and 3 did not significantly shift when the host matrix was changed from the cubic $Zr(BH_4)_4$ crystal to an amorphous methylcyclohexane (MCH) glass. The structure of $Np(BH_4)_4$ retains its T_d symmetry in both host materials.

The EPR spectrum of pure $Np(BD_4)_4$ consisted of one broad resonance (FWHH = 5000 gauss) centered at approximately $g = 2.0 \pm .2$. The extreme broadness of the band is mainly due to the magnetic dipole-dipole interaction.

References

[1(a)] Orton, J. W. "Electron Paramagnetic Resonance." London ILIFFE Books, Ltd. London, 1968.

[(b)] Abragam, A.; Bleaney, B. "Electron Paramagnetic Resonance of Transition Ions." Oxford University Press. London, 1970.

[2] Hutchings, M. T. Solid State Physics 16 227 (1965).

[3] Stevens, K. W. H. Proc. Phys. Soc. (London) A65 209 (1952).

[4] Lea, K. R.; Leask, M. J. M.; Wolf, W. P. J. Phys. Chem. Solids 23 1381 (1962).

[5] Bernstein, E. R.; Keiderling, T. A. J. Chem. Phys. 59 2105 (1973).

[6] Hutchison, Jr., C. A.; Weinstock, B. J. Chem. Phys. 32 56 (1960).

[7] Ramsey, N. F. "Molecular Beams." Oxford University Press. London, 1963, p. 76.

[8] Marks, T. J.; Kolb, J. R. Chem. Rev. 77 263 (1977).

[9] Bleaney, B. Proc. Roy. Soc. (London) A277 289 (1964).

[10] Axe, J. D.; Stapleton, H. J.; Jeffries, C. D. Phys. Rev. 121 1630 (1961).

[11] Lewis, H. R.; Sabisky, E. S. Phys. Rev. 130 1370 (1963).

[12] Baker, J. M.; Bleaney, B. Proc. Roy. Soc. (London) A245 156 (1958).

[13] Lewis, W. B.; Mann, J. B.; Liberman, D. A.; Cromer, D. T. J. Chem. Phys. 53 809 (1970).

Chapter 5

OPTICAL SPECTRA OF $Np(BH_4)_4$ AND $Pa(BH_4)_4$

Introduction

There are numerous reports[1-5] of spectroscopic studies of f-electron ions in crystalline ligand fields which have furnished much information on the electronic energy level structures of the lanthanide and actinide ions. In systems where the symmetry of the ligand fields is high, assignments of the spectral bands have been made and have led to the determination of free ion and crystal field Hamiltonian parameters. In conjunction with theory, spectral studies have formed the basis of the understanding of the quantum mechanical properties of these ions.

Optical spectra of $Np(BH_4)_4$ and $Np(BD_4)_4$ in pure form and diluted in $Zr(BH_4)_4$ and $Zr(BD_4)_4$ were found to be dominated by vibronic transitions. Results from the normal coordinate analysis (see chapter 3) were used in assigning vibronic bands of the $\Gamma_6(^4I_{9/2}) \rightarrow \Gamma_8^{(1)}(^4I_{11/2})$ transitions. The vibrational modes found are expected to appear with the other electronic bands within the $5f^3$ configuration. Assignment of these remaining spectral bands have not been done and must wait for results from Zeeman, resonance Raman, low-temperature-far infrared, and fluorescence spectra.

Preliminary spectra of $Pa(BH_4)_4$ and $Pa(BD_4)_4$ are also given in this chapter.

Experimental

Pure Compound Spectra

All spectra presented in this chapter were recorded on a Cary 17 spectrophotometer. Single crystals of $Np(BH_4)_4$ and $Np(BD_4)_4$ of 30 μ path length and 1 mm thick $Zr(BH_4)_4$ and $Zr(BD_4)_4$ crystals were grown as described in chapter 3. Spectra were taken from 350-2500 nm at 2K, 77K, and 300K.

Diluted Compound Spectra

Mixed crystals, $Np(BH_4)_4/Zr(BH_4)_4$ and $Np(BD_4)_4/Zr(BD_4)_4$, were grown from the vapor according to the method of Bernstein and Keiderling.[6] $Np(BH_4)_4$ and $Np(BD_4)_4$ isolated in a methylcyclohexane (MCH) glass were found to give slightly broader but equivalent spectra.

In the photographic region, 300-1000 nm, low temperature spectra of $Np(BH_4)_4/Zr(BH_4)_4$ were recorded on a 3/4 m Jarrell Ash spectrograph. No additional structure was observed.

At room temperature $Pa(BH_4)_4$ does not dissolve in $Zr(BH_4)_4$ or MCH, but small amounts can be made to dissolve in them if the mixtures are heated to 60-70° for approximately 1 hour in a sealed glass tube.[7] Five mg $Pa(BH_4)_4$ were added to a quartz optical cell in an inert atmosphere drybox. After evacuating the cell at room temperature, 300 mg $Zr(BH_4)_4$ was condensed into the cell which was subsequently sealed off under vacuum. A yellow solution was obtained upon heating as the $Pa(BH_4)_4$ dissolved. Crystals grown by slow cooling of the solution were very inhomogenous and the $Pa(BH_4)_4$ did not appear to incorporate itself into

the $Zr(BH_4)_4$ lattice. Dark yellow and colorless areas in the crystals were observed with the former presumably being pure $Pa(BH_4)_4$. This crystal was not suitable for spectroscopic measurements. Single crystals grown from the vapor were colorless $Zr(BH_4)_4$ crystals since the $Pa(BH_4)_4$ did not cosublime with $Zr(BH_4)_4$.

Suitable quality samples of $Pa(BH_4)_4$/MCH-d_{14} and $Pa(BD_4)_4$/MCH-d_{14} for optical spectra were made by dissolving the Pa compound in MCH-d_{14} as above. Transparent glasses were formed when the solutions were quickly cooled with liquid helium in the optical dewar. As will be discussed later, the structure of $Pa(BH_4)_4$ in the organic glass is not known with certainty. Spectra were taken in the range 2100-300 nm at 2K and 300K.

Theory

The energy levels of an ion in a crystalline electric field (e.g. Np^{4+} in $Np(BH_4)_4$ or Pa^{4+} in $Pa(BH_4)_4$) can be approximately calculated using a Hamiltonian of the form[4]

$$\mathcal{H} = \mathcal{H}_f + \mathcal{H}_c \tag{1}$$

The $\mathcal{H}_f$ term is the free ion Hamiltonian and consists of the sum of the kinetic energies of the electrons, the potential energy of all the electrons in the field of the nucleus, the electrostatic repulsion of pairs of electrons, and the spin orbit interaction between the spin and orbital angular momenta for each electron. The second term, $\mathcal{H}_c$, is the

crystal field contribution which accounts for the splitting of free ion J levels by the electric field produced by the ligand change. The free ion Hamiltonian is

$$\mathcal{H}_f = \sum_{i=1}^{N} \frac{\hbar^2}{2m} \nabla_i^2 - \sum_{i=1}^{N} \frac{Ze^2}{r_i} + \sum_{i<j}^{N} \frac{e^2}{r_{ij}} + \sum_{i=1}^{N} \xi(r_i)\vec{s}_i \cdot \vec{\ell}_i \qquad (2)$$

when the nucleus of atomic number Z is assumed to have infinite mass. Usually the central field approximation[8] is made where each electron moves in a spherically symmetric potential, $-U(r_i)/e$. $\mathcal{H}_f$ becomes

$$\mathcal{H}_f = \left[\sum_{i=1}^{N} \frac{-Ze^2}{r_i} - U(r_i)\right] + \sum_{i<j}^{N} \frac{e^2}{r_{ij}} + \sum_{i=1}^{N} \xi(r_i)\vec{s}_i \cdot \vec{\ell}_i \qquad (3)$$

The first term in Eq. (3) shifts all levels in the same ℓ^N configuration equally and can be ignored. The magnitude of the second term depends on the particular electronic state of the configuration and matrix elements of the type

$$\langle f^N\, UWSLJM_J | \sum_{i<j}^{N} \frac{e^2}{r_{ij}} | f^N\, U'W'S'L'J'M'_J \rangle$$

are needed.

Tensor operators are very useful in the calculation of matrix elements and that above can be written as

$$\langle f^N\, UWSLJM_J | \sum_{i<j}^{N} \frac{e^2}{r_{ij}} | f^N\, U'W'S'L'J'M'_J \rangle = \sum_{\substack{k=0 \\ \text{even}}}^{6} f^K F_K(nf,nf) \qquad (4)$$

where f^K are the angular parts of the interaction and F_K are the Slater integrals

$$F_K = \frac{e^2}{D^K} \int_0^\infty \int_0^\infty \frac{r_<^K}{r_>^{K+1}} R_{nf}^2(r_i) R_{nf}^2(r_j) dr_i dr_j \qquad (5)$$

The D^K are numerical factors; $D^2 = 225$, $D^4 = 1089$, and $D^6 = \frac{25}{184041}$.

These F_K do not appear in the free ion Hamiltonian for Pa^{4+} ($5f^1$) since it has only one 5f electron.

Matrix elements of the spin . bit operator can be expressed in tensor operator form as

$$\langle f^N\, UWSLJM_J | \zeta_{nf} \sum_{i=1}^{N} \vec{s}_i \cdot \vec{\ell}_i | f^N\, U'W'S'L'JM_J \rangle = \zeta_{nf} (-1)^{J+L+S'}$$

$$\times \left[\ell(\ell+1)(2\ell+1)\right]^{\frac{1}{2}} \begin{Bmatrix} L & L' & 1 \\ S' & S & J \end{Bmatrix} \langle f^N\, UWSL || V^{(11)} || f^N\, U'W'S'L' \rangle \qquad (6)$$

where $\zeta_{nf} = \int_0^\infty R_{nf}^2\, \xi(r) dr$ and $\langle f^N\, UWSL || V^{(11)} || f^N U'W'S'L' \rangle$

is the reduced matrix element of $V^{(11)}$, tabulated by Nielsen and Koster[9]

Using the hydrogenic ratios for the Slater radial integrals, F_4/F_2 and F_6/F_2, the free ion energy matrix can be expressed in terms of two parameters, F_2 and ζ_{nf}, to be determined from experiment.

Previous studies on Np^{4+}[10-12] have found that F_2=200-250 cm^{-1} and ζ_{5f} = 1950-2150 cm^{-1} compared to F_2 = 320-340 cm^{-1} and ζ_{4f} = 800-900 cm^{-1} for Nd^{3+} ($4f^3$).[4,13] For nf^1 systems, ζ_{5f} = 1500 cm^{-1}[14] for Pa^{4+} and ζ_{4f} = 640 cm^{-1} for Ce^{3+}.[15]

When an ion is placed in a static electric field of a crystal, the spherical symmetry of the free ion J levels is reduced to that of the crystals and each (2S+1)(2L+1)-fold degenerate J state splits into crystal field states labelled by Γ_i. The Hamiltonian for a T_d crystal field was given in chapter 4 as

$$\mathcal{H}_c = B_4 (O_4^0+5O_4^4) + B_6 (O_6^0-21O_6^4) \tag{7}$$

whose matrix elements are tabulated by Hutchings.[16] In tensor operator notation, $\mathcal{H}_c$, is

$$\mathcal{H}_c = B_0^4[C_0^{(4)} + (5/14)^{\frac{1}{2}}(C_4^{(4)}+C_{-4}^{(4)})] + B_0^6[C_0^{(6)}-(7/2)^{\frac{1}{2}}(C_4^{(6)}+C_{-4}^{(6)})] \tag{8}$$

In Eq. (8), $C_q^{(K)}$ is a tensor operator of rank K and $B_0^4 = \frac{8B_4}{\beta}$ and $B_0^6 = \frac{16B_6}{\gamma}$ where β and γ are the 4th and 6th degree operator equivalent factors.[17,18]

All 41 J states of Np^{4+} and 2 J states of Pa^{4+} in a T_d crystal field break up into either Γ_6, Γ_7, or Γ_8 states where the Γ_6 and Γ_7 levels are doubly degenerate and the Γ_8 states are four-fold degenerate.

The total Hamiltonian in Eq. (1) contains four parameters, F_2, ζ_{5f}, B_0^4, and B_0^6 for Np^{4+} and three parameters, ζ_{5f}, B_0^4, and B_0^6 for Pa^{4+} which are determined by a least squares fitting process that minimizes the difference between the observed and calculated energies of the crystal field states. Using the values F_2 = 204 cm^{-1} and ζ_{5f} = 2116 cm^{-1},

crystal field levels for $Np(BH_4)_4$ were calculated for various values and ratios of B_0^4/B_0^6. Plots of the levels are shown in Figs. 1-3. The range of B_0^4 and B_0^6 values used in the plots were such that the actual values for $Np(BH_4)_4$ would be represented. These plots are helpful in assigning the spectral bands.

Results and Discussion

Neptunium Borohydride

As seen in the energy level diagrams in Figs. 1-3, the Γ_6 level of the $^4I_{9/2}$ manifold is the ground state, in agreement with the EPR results (see chapter 4). The two Γ_8 states of that manifold are well below the other manifolds yet they were not identified in the IR spectra (see chapter 3).

The next higher lying manifold is $^4I_{11/2}$ which breaks up into $\Gamma_6 + \Gamma_7 + 2\Gamma_8$ states in which one of the Γ_8 states is lowest. This one is identified in the optical spectra and is discussed later. Above these manifolds the states become closer together and their assignment is very difficult without large amounts of experimental data. Spectral analyses of f^3 configurations which have been reported considered only the lowest six J manifolds.[13,19,20]

The optical spectra of $Np(BH_4)_4$ and $Np(BD_4)_4$ at 2K are shown in Figs. 4-7. Similar spectra of $U(BH_4)_4$ and $U(BD_4)_4$ in $Hf(BH_4)_4$ and $Hf(BD_4)_4$ were taken by Bernstein and Keiderling[6] which, like the spectra presented here, revealed extensive vibronic structure. In general the deuteride spectra are sharper than those of the hydride and considerable broadening was observed with samples at 77K and 300K.

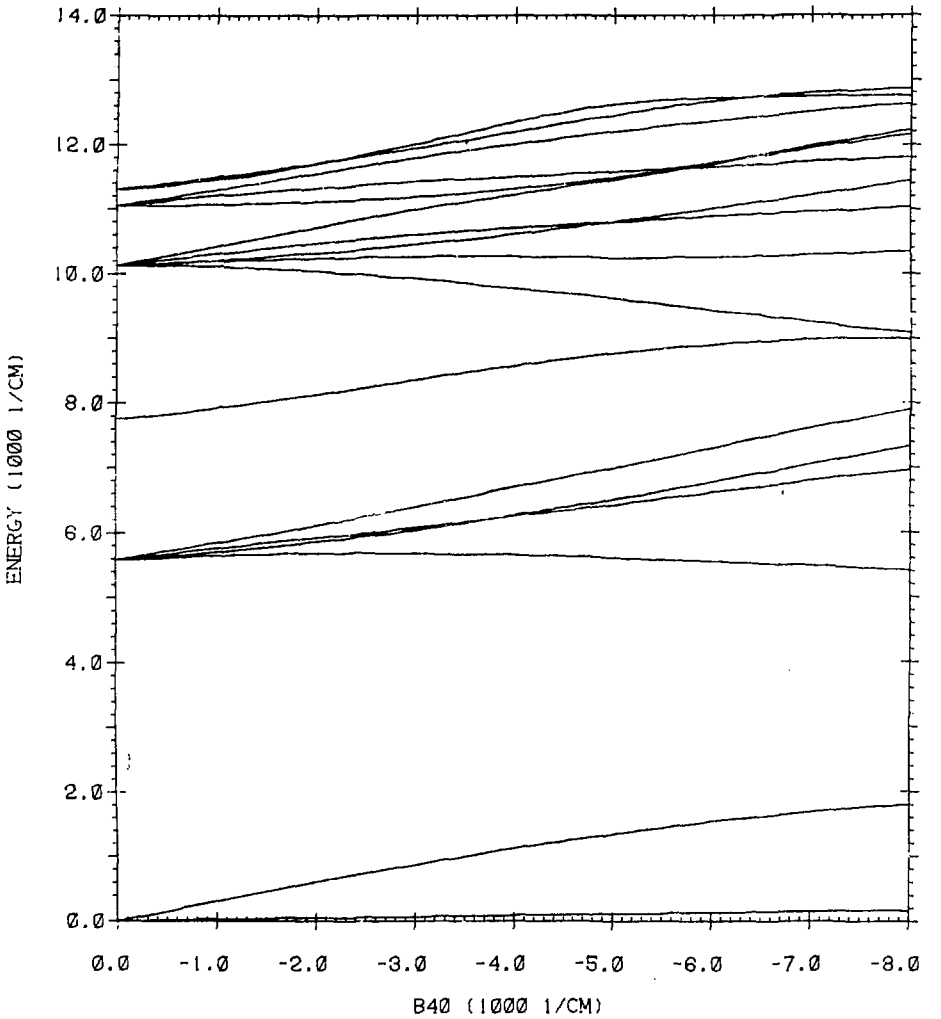

CRYSTAL FIELD STATES OF NP(BH4)4; B40/B60 = 1.31

XBL 7912-13705

Figure 1.

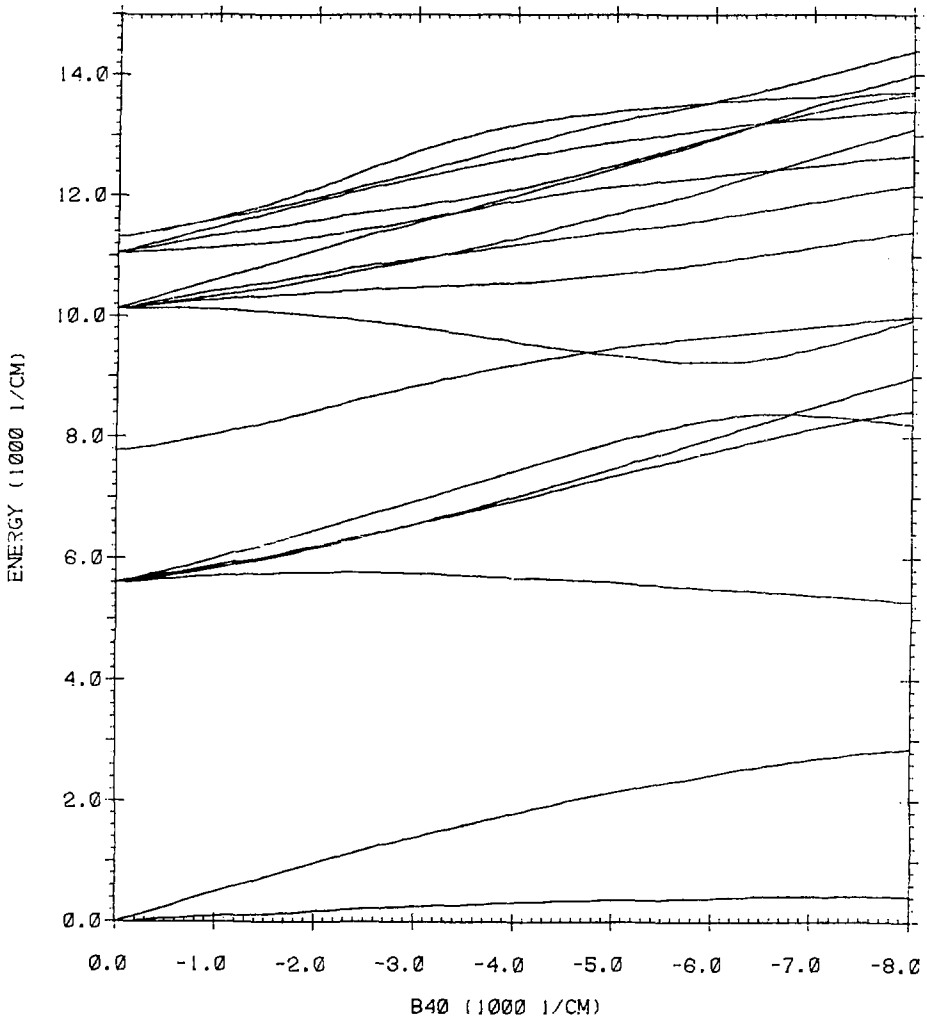

CRYSTAL FIELD STATES OF NP(BH4)4; B40/B60 = 0.35

XBL 7912-13704

Figure 2.

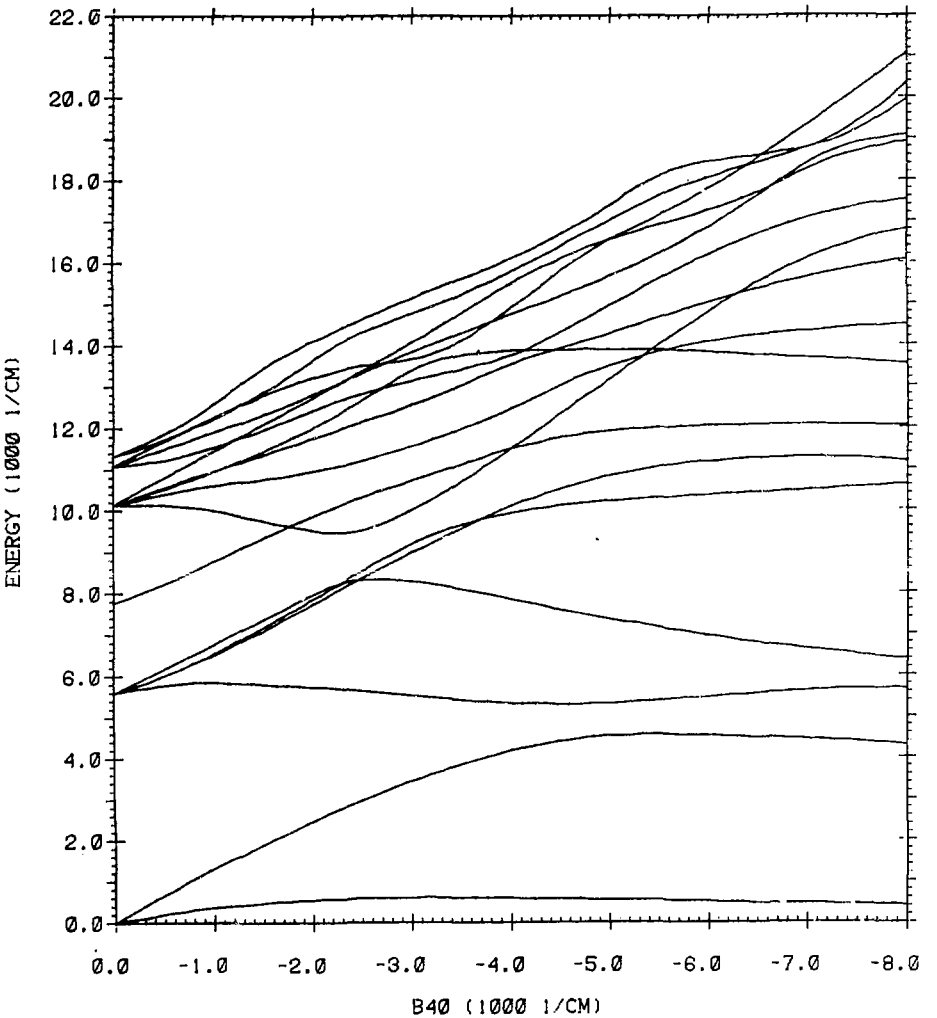

CRYSTAL FIELD STATES OF NP(BH4)4, B40/B60 = 0.33

XBL 7912-13706

Figure 3.

Figures 4-7. Optical Absorption Spectra of $Np(BH_4)_4$ and $Np(BD_4)_4$ in the Near Infrared and Visible Regions at 2K.

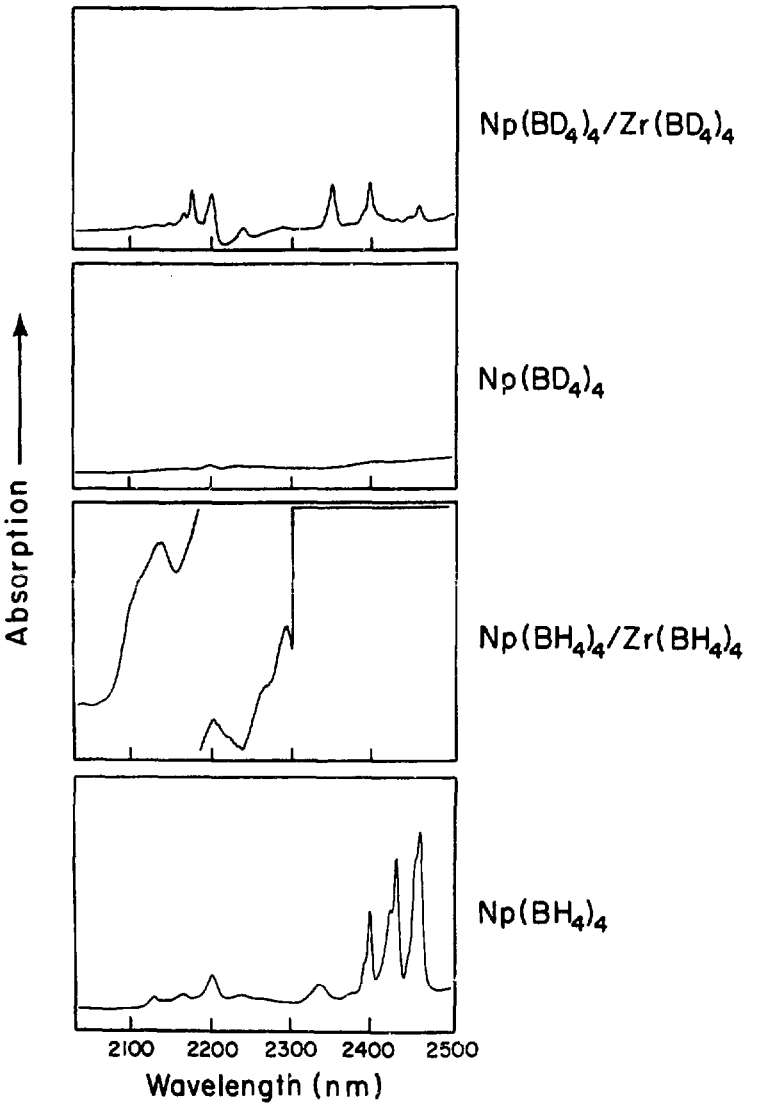

Figure 4. XBL7911-13258

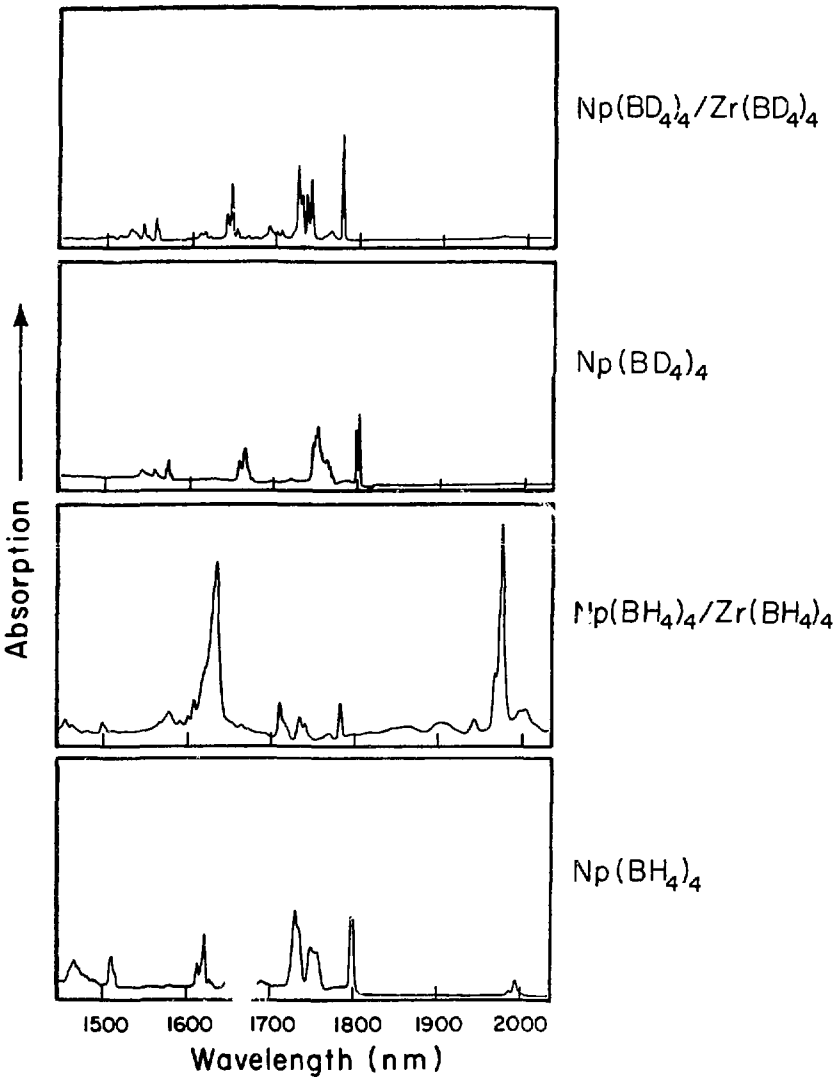

Figure 5. XBL79:1-13259

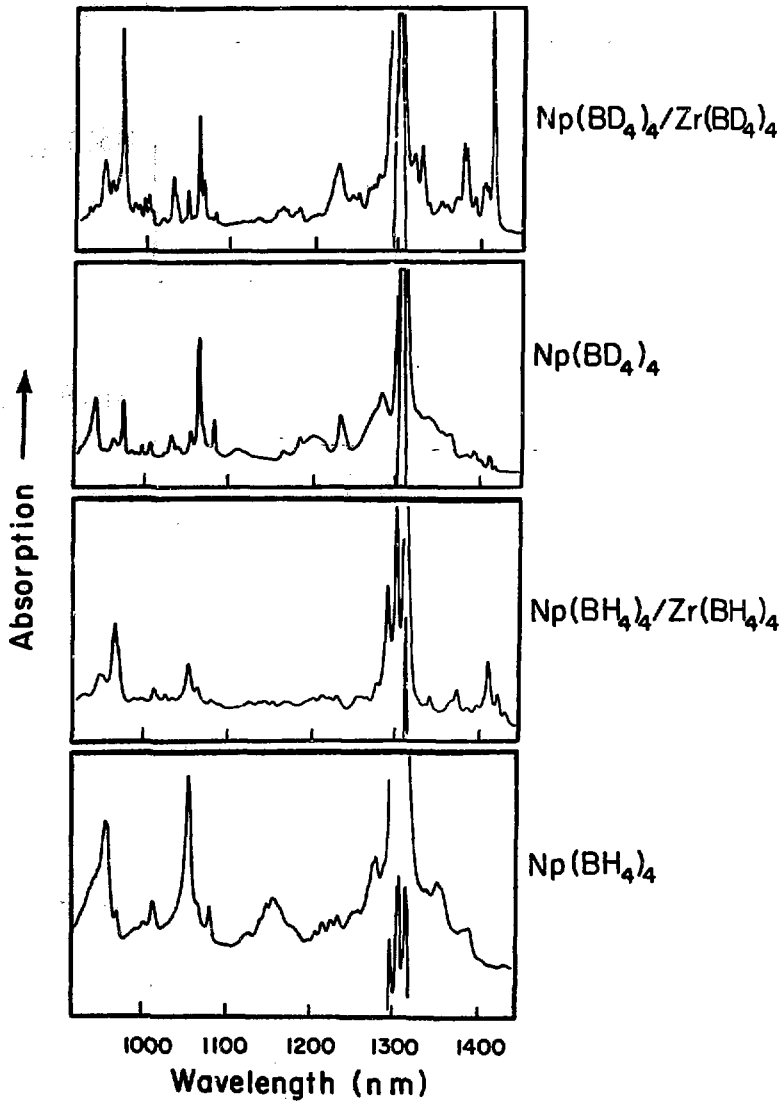

Figure 6. XBL7911-13260

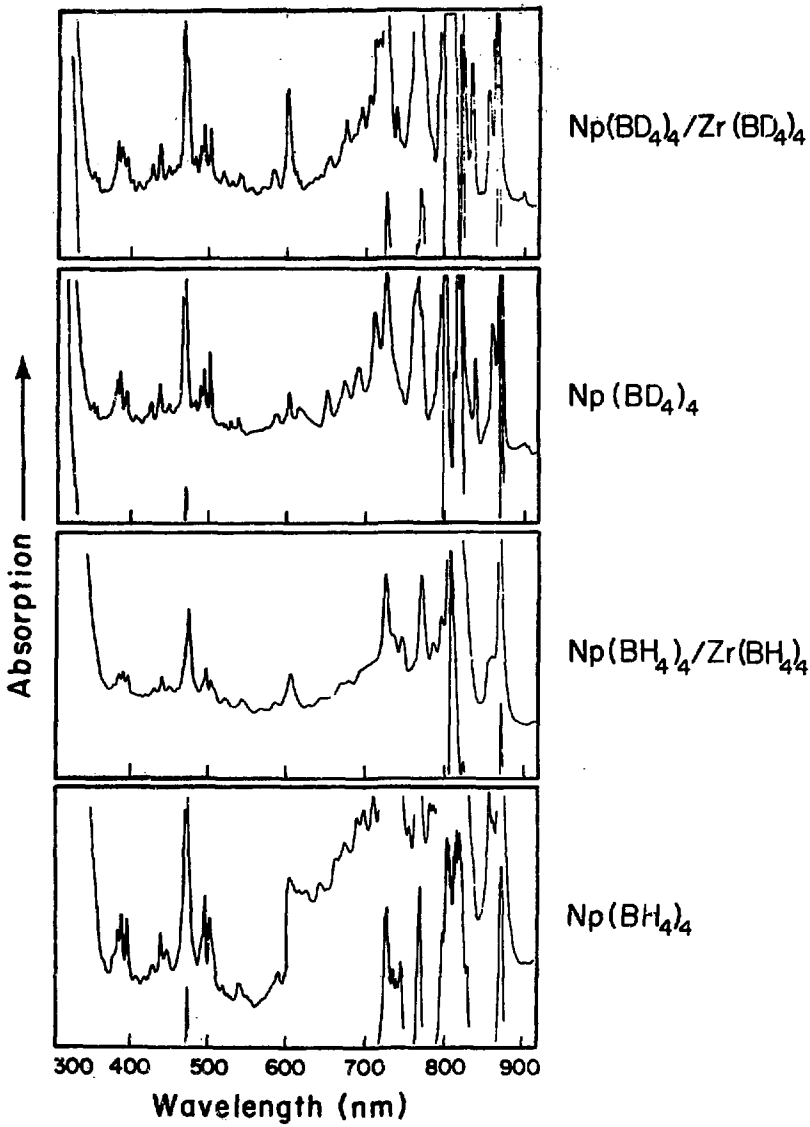

XBL7911-13255

Figure 7.

For molecules lacking a center of inversion, forced electric dipole transitions are allowed although the transition intensities are expected to be weak. Magnetic dipole transitions are allowed but they are usually 10^4 times weaker than those of electric dipole origin and are not observed. For $Np(BH_4)_4$ having a Γ_6 ground state, the only forbidden electronic and vibronic transitions are

$$\Gamma_6 \rightarrow \Gamma_6'(0\rightarrow 0);\ \Gamma_6 \rightarrow \Gamma_7 + \nu^{A_2};\ \Gamma_6 \rightarrow \Gamma_6' + \nu^{A_1}.$$

It is difficult to locate Γ_6 levels since they are forbidden but vibronic transition terminating on non-totally symmetric vibrational levels can have appreciable intensity.

The spectral bands in Fig. 4 are all vibrational overtone or combination bands (see chapter 3). The absence of electronic bands in this low energy region is due to the large spin orbit interaction which separates the J = 9/2 and J = 11/2 states of the ^4I manifold by about 5600 cm^{-1}.[10]

The spectra shown in Fig. 5 clearly exhibit the $(^4I_{9/2}) \rightarrow \Gamma_8^{(1)}$ $(^4I_{11/2})$ 0-0 Stark transition at 1783.8 nm (5604.5 cm^{-1}) for $Np(BD_4)_4/Zr(BD_4)_4$ and 1783.5 nm (5605.4 cm^{-1}) for $Np(BH_4)_4/Zr(BH_4)_4$. Vibronic bands extending to higher energies are obvious and follow the decreasing Franck-Condon envelope. According to the Franck-Condon principle, the geometries of the electronic states involved in the transition are similar. Adiabatic (vertical) transitions from the ground to excited states therefore are expected to be the most intense while the vibronic transitions become weaker for those transitions ending on the higher vibra-

tional states of the excited electronic level. Basic line shapes and relative intensities of the vibronic bands are similar for the hydride and deuteride and corresponding vibronic bands show the expected increase in energy from the deuteride to hydride. Assignment of these bands were based on the results of the normal coordinate analysis and are listed in Table 1.

The vibronic transitions which originate from the ground vibrational state of Γ_6 ($^4I_{9/2}$) (kT = 1.4 cm^{-1} at 2K), terminate on the various vibrational states of the $\Gamma_8^{(1)}$ ($^4I_{11/2}$) electronic level. In Table 1 and Fig. 4 (chapter 3), it is seen that the highest-energy vibronic transitions for the hydride and deuteride are the highest-energy νMH_b (νMD_b) fundamental modes. The $\nu BH_{t,b}$ modes do not couple well to electronic transitions of the metal ion and also would not be expected to be strong from Franck-Condon arguments. The fundamental vibrations listed in Table 1 were also seen in the spectra of $U(BH_4)_4/Hf(BH_4)_4$ and $U(BD_4)_4/Hf(BD_4)_4$[6] and should be seen with other electronic transitions in the spectra shown in Figs. 6 and 7.

The strong bands at 1600-1650 nm and 1900-2000 nm in the spectrum of $Np(BH_4)_4/Zr(BH_4)_4$ are due to $3\nu_3^{T_2}$ and $2\nu_1^{T_2}$ modes of $Zr(BH_4)_4$ respectively (see Table 18, chapter 3).

In the pure $Np(BH_4)_4$ and $Np(BD_4)_4$ spectra, the corresponding bands shift to lower energies by approximately 50 cm^{-1} and broaden with a loss of detail. The $\Gamma_8^{(1)}$ ($^4I_{11/2}$) becomes a doublet with a separation of 10 cm^{-1}.

Table 1

Vibronic Bands of the Γ_6 ($^4I_{9/2}$) → $\Gamma_8^{(1)}$ ($^4I_{11/2}$) 0-0 Stark Transition

Wavelength (nm)	Energy (cm^{-1})	Difference (cm^{-1})	Assignment
		$Np(BH_4)_4/Zr(BH_4)_4$	
1783.5	5605	----	$\Gamma_8^{(1)}$ ($^4I_{11/2}$)
1741.3	5741	136	$\Gamma_8^{(1)} + \nu_9^{T_2}$
1735.2	5762	157	$\Gamma_8^{(1)} + \nu_5^{E}$
1711.2	5842	237	$\Gamma_8^{(1)} + \nu^{A_2}$ *a*
1665.0	6004	399	$\Gamma_8^{(1)} + \nu_5^{T_1}$ *b*
1627.1	6144	586	$\Gamma_8^{(1)} + \nu_4^{E}$ *b,c*
1608.1	6217	612	$\Gamma_8^{(1)} + \nu_8^{T_2} + \nu_9^{T_2}$
1601.2	6244	639	$\Gamma_8^{(1)} + \nu_8^{T_2} + \nu_5^{E}$
1502.1	6656	1051	$\Gamma_8^{(1)} + \nu_3^{E}$
1498.8	6670	1065	$\Gamma_8^{(1)} + \nu_3^{T_1}$ *b*
1481.1	6750	1145	$\Gamma_8^{(1)} + \nu_6^{T_2}$
1462.3	6837	1232	$\Gamma_8^{(1)} + \nu_5^{T_2}$
1453.9	6876	1271	$\Gamma_8^{(1)} + \nu_4^{T_2}$
		$Np(BD_4)_4/Zr(BD_4)_4$	
1783.8	5604	----	$\Gamma_8^{(1)}$ ($^4I_{11/2}$)
1746.1	5725	121	$\Gamma_8^{(1)} + \nu_9^{T_2}$
1740.9	5743	139	
1735.4	5761	157	$\Gamma_8^{(1)} + \nu_5^{E}$
1730.6	5777	173	$\Gamma_8^{(1)} + \nu^{A_2}$ *a*
1695.7	5896	292	$\Gamma_8^{(1)} + \nu_5^{T_1}$
1662.4	6014	410	$\Gamma_8^{(1)} + \nu_4^{E}$ *b*
1656.5	6035	431	$\Gamma_8^{(1)} + \nu_7^{T_2}$
1650.6	6057	453	$\Gamma_8^{(1)} + {}^{10}B(\nu_7^{T_2})$
1644.6	6079	475	$\Gamma_8^{(1)} + \nu_4^{A_1}$
1562.6	6398	794	$\Gamma_8^{(1)} + \nu_3^{E}$

Table 1 (continued)

Wavelength (nm)	Energy (cm^{-1})	Difference (cm^{-1})	Assignment[b]
1560.1	6408	804	$\Gamma_8^{(1)} + \nu_3^{T_1}$
1545.0	6471	867	$\Gamma_8^{(1)} + \nu_6^{T_2}$
1533.5	6519	915	$\Gamma_8^{(1)} + \nu_5^{T_2}$
1530.0	6534	930	$\Gamma_8^{(1)} + \nu_4^{T_2}$

[a]The A_2 mode was not observed or calculated for $Np(BH_4)_4$ and $Np(BD_4)_4$ so this assignment has not been confirmed.

[b]These assignments are based on frequency calculations (see chapter 3).

[c]Due to interference from $3\nu_3^{T_2}$, this band was taken from pure $Np(BH_4)_4$ spectra.

Spectra in Figs. 6 and 7 are very complicated and no assignments of the bands were made. The next electronic band is probably that at 1411.4 nm (7038.2 cm^{-1}) for $Np(BD_4)_4/Zr(BD_4)_4$ seen as an intense, sharp peak in Fig. 6. It is too far removed from the 5604 cm^{-1} level to be vibronic and is also too intense. Strangely, it is only weakly observed as a close doublet in the $Np(BD_4)_4$ spectrum.

Consistent with spectra of other $5f^3$ ions,[10,21,22] very strongly absorbing regions occur at 1300 nm (Fig. 6) and 740, 780, 810, 880 nm (Fig. 7).

The g value (1.89) found for the Γ_6 ground state of $Np(BH_4)_4$ differed significantly from that calculated from crystal field theory without J mixing. Eigenvectors from the energy level calculations of Figs. 1-3 showed that substantial J mixing occurred. Although some of the g-value deviation may be due to covalency effects, the correct g value was calculated if certain values of B_0^4, B_0^6, and ζ_{5f} were used. A plot of g value vs. B_0^4 (with constant B_0^4/B_0^6) were made for various B_0^4/B_0^6 ratios and is shown in Fig. 8. It is evident that for small values of the B_0^4/B_0^6 ratio, J mixing is strong (see also Figs. 1-3). Lines of constant g (g = 1.89) were drawn for various values of B_0^4 and B_0^6 and for three values of ζ_{5f}. This graph is given in Fig. 9. A satisfactory fit of $\Gamma_8^{(1)}$ ($^4I_{11/2}$) was obtained for g = 1.89 but the next higher-lying crystal field state was calculated at ~7700 cm^{-1} suggesting that the intense absorption at 7083 cm^{-1} mentioned earlier is vibronic. Additional spectroscopic data are needed before reliable assignments can be made.

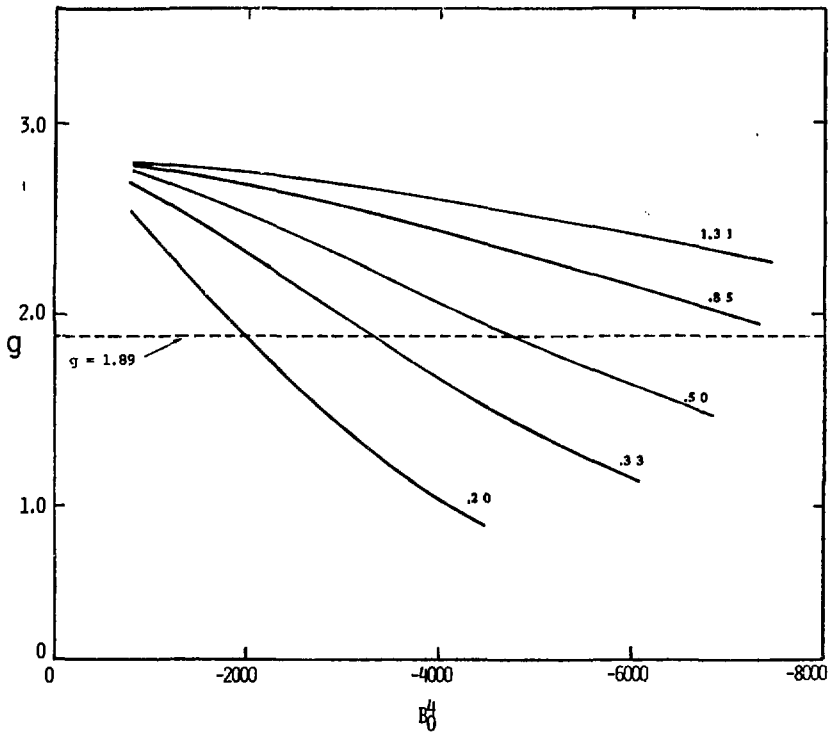

Figure 8.

g Value vs. B_0^4

The number next to a curve indicates the B_0^4/B_0^6 ratio.

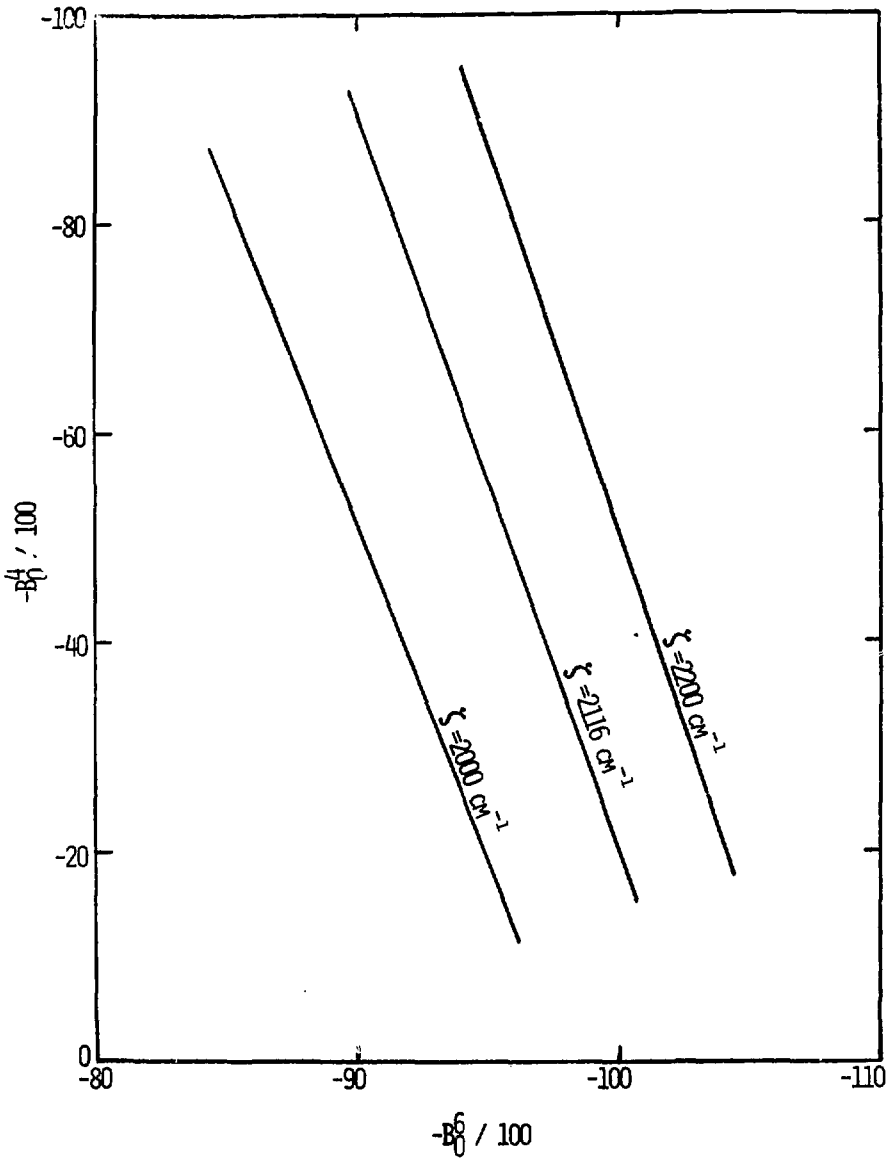

XBL 7912-13707

Figure 9.

Protactinium Borohydride

The $5f^1$ configuration of Pa^{4+} has one LS state, ^2F, which breaks up into a $^2F_{5/2}$ ground state and $^2F_{7/2}$ excited state by the spin orbit interaction with a separation of $7/2\zeta_{5f}$. A crystal field of the type given as Eq. (8) causes the further splitting of the free ion levels into $^2F_{5/2} \rightarrow \Gamma_7 + \Gamma_8$ and $^2F_{7/2} \rightarrow \Gamma_6 + \Gamma_7' + \Gamma_8'$. According to the H(12) crystal field model, $B_0^4 < 0$ and the Γ_8 ($^2F_{5/2}$) state is the ground state.[23] Although this prediction has not been confirmed by EPR experiments, it is probably correct since the H(12) model was correct for $U(BH_4)_4$ and $Np(BH_4)_4$.

Transitions between the $J = 5/2 \rightarrow J = 7/2$ manifold for f^1 ions occur in the near infrared. The lowest Γ_7 state is predicted to lie approximately 1300 cm^{-1} above the Γ_8 ground state and was not observed in the Cary 17 spectra. The low temperature optical spectra of the hydride and deuteride in a MCH-d_{14} glass are shown in Fig. 10. Three bands are seen which, if the symmetry of $Pa(BH_4)_4$ were tetrahedral, would be the Γ_6, Γ_7', and Γ_8' of the $J = 7/2$ level. But Keiderling[24] discovered that when a hydrocarbon solution of $U(BH_4)_4$ was frozen, the monomeric, tetrahedral structure of $U(BH_4)_4$ reverted into the polymeric, C_2 symmetry structure. This same phenomenon is presumed to occur for $Pa(BH_4)_4$ and would result in the splitting of the Γ_8 states. A crystal field Hamiltonian consisting of nine crystal field parameters would then be needed to analyze the spectra.

While it is very tempting to assign the three observed bands on the basis of the tetrahedral structure, comparison of these spectra to

pure crystal spectra is necessary before any definitive conclusions can be reached.

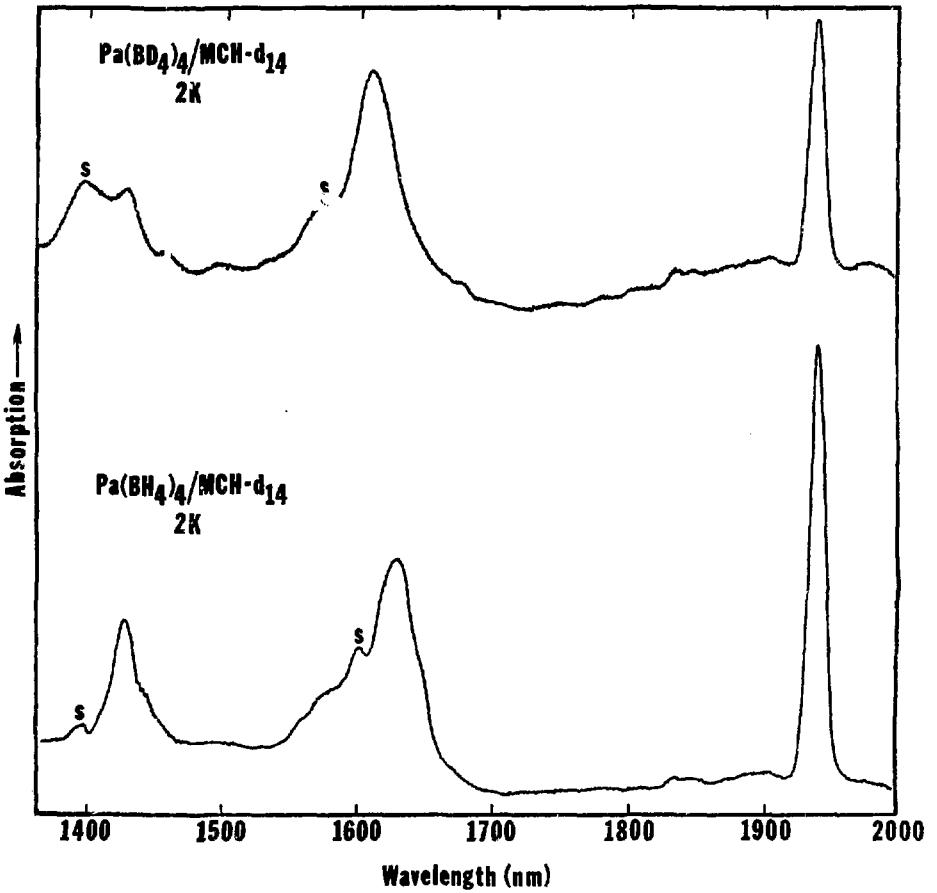

XBL 798-11146

Figure 10.

References

[1]Dieke, G. H. "Spectra and Energy Levels of Rare Earth Ions in Crystals." John Wiley and Sons. New York, N.Y., 1968.

[2]Crosswhite, H. M.; Crosswhite, H.; Kaseta, F. W.; Sarup, R. J. Chem. Phys. 64 1981 (1976).

[3]Carnall, W. T.; Crosswhite, H.; Crosswhite, H. M.; Conway, J. G. J. Chem. Phys. 64 3582 (1976).

[4]Wybourne, B. D. "Spectroscopic Properties of Rare Earths." John Wiley and Sons. New York, N.Y., 1965.

[5]Mulak, J.; Suski, W.; Troc, R., Eds. "Proceedings of the 2nd International Conference on the Electronic Structures of the Actinides." Wroclaw, Poland, 1976.

[6]Bernstein, E. R.; Keiderling, T. A. J. Chem. Phys. 59 2105 (1973).

[7]Banks, R. H.; Edelstein, N. M.; Spencer, B.; Templeton, D. H.; Zalkin, A. J. Am. Chem. Soc. 102 0000 (1980).

[8]Judd, B. R. "Operator Techniques in Atomic Spectroscopy." McGraw-Hill Book Co. New York, N.Y., 1963.

[9]Nielsen, C. W.; Koster, G. F. "Spectroscopic Coefficients for the p^n, d^n, and f^n Configurations." MIT Press. Cambridge, Mass., 1963.

[10]Conway, J. G. J. Chem. Phys. 41 904 (1964).

[11]Menzel, E. R.; Gruber, J. B. J. Chem. Phys. 54 3857 (1971).

[12]Menzel, E. R.; Gruber, J. B.; Ryan, J. L. J. Chem. Phys. 57 4287 (1972).

[13]Caspers, H. H.; Rast, H. E.; Buchanan, R. A. J. Chem. Phys. 42 3214 (1965).

[14]Axe, J. D. Ph. D. Thesis. University of California, 1960.

[15]Lang, R. Can. J. Res. A13 1 (1935); A14 127 (1936).

[16]Hutchings, M. T. Solid State Phys. 16 227 (1964).

[17]Kassman, A. J. J. Chem. Phys. 53 4118 (1970).

[18]Stevens, K. W. H. Proc. Phys. Soc. (London) A65 209 (1952).

[19]Menzel, E. R. Ph.D. Thesis, Washington State University, 1970.

[20]Drozdzynski, J.; Conway, J. G. J. Chem. Phys. 56 883 (1972).

[21]Reference 4, p. 193.

[22]Phillips, W.; Feldman, J. M. J. Chem. Phys. 42 2933 (1965).

[23]Lea, K. R.; Leask, M. J. M.; Wolf, W. P. J. Phys. Chem. Solids 23 1381 (1962).

[24]Keiderling, T. A. Ph. D. Thesis, Princeton University, 1974.

CONCLUSIONS AND FUTURE WORK

The physical properties and molecular structures of thorium and uranium borohydrides are very similar and it was expected that those of other actinide borohydrides would resemble them. When $Pa(BH_4)_4$ was synthesized, it was found to be isostructural to $Th(BH_4)_4$ and $U(BH_4)_4$ and have intermediate physical properties (e.g. vapor pressure, solid-state density, etc.). However, the tetrakis-borohydrides of Np and Pu are very different from the other three actinide compounds both in their behavior and molecular structures.

The molecular structure of $Np(BH_4)_4$ was studied by single crystal Xray diffraction and compared to those of other metal tetrakis-borohydrides. Additional insight into the understanding of bonding and properties of these compounds would be obtained by studying the structures of alkyl derivatives and coordination complexes. Single crystal neutron diffraction techniques would be necessary in accurately locating the hydrogen atoms. Complementing this work would be an investigation of actinide borohydride chemistry, especially of $Np(BH_4)_4$ and $Pu(BH_4)_4$, which is essentially unknown.

The vibrational spectra of $Np(BH_4)_4$ and $Np(BD_4)_4$ were analyzed and the results were found useful in the preliminary interpretation of the electronic spectra of the Np compounds. High resolution gas phase infrared and Raman spectra would aid in substantiating uncertain vibrational assignments and identify unknown bands. Vibrational spectra of the pure isotopic molecules (e.g. $Np(^{10}BH_4)_4$ would be of great value in explaining the origins of weak satellite peaks.

Vibronic transitions were observed to dominate the optical spectra of covalent Np borohydride and additional spectral information seems to be needed before the identification of pure electronic transitions can be accomplished. Zeeman, resonance Raman, fluorescence, and low temperature-far infrared spectra of $Np(BH_4)_4/Zr(BH_4)_4$ and $Np(BD_4)_4/Zr(BD_4)_4$ would be useful in the determination of the electronic states of $Np(BH_4)_4$.

While it is clear that there is much to be learned about these compounds, the work reported in this thesis should provide a firm foundation for any future studies which may follow.

U.S.GPO:1980-698-169/F-108